Creation of a Strongly Interacting Fermi-Fermi Mixture of ^{6}Li and ^{40}K

dissertation

by

Andreas Trenkwalder

submitted to the Faculty of Mathematics, Computer Science and Physics of the University of Innsbruck

in partial fulfillment of the requirements for the degree of doctor of science

advisor:
Univ.Prof. Dr. Rudolf Grimm,
Institute of Experimental Physics, University of Innsbruck,
Institute for Quantum Optics and Quantum Information
of the Austrian Academy of Sciences

Innsbruck, July 2011

Summary

In the field of ultracold atoms, new experiments devoted to fermions have been started recently. Fermions show features unknown to bosons like the Pauli exclusion principle or the BEC-BCS crossover. They are rewarding in terms of basic science but challenging in experiment as well as in theory. Fermions are in the center of many fundamental questions physicists aiming to answer. From nuclear physics, condensed matter physics to astronomy and high energy physics. Example research lines are high-T_c superconductivity, the phase diagram of the quark-gluon plasma or dense neutron matter. Strongly interacting fermionic few- and many-body systems pose hard problems for theory and experiments are highly welcome. Mixtures of different fermionic species give additional degrees of freedom, new phases are expected to emerge and a multitude of possible configurations, dimensions, lattices and forms of imbalanced systems are thinkable. Current experiments are about to explore these fascinating new possibilities. In our group we set up a new experiment involving the Fermi-Fermi mixture of ^{6}Li and ^{40}K. Other groups recognized the versatility of this mixture as well such that we have now several experiments worldwide working with this mixture. The individual species were already well known but the properties of the mixture were unknown. The first question to answer was about the two-body properties of the mixture. The scattering length and possible resonances needed to be evaluated. We could identify several resonances of the system and with theory input the singlet and triple scattering lengths were found. The resonances are closed-channel dominated which means they are narrow. The next step was to verify that the mixture remains stable and thermalizes in the vicinity of a broad homonuclear ^{6}Li resonance that we intended to use for evaporative cooling. This is a necessity to reach a low enough temperature before we could obtain molecules on two of the found resonances. The 155-G resonance was then identified to be the ideal resonance of our choice and thoroughly characterized. Although the resonance is quite narrow, we improved the stability of our machine such that we could enter the strongly interacting regime of the ^{6}Li-^{40}K mixture by the observation of hydrodynamic expansion. This opens up the possibility of many new experiments on the BEC-BCS crossover of this mixture.

Zusammenfassung

In den letzen Jahren hat sich das Gebiet der ultrakalten Quantengasen stark entwickelt, neue vielversprechende Experimente, insbesondere mit Fermionen konnten aufgebaut werden. Fermionen zeigen zusätzliche Eigenschaften gegenüber Bosonen, wie das Pauli'sche Ausschlussprinzip oder der BEC-BCS Übergang. Allerdings sind Experimente mit Fermionen meist schwieriger durchzuführen und die Theorie von Fermi Gasen ist komplex. Gerade aber Fermionen spielen eine zentrale Rolle auf vielen verschiedenen Gebieten der Physik: wie etwa bei Hochtemperatur-Supraleitern, in Neutronensternen oder dem Phasendiagramm vom Quark-Gluonen Plasma. Stark wechselwirkende Mehr- oder Vielteilchensysteme stellen die Theorie vor große Probleme und Experimente werden dringend benötigt. Mischungen von verschiedenen fermionischen Spezies liefern zusätzliche Freiheitsgrade, neue Phasen werden erwartet und eine Vielzahl an Konfigurationen, Dimensionen, Gittern und Formen von Imbalanz sind denkbar. Aktuell stehen wir an der Schwelle diese neuen Möglichkeiten zu erkunden. Wir haben in unserer Gruppe ein neues Experiment aufgebaut welches eine Mischung von ^{6}Li und ^{40}K vorsieht. Diese Spezies sind bereits sehr gut untersucht, aber die Mischung ist neu. Dies haben auch andere Gruppen erkannt, sodass wir heute über weltweit mehrere solcher Experimente verfügen. Zuerst mussten grundlegende Eigenschaften dieser Mischung, wie die Streulänge und mögliche Resonanzen gefunden werden. Dies ist uns gelungen. Mit Hilfe von theoretischer Seite kennen wir jetzt die Singlet- und Triplet-Streulängen. Allerdings erwiesen sich die Resonanzen als schmal, was Experimente damit schwierig macht, aber ebenso neue Einsichten erlaubt. Wir konnten zeigen, dass die Mischung stabil bleibt, sogar an einer breiten Einzelspezies ^{6}Li-Resonanz. Das ist wichtig da wir diese Resonanz zum kühlen verwenden. Damit war der Weg bereitet um heteronukleare Moleküle herzustellen. Wir indentifizierten die 155-G Resonanz als unsere ideale Resonanz und charakterisierten diese gründlich. Aktuell konnten wir an dieser Resonanz ein stark wechselwirkendes Fermi Gas nachweisen indem wir die hydrodynamische Expansion beobachtet haben. Dies bereitet den Weg um vielleicht schon bald den BEC-BCS Übergang für diese Mischung zu untersuchen.

Thanks! Danke!

Hee that is thy friend indeed,
Hee will helpe thee in thy neede:
If thou sorrowe, hee will weepe;
If thou wake, hee cannot sleepe:
Thus of euerie griefe, in hart
Hee, with thee, doeth beare a Part.
These are certaine signes, to knowe
Faithful friend, from flatt'ring foe.

Richard Barnfield[†]

This thesis would not have been possible without the help of many colleagues and friends. I owe many of you so much! First of all I would like to thank Rudi Grimm for giving me the opportunity to work on this great experiment. It needs a lot of management not always seen from outside before a large and complex apparatus can be setup. Despite of his limited time he managed to join our lab meetings, helped a lot with advices or played the devil's advocate to point us to some misconceptions. I have to admit that sometimes, some slight pressure helped to speed up things.

Florian Schreck and Eric Wille built the experiment when I joined the team as a diploma student. I could learn many new things from both of you. To share with Gabriel Kerner the office was always fun and I enjoyed to work with you and to learn from you. We had very nice video evenings in your house. Unfortunately, I could not learn Hebrew better than to say תודה רבה (toda raba). With Devang Naik it was easy going despite that we worked quite hard. I owe you many new insights and good ideas. We had a very good time in the lab together. With Frederik Spiegelhalder it was sometimes difficult because we are so different personalities. I hope you had still a good time in Innsbruck and I wish you all the best in Amsterdam! Mit'm Gerhard Hendl wårs immer a Hetz! Und ohne Deine Elektronik hatten mir no nit amål a MOT. Very special thanks go to Clarice Aiello! Your coils work perfectly. I am sorry that you left the lab so early. Many thanks to the new team members Matteo Zaccanti, Michael Jag and Christoph Kohstall! I am sure you will make very nice experiments and I hope I can share still some good time with you in the lab! I remember the nice hiking day of the FeLiKx-team we did in spring last year together with Bo Gao, Andrei Sidorov and other people from the group. We should do this more often!

[†]excerpt from [Bar98]

Vielen Dank an das IQOQI administrative Team: Doris Corona, Elisabeth Huck, Valentin Staubmann, Andreas Knabl, Thomas Mayr, Michael Jäger und Herrn Knabl. Die IQOQI Wandertage waren immer super! Vielen Dank auch an Christine Götsch-Obmascher und Nicole Jorda! Die Werkstätte verdient ein ganz großes Lob: Andreas Strasser und Stefan Haslwanter haben vieles von unserem Experiment hergestellt. Man kriegt genau was man braucht, ihr wisst immer guten Rat und ein kurzer "Plauderer" geht sich auch immer noch aus. Thank you to the interns helping to set up the experiment: Regis Danielian, Yang Liu, Raquel Chulia-Jordan, Eileen Spiegelhalder and many more. Staying in the Grimm group was always a pleasure. I liked a lot the cakes and parties and one always found an expert when one had a question. Thank you all!

Ich bin sehr froh mit Simon Stellmer das Büro zu teilen! Ich schulde dir schon so viele Kekse. Da wir beide gerne jegliche Art von Früchten mögen siehts bei uns manchmal aus wie auf einer Bananenfarm. Wir können gut über Physik diskutieren aber auch ganz gut "blödeln". Es ist immer lustig mit dir. With Meng Khoon Tey I liked always to discuss things, equally work or personal. 谢谢(xie xie) to you and to Bo Huang for the excellent Chinese food!

¡Muchas gracias a Edmundo Sánchez! Nos hemos encontrado al inicio en Les Houches y fuimos amigos todos los años. Me recuerdo con gusto caminar juntos en la montaña, especialmente con tu hija Inés Helena.

Tack till mina svenska vänner: Martin & Camilla Amft med Emilia, Torsten Dorniok och Christoph Knappe! Tyvärr har jag inte hunnit hälsa på er så ofta. Tack för att det alltid fanns en plats hos er att sova över. Jag hoppas att träffas snart igen och går på en jätte fotvandring tillsammans.

Ein ganz großes Dankeschön geht an Bettina Fischer fürs Korrekturlesen! Wir hatten eine sehr schöne Zeit in China.

Vielen Dank an meine Freunde und Kollegen, die ich jetzt gar nicht alle erwähnen kann!

Zu guter letzt, vielen Dank an meine Eltern Ignaz und Margreth Trenkwalder, an meine "kleine" Schwester Angelika, die ich immer noch gerne necke, an meine Brüder, Luis mit Petra und Katharina und Siggi mit Anneliese, Martin und dem "Poppele"! Ich bin so froh euch um mich herum zu haben. Danke für die vielen schönen Wochenenden an denen wir etwas gemeinsam unternommen haben!

Contents

Chapter 1

Introduction

1.1 Overview

This thesis covers the experiments performed so far on the ^{6}Li-^{40}K mixture in our group. It is aimed to give an overview for new students intending to work on our experiment. Since several groups work on this mixture it might be useful for them as well. The format as a "papers thesis" does not allow to present many details, therefore, it was tried to give the relevant references for further reading.

The introduction consists of two parts where first a brief overview of the basic concepts of Fermi gases is given. The second part is more experimental and will describe the approaches of different groups to perform experiments with the ^{6}Li-^{40}K mixture. An overview of the scientific achievements is given before the status of our experiment is briefly discussed. The outlook will mention possible near-future experiments. The core of the thesis are the publications of our experiment. In the appendices some unpublished measurements will be presented and some technical details are discussed. We have observed a high field heteronuclear resonance and the p-wave resonance splitting has been measured. With the help of a magnetic field modulation technique the binding energy of molecules on one resonance was measured. The narrow resonances require a well determination and stability of the magnetic field. Radio-frequency transitions are driven and with the presented Breit-Rabi formula the field is determined. The last appendix shows how we stabilize the magnetic field.

1.1.1 History

In the beginning 20^{th} century three phenomena were discovered which only occur at very low temperature and indicate that at low temperature matter behaves different than at high temperature.

In 1908, helium was first liquified by Heike Kamerlingh Onnes at the university of Leiden in the Netherlands. With the help of this achievement he discovered in the year 1911 that the electrical resistivity of mercury and other metals vanishes when the temperature is lowered below a critical temperature (see references in [Del10]). He realized that a new phase must have emerged at this temperature and called it "superconductivity". He could show that an induced current in a superconducting ring was persisting to flow during one hour. Onnes was

also the first who described that liquid helium creeps out of a container if not well sealed, which is called the "Onnes-effect"[1].

In the year 1937 John Allen, Don Misener and Piotr Kapitza observed that for liquid helium-4 if cooled below a critical temperature the viscosity vanishes [All38, Kap38]. The fluid behaves as if it had no friction earning it the name "superfluid". In a similar experiment as Onnes they showed that a superfluid will persist to flow when filled into a tube forming a closed loop. The Onnes effect can be understood by the vanishing viscosity but why this happens was unclear.

In 1924 Satyendra Nath Bose, an Indian physicist, published an article [Bos24] where he derived Planck's emission law with methods from statistical mechanics. Einstein followed this idea and applied statistical mechanics on atoms as well in his publication "quantum theory of monatomic ideal gases" [Ein24, Ein25]. He found that when a gas is compressed beyond a critical density a macroscopic number of particles will "condense" into the ground state. This state is known as Bose-Einstein condensation (BEC) and occurs for bosons (see below) at very low temperatures (in the 10^{-9} K=nK regime, also known as the "ultracold" regime).

Bosons and fermions

While BEC was a prediction coming from theory, superfluidity, and superconductivity were experimental observations. The direct connection between these phenomena is not obvious, but they occur all at low temperature. So what is the role of temperature and how are these phenomena related or different? The answer comes from quantum mechanics, developed at the time of these discoveries. In quantum mechanics, particles are not point-like but they are described by a wave function. It describes the probability to find one particle in a particular state. The wave function has a wavelength, called "de Broglie wavelength". It depends on the energy of the particle, with a large energy giving a small wavelength and vice versa. High temperature means large energy, i.e. the de Broglie wavelength is so small that we can treat the particle as point-like. It obeys the common laws of classical mechanics and thermodynamics. But as we decrease the temperature, the de Broglie wavelength becomes larger until it becomes equal to the size of the interparticle distance. The wave functions of neighboring particles start to overlap and at such a low temperature classical physics ceases to give correct predictions.

Here quantum statistics takes over: we distinguish between two fundamental types of particles, bosons and fermions. Bosons, named after Satyendra Nath Bose, have an even wave function. This means that if one exchanges two bosons, the wave function does not change. This is contrary to fermions which are named after Enrico Fermi, an Italian physicist. Fermions have an odd wave function[2] which means that if one exchanges two fermions the wave function changes its sign. The consequence is that indistinguishable fermions can not

[1] Without realizing it, Onnes had also observed the superfluid transition of liquid helium in the same measurement when he discovered the superconductivity of Mercury [Del10].

[2] Bosons have integer spin and fermions half-integer spin. "Spin" refers to a "spinning" particle in a classical picture but which is a rather crude description. It should be better seen as an additional degree of freedom giving a certain angular momentum. Half-integer spin means half-integral angular momentum in units of the reduced Planck's constant $\hbar$, i.e. $\hbar/2$, $3\hbar/2$, $5\hbar/2$, etc.

occupy the same state, while bosons can. In other words, when the wave functions overlap, for indistinguishable fermions the probability of finding a particle in the overlapping region vanishes. This is called the Pauli exclusion principle. Another consequence is that equal fermions can not be compressed into an infinitesimal volume but oppose by the so-called "Fermi pressure" against compression. Bosons behave differently. The probability becomes even larger to find a particle in an overlapping region of the wave functions.

Bose-Einstein condensate

These quantum-mechanical properties are the key to understand the phenomena described above. The simplest is Bose-Einstein condensation. At low temperature, the wave functions of bosons overlap and at sufficiently low temperature, all particles occupy the same state described by a single wave function. There is a phase transition from the normal to the BEC state. It was believed that such a state could never be created but atomic physics provided the tools. Seventy years after the predictions from Bose and Einstein the first BEC could be realized in 1995 by the groups of Carl Wieman and Eric Cornell (^{87}Rb), Randall Hulet (^{7}Li) and Wolfgang Ketterle (^{23}Na) [And95, Bra95, Dav95]. For a review see for example [Leg01].

Superconductivity and superfluidity

The theory describing superconductivity is known as BCS theory, named after John Bardeen, Leon Neil Cooper and John Robert Schrieffer, who essentially describe superconductivity as a condensation of bosonic "Cooper pairs" [Coo56, Bar57a, Bar57b]. A simple picture describes the effect for a normal crystalline superconductor as follows: The electrons move through the crystal of ions which form the solid. The ions "feel" the interaction with the electrons and get displaced slightly. This forms a sound wave, called "phonon", which propagates through the crystal[3]. The phonons travel frictionless until at a characteristic distance they scatter another electron. The two electrons involved form the "Cooper pair" which can Bose condense. The coupling between the electrons is in momentum space and the interaction is mediated by phonons.

Although the BCS theory can explain most features of superconductivity very well, the so-called high-T_c-superconductors, i.e. superconductors with a high critical transition temperature [Ore00], are not yet understood. It would be a major breakthrough if a superconductor would be made available at room temperature or at technologically easier achievable temperatures[4].

Superfluid helium is more difficult to understand. Helium has two naturally occurring isotopes, ^{4}He and the much less abandoned ^{3}He, with the former being a boson and the latter a fermion. Superfluidity of ^{4}He is another manifestation of a BEC. But the fermionic ^{3}He shows superfluid behavior as well, but at much lower temperature [Osh72]. It took longer to understand how superfluidity in a gas of fermions can occur. In the 1950'ies Lev Landau and Vitaly Ginzburg developed a thermodynamic theory which could describe it in a two-fluid picture with sound waves as excitations [Lif80]. However, a microscopic description of

[3]The electron and the phonons can be described as one so-called "quasi-particle" called "polaron". Experiments on polarons are briefly discussed on page 8.

[4]Current high-T_c-superconductors involve Copper-Oxides with the highest reported T_c=133 K[Sch93].

superfluidity is similar to BCS theory since here also Cooper pairs are formed. Recent reviews of Fermi gases and fermionic superfluidity can be found in [Leg06, Gio08, Ing08, Blo08].

Superfluidity in BEC experiments

After the first BECs became experimentally available this new phase of matter was thoroughly investigated. Among the properties of interest was also superfluidity. It was understood that a BEC is superfluid but a superfluid is not necessarily a BEC. To proof superfluidity is not as simple as to proof BEC[5]. A superfluid, when stirred, stays at rest for slow stirring velocity. If one stirs above a critical velocity, holes in the density distribution appear which are called vortices. In the year 1999 it could be proved experimentally that a BEC is also superfluid by observation of vortices [Mat99, Mad00b, AS01].

Fermi gases

No phase transition to a BEC exists when non-interacting fermions are cooled down since they are not allowed to occupy the same state. At zero temperature, every possible state is filled with exactly one fermion up to the energy called Fermi energy E_F. The temperature associated with this energy is the Fermi temperature $k_B T_F = E_F$. For energies below the Fermi energy, quantum effects become observable. For $T > T_F$ the gas can be regarded as classical, for $T \ll T_F$ one speaks of a "degenerate Fermi gas". Note that the transition from a classical gas to a quantum gas is not a sharp transition as for a BEC but it is smooth. So no clear boundary can be given, but the shape of the cloud below $T/T_F \approx 0.5$ is clearly different to a classical gas. This smooth transition makes it more difficult to observe quantum behavior for fermions. Nevertheless, already in the year 1999 the group of Deborah Jin could demonstrate a degenerate Fermi gas of ^{40}K atoms [DeM99] followed by the groups of Christophe Salomon, Randall Hulet, Wolgang Ketterle and John Thomas who could show degeneracy of ^{6}Li [Sch01, Tru01, Had02, Gra02]. These two species are the only alkali fermions which can be trapped easily[6]. Reviews on Fermi gases can be found in [Ing08, Gio08].

Non-alkali fermions are investigated as well. A degenerate Fermi gas of metastable ^{3}He was observed in the group of Wim Vassen [McN06], ^{171}Yb and ^{173}Yb have been cooled to degeneracy in the group of Yoshiro Takahashi [Fuk07, Fuk09] and degeneracy of the alkali-earth ^{87}Sr has been achieved in the group of Thomas Killian and within our group [DeS10, Tey10].

[5] The density profile of a BEC is different from a thermal distribution. Usually, one makes absorption images of the cloud and watches out for a high-density peak inside a thermal (Gaussian) background.

[6] The only stable fermionic alkali metals are ^{2}H (deuterium) and ^{6}Li. ^{40}K is among the naturally occurring unstable elements with a very long half-life time of 10^9 years such it can essentially be treated as stable. Francium has several fermions but all of them have a very short lifetime. Magnetic-optic trapping of deuterium [Wie10] and for example of ^{210}Fr [Sim96] have been reported. The unstable ^{82}Rb was trapped in a magnetic trap [Cra01].

1.1.2 Tuning interactions

While simple theories were originally assuming non-interacting particles, the actual experiments were done with interactions and the question how these change the behavior needed to be answered.

The scattering length

In scattering theory, the outgoing particles are described in a partial wave expansion of increasing angular momentum $\ell = 0, 1, 2$, etc. [Sak94]. The lowest partial waves are called s-wave, p-wave and d-wave, respectively. The s-wave is spherical and one can give a single parameter describing the entire scattering process. It is the so-called "scattering length" a which has the unit of length and essentially gives the distance at which particles typically collide[7]. It is positive for repulsion and negative for attraction. For gases at very low temperatures, only the lowest partial waves need to be considered and for ultracold gases only s-wave collisions. Since fermions can not occupy the same state, s-wave collisions of indistinguishable fermions are forbidden. Only p-wave collisions (or higher odd partial waves) are allowed. But p-wave collisions can not occur anymore at ultralow temperatures. Therefore, ultracold indistinguishable fermions do not collide.

Feshbach resonances

In the field of ultracold gases we have at hand one of the most powerful tools which enables us to tune interactions: Feshbach resonances [Chi10], named after Herman Feshbach, an American nuclear physicist. Such a resonance occurs when the energy of atoms in a scattering state becomes equal to the energy of a bound state of a different (spin) channel. In our case the bound state is a diatomic molecule (dimer). Interactions of the two states lead to an avoided crossing allowing to convert the unbound atoms into a bound dimer by ramping adiabatically over the resonance[8]. When the states involved have different magnetic moments, one can do this by simply changing the magnetic field. While ramping over the resonance, the scattering length changes dramatically: At the center of the resonance the scattering length is infinite and across the resonance it changes its sign. This allows to tune the interaction strength in a large range. Most notably, the interaction can be made attractive or repulsive or even zero, at which a perfectly non-interacting gas can be created. Across the resonance, the interaction strength is described by the product of the scattering length a with the Fermi momentum $k_F = \sqrt{2\,m\,E_F}/\hbar$. If the absolute value becomes $|k_F\,a| > 1$ then the Fermi gas is considered as "strongly interacting"[9]. This means, that collisions dominate the entire properties of the gas. The details of the interactions and of the particles involved

[7] The scattering length a is defined as $\lim_{k\to 0} k\,cot(\delta_0) = -1/a$, with k the relative momentum of the particles and δ_0 the phase of the outgoing wave. For a square-shaped potential of radius R the tangent on the wave function at R intersects with the r-axis at radius a [Sak94].

[8] The atomic scattering state is often referred as "open channel" while the bound state is referred as "closed channel".

[9] Note that we often speak of "strong interactions" but this should not be confused with the "strong interaction" or "strong force" binding the quarks together. Protons and neutrons consist of quarks and are bound in the nucleus by the residue of the strong force. The strong force is mediated by gluons.

become irrelevant. On the center of the resonance, in the "unitary limit" $a \to \pm\infty$, the properties of the strongly interacting Fermi gas can be calculated exactly [Hei01, Ho04].

It is remarkable that in the strongly interacting regime the physics of ultracold gases is the same as for completely different systems at orders of magnitude of different energies: condensed matter physics, high-T_c superconductors, dense neutron matter, heavy ion collisions, and the quark-gluon plasma [Blo08, Che05a, Ore00, Gel05, Gez08, Bra07, Joh10, Tho10, Jac10, Sch09a]. Therefore, one speaks of "universal physics".

The first experimental observations of a Feshbach resonance are reported for bosons in 1998 [Cou98, Ino98] and since then many experiments have been carried out using this tool. But these resonances are not only useful, they can cause problems as well. When the scattering length is negative, a BEC becomes unstable and the cloud collapses. This is sometimes called "bosenova". For large positive scattering length, the large collision rate can lead to enhanced loss of atoms due to three-body collisions. Therefore, for bosons the strongly interacting region is not easily accessible. But these restrictions are not the case for fermions.

For fermions Feshbach resonances do exist as well. One needs two different spin states, otherwise fermions can not collide and form molecules[10]. Deeply bound molecules formed from fermions become bosons[11]. This means that the statistics changes from fermionic to bosonic when molecules are formed. Although fermions can not Bose condense, molecules formed of fermions can Bose condense. It was a great achievement when in 2003 the first molecular BECs of $^6Li_2$ and of $^{40}K_2$ were created in our group and the groups of Deborah Jin and Wolfgang Ketterle [Joc03b, Gre03, Zwi03]. It was surprising that these molecules are long lived on the Feshbach resonance [Reg03b, Cub03, Str03, Joc03a, Reg04a]. The observation showed a stable gas even with attractive interactions and less atom loss on resonance than expected. The reason is the Pauli exclusion principle which stabilizes the gas by the Pauli pressure and reduces collisions with molecules [Pet04b].

1.1.3 Strongly interacting Fermi gases

The critical temperature for superfluidity of a weakly interacting Fermi gas is extremely small. Therefore, one thought that fermionic superfluidity besides of liquid ^{3}He will never be observable[12]. But it turned out that in the strongly interacting regime of a Feshbach resonance the superfluid phase should already appear at accessible temperatures.

First evidence of a strongly interacting Fermi gas of ^{6}Li atoms was observed in the groups of John Thomas and Christophe Salomon [O'H02, Bou03]. The cold gas was released from an asymmetric trap. If the collision rate during expansion is much larger than the trapping

[10] Here we consider only s-wave pairing. Several p-wave Feshbach resonances have been identified in different fermionic systems. For example for ^{6}Li [Sch05], ^{40}K [Reg03c] and ^{6}Li-^{40}K, chapter 2. Indications of p-wave molecules have been reported by the groups of Christophe Salomon and Claus Zimmermann & Philippe Courteille [Zha04, Mai10] and p-wave molecules have been directly observed in the group of Deborah Jin [Gae07]. In appendix B one of the p-wave resonances in our system is presented in more detail.

[11] These bosons are often referred as "composite bosons". In nuclear physics composite bosons are called mesons and consist of one quark and one anti-quark, for example pions. There exist composite fermions as well, called baryons, with protons and neutrons the most famous. They consist of 3 quarks.

[12] Since ^{3}He is a liquid interactions are intrinsically very strong in this system.

frequency then the cloud expands slower and asymmetric. The atoms experience many more collisions along the tight axis than along the weak axis. This leads to an inversion of the aspect ratio during expansion. One speaks of "hydrodynamic" behavior since the cloud behaves like a liquid. This is not a proof of superfluidity but indicates that collisions dominate the expansion, i.e. the interactions are strong, a necessity for fermionic superfluids. In chapter 6 our experiment on hydrodynamic expansion of ^{6}Li-^{40}K is presented.

BEC-BCS crossover

The crossover regime around the Feshbach resonance, where the gas changes from weakly interacting fermions (BCS regime) to strongly interacting (on the resonance) to a BEC of tightly bound bosonic molecules (BEC), is called the "BEC-BCS-crossover" [Eag69, Leg80, Noz85, Sa 93, Eng97]. After the first hydrodynamic expansion experiments showed strong interactions, numerous others followed investigating the crossover regime [Bar04b, Bou04, Reg04b, Zwi04]. For example, with the help of "collective oscillations", i.e. oscillations of an ensemble of atoms, superfluid hydrodynamics could be characterized indirectly across the resonance [Bar04a, Kin04b, Kin04a, Kin05a, Alt07a, Alt07b, Wri07]. Another method was to use radio-frequency spectroscopy [Reg03b, Reg03a, Gup03, Chi04, Shi07]. In the year 2005 the group of Wolfgang Ketterle could directly proof superfluidity of a Fermi gas by observing vortices across the BEC-BCS crossover [Zwi05]. Soon after, the same group could directly observe the transition to the superfluid phase [Zwi06a].

Experiments on strongly interacting Fermi gases

In the last years, many interesting experiments of strongly interacting Fermi gases have been performed on different topics and systems. Thermodynamic quantities and the equation of state were measured for ^{6}Li and critical temperatures[13] and critical imbalance (see below) of the superfluid-normal transition could be extracted [Shi08a, Shi08b, Luo09, Nas10, Nav10]. The interaction energy on resonance was measured already earlier[14] [O'H02, Geh03b, Bar04b, Bou04, Per04, Kin05b] and more recently has been extracted from thermodynamic measurements for ^{6}Li and ^{40}K with excellent agreement [Par06a, Ste06, Luo07, Hu07, Luo09]. The universal "contact" parameter is defined as the amplitude of the high-momentum $1/k^4$-tail in the density distribution $n(k)$ at unitarity: $C \equiv \lim_{k\to\infty} k^4 n(k)$ [Ste10b]. It was introduced by Shina Tan [Tan08a, Tan08c, Tan08b] and has been measured by the group of Deborah Jin [Ste10b] and by the group of Chris Vale with the use of Bragg spectroscopy [Kuh10, Kuh11]. The so-called "pseudo-gap" regime is under investigation from theory and experiment [Kin05b, Che05a, Che09, Gae10, Per11]. John Thomas measured the heat capacity [Kin05b], the speed of sound [Jos07] and the viscosity of the strongly interacting Fermi gas [Cao11]. So-called "Efimov" trimer states [Efi70] have been observed in our group and several others in bosonic [Kra06, Zac09, Kno09, Bar09, Pol09, Gro09, Gro10] and fermionic systems [Ott08, Huc09, Wil09b, Nak10]. Experiments in lower dimensions

[13] On resonance the numbers converge towards T_c=0.19(2) T_F for a trapped gas [Nas10].

[14] Related to this is the universal parameter β which is defined as $\mu = E_F(1+\beta)$ at unitarity and $T = 0$. It gives the mean interaction energy per particle in units of the Fermi energy. It was found to be negative, meaning attraction on resonance. [Luo09] summarizes latest results giving $\beta \approx -0.6$.

or lattices are performed where some phases might be easier to observe, see for example [Blo08, Gio08, Gün05, Pet07, Ors07, HM10, Frö11, Nis09a]. The "polaron" state, an impurity in a "Fermi sea", has been observed in the group of Martin Zwierlein [Sch09b] and the group of Wolfgang Ketterle has investigated "itinerant ferromagnetism" [Jo09, Zwe09, Pek11][15] but still many questions remain open.

1.1.4 Imbalanced systems

The mechanisms of pairing are not completely understood. One question was under which conditions pairing occurs or vanishes. The idea was to introduce some imbalance into the system and to test when pairing breaks down.

The easiest form of imbalance was to have a spin mixture with different atom number per state, i.e. population imbalance. The groups of Wolfgang Ketterle [Zwi06b, Zwi06a, Shi06] and of Randall Hulet [Par06a, Par06b] showed in the year 2006 that a spin-imbalance introduces phase separation into a superfluid core of fully paired atoms and an outer shell in the normal phase consisting of the excess majority atoms (for a review see [Che10]). The phase diagram for the imbalanced mixture on resonance was measured by the group of Wolfgang Ketterle [Shi08b].

In an impressing experiment, the group of Christophe Salomon measured the equation of state for the imbalanced Fermi gas [Nas10]. They showed that the fully-paired superfluid phase can be described as a non-interacting perfect Fermi liquid with a renormalized pressure representing the imbalance. The normal phase consists of two ideal gases: One is formed of bare majority atoms and the other one is formed of "polarons".

Fermi-Fermi mixtures

Another interesting possibility to introduce imbalance is to combine different species. The phase diagram will change dramatically and new phases might appear [Gio08, Bau09, Gez09, Ful64, Lar65, Sar63, Liu03, Gub03, Liu04, Pet07, Nis09a, Par07, Gub09]. The different species can be trapped individually with different potential depth or different lattices. By this the density or Fermi energy could be made imbalanced or different boundary conditions could be introduced. Another feature is that the species could be manipulated and detected individually.

The ^{6}Li-^{40}K mixture came into the focus since the individual species were already successfully cooled and trapped. But new experiments had to be built. One of them is the fermionic-^{6}Li-^{40}K-experiment (FeLiKx) on which the experiments of this thesis were performed. In the following section the experiments and achievements of the ^{6}Li-^{40}K mixture will be discussed in detail.

[15] The electrons of an "itinerant ferromagnet" have their spins aligned creating the magnet while they simultaneously flow as electrical current. Ref. [Jo09] has been measured on the "repulsive branch" of the resonance where the gas is unstable and decays into the molecular state. The polaron of ref. [Sch09b] has been investigated on the molecular, i.e. "attractive" branch.

1.2 Experiments on the ^{6}Li-^{40}K Fermi-Fermi mixture

In this section we will review the different experimental setups used by the several groups working on the ^{6}Li-^{40}K mixture. Among our group, these are the groups of Kai Dieckmann in Munich, Jook Walraven in Amsterdam, Christophe Salomon in Paris and the group of Martin Zwierlein in Cambridge. The scientific achievements will be discussed briefly. A more technical part will follow giving the status of our experiment and recent and near-future improvements on the machine are described. An outlook of ongoing research and future experiments will be given at the end.

1.2.1 Different approaches

The group of Kai Dieckmann at the Ludwig-Maximilian University in Munich[16] (now National University of Singapore[17]) uses ^{87}Rb as coolant [Tag06]. The elements ^{40}K and ^{87}Rb are loaded from dispensers and ^{6}Li is loaded from a Zeeman slower into a triple species magneto-optical trap (MOT). From there, the mixture is transferred into another chamber by magnetic transport. There, evaporation with ^{87}Rb as a coolant can be performed in a magnetic trap and the two fermions are cooled sympathetically. At the end of the evaporation they have a Bose condensate of ^{87}Rb together with a double-degenerate Fermi-Fermi mixture [Tag08]. The mixture is loaded into an optical dipole trap afterwards[18]. Although ^{87}Rb and ^{40}K thermalize well[19], thermalization with ^{6}Li is slow due to the small interspecies scattering length between ^{6}Li and ^{87}Rb of $20\,a_0$ [Sil05] (a_0 is the Bohr radius with $a_0 = 0.52917720859 \times 10^{-10}\,\mathrm{m}$ [Moh08]). Nevertheless, the group achieves good atom numbers of about 10^5 atoms for both species at a temperature of $0.4\,T_F$ for ^{6}Li and $0.6\,T_F$ for ^{40}K [Voi09]. The group has recently moved to Singapore.

The group of Jook Walraven at the University of Amsterdam[20] does not use a Zeeman slower for ^{6}Li but 2D MOTs for both species to get a high flux before ^{6}Li and ^{40}K are trapped in a combined 3D MOT [Tie09a, Tie09b]. Using the background scattering length of ^{40}K of about $170\,a_0$ [Tie09a, Fal08] ^{6}Li is cooled sympathetically. The interspecies scattering length of $63\,a_0$ (chapter 2) is sufficient for thermalization. They could load more ^{6}Li but then it would exert too large a heat load on ^{40}K during evaporation. This is because the temperature of ^{6}Li out of the MOT is much larger than that of ^{40}K. After evaporation, they transfer the mixture into an optical dipole trap and have to spin-clean their sample. The mixture is transported into a small quartz appendix of the main chamber by moving a lens of the dipole trap. There, the optical access to the sample is less restricted. The atom number is about 4×10^3 for ^{6}Li and 2×10^4 for ^{40}K and the temperature is about $20\,\mu$K [Tie10a].

[16] Department für Physik der Ludwig-Maximilians-Universität, Schellingstrae 4, 80799 Munich, Germany and Max-Planck-Institut für Quantenoptik, Hans-Kopfermann-Straße 1, 85748 Garching, Germany.

[17] Centre for Quantum Technologies and Department of Physics, National University of Singapore, 3 Science Drive 2, Singapore 117543.

[18] For the experiments involving only the fermions more ^{6}Li can be loaded which depletes ^{87}Rb completely during the evaporation. With this a pure ^{6}Li-^{40}K mixture is left in the trap.

[19] The scattering properties of ^{40}K-^{87}Rb were measured for example in [Fer06].

[20] van der Waals-Zeeman Institute of the University of Amsterdam, Valckenierstraat 65, 1018 XE, The Netherlands.

The atom number and temperatures are not yet sufficient for experiments on the mixture in the ultracold regime.

In the group of Christophe Salomon at ENS Paris[21], a new ^{6}Li-^{40}K experiment has been set up [Rid11]. There a Zeeman slower for ^{6}Li, a 2D MOT for ^{40}K and a combined 3D MOT is used. The experiment still needs to be completed by a magnetic transport of the cloud into another chamber. There the mixture will be cooled by evaporation in the magnetic trap using ^{40}K as a coolant as is done in Amsterdam. After evaporation, the cold cloud will be loaded into an optical dipole trap. The atom sources have been characterized, the combined MOT has been optimized and the group reports on first results about inter-species collisions [Rid11]. Currently, the magnetic transport is tested.

At the MIT in Cambridge[22] the group of Martin Zwierlein has built a new ^{6}Li-^{40}K experiment [Wu11]. Two Zeeman slowers and a combined MOT are used. The atoms are loaded into a magnetic trap where they are cooled sympathetically by ^{23}Na. In a first stage of their experiment, they used ^{41}K as a coolant which worked already very well. They achieve triple quantum degeneracy with 1.6×10^5 ^{6}Li atoms and 1.1×10^5 ^{41}K atoms and 2.0×10^5 ^{40}K atoms at a temperature of $0.16\,T_F$ for ^{6}Li and $0.51\,T_F$ for ^{40}K [Wu11].

In our group we use an all-optical approach, which is different to the other groups, see chapter 4 and [Wil09a]. Lithium and potassium are loaded from a triple-species oven[23] via a common Zeeman slower into a combined MOT. The mixture is transferred into an optical dipole trap where it is cooled by forced evaporation. To enhance the scattering length, this is done at 1180 G, on the BCS side of the broad 834-G ^{6}Li-^{6}Li Feshbach resonance in two spin states of ^{6}Li. The elastic scattering length between ^{6}Li and ^{40}K of $63\,a_0$, see chapter 2, is sufficient such that ^{40}K can be cooled sympathetically by ^{6}Li, see chapter 3. After the evaporation, one of the two spin states of ^{6}Li has to be removed to avoid ^{6}Li$_2$ molecule formation in the following magnetic field ramp over the 843-G resonance. The destination field of the ramp is the heteronuclear Feshbach resonance located at 155 G where most of our experiments are performed. Typical atom numbers and temperatures are 2×10^5 at $0.2\,T_F$ for ^{6}Li and 2×10^4 at $0.5\,T_F$ for ^{40}K. Note that for our system we have much less ^{40}K than ^{6}Li since we evaporate the lighter species and have to ensure to load not too many of the ^{40}K atoms, otherwise we would deplete ^{6}Li completely.

1.2.2 Scientific achievements

By now the basic two-body interspecies properties are very well characterized. We observed Feshbach resonances of the system and could assign them to several *s*- and *p*-wave resonances, see chapter 2. This was the result of a collaboration with other groups: Eite Tiesinga and Paul Julienne from NIST provided the coupled channels calculations and Tobias Tiecke, Jook Walraven and Servaas Kokkelmans developed a new model that allows a fast and

[21] Laboratoire Kastler Brossel, École Normale Supérieure, CNRS, Université Pierre et Marie-Curie, 24 rue Lhomond, 75231 Paris Cedex 05, France.

[22] Department of Physics, MIT-Harvard Center for Ultracold Atoms, and Research Laboratory of Electronics, Massachusetts Institute of Technology, Cambridge, Massachusetts 02139, USA.

[23] Originally, strontium was implemented in our system [Wil09a] but has been removed since a new lab was built which was successfully devoted for strontium [Ste09, Tey10, Ste10a].

simple calculation of resonances [Tie10b]. By fitting the energies of the singlet and triplet potentials, we could obtain the singlet and triplet scattering lengths of $+52.1(3)\,a_0$ and $+63.5(1)\,a_0$, respectively. Since they are very similar, the background scattering length of all resonances is in the same range; see table 5.2. It turned out that all of the observed resonances are rather narrow which means that they are closed-channel dominated [Chi10]. The coupling between the atomic scattering state and the molecular state is weak. Therefore, the universal regime at these resonances is small. This non-universality is expressed in terms of a "finite range" [Pet04a, Chi10] which is not zero as in the ideal case but finite. However, such resonances might be favorable for certain types of experiments[24]. We could find a high-field resonance at 2335 G but which is not yet assigned; see appendix A. It was surprising that the *p*-wave resonances in the ^{6}Li-^{40}K-mixture are very broad, which can be attributed to a small difference in the magnetic moments of the states involved. This stretches out the resonance. In appendix B the Li$|1\rangle$K$|1\rangle$ *p*-wave resonance is discussed in more detail.

After performing the Feshbach spectroscopy, we investigated the stability of the mixture close to the ^{6}Li-^{6}Li resonance at 834 G; see chapter 3. A stable mixture is needed since we use the strongly interacting ^{6}Li as a cooling agent for ^{40}K. We could show that on the BCS side and even on resonance the mixture remains stable. On the BEC side, as soon as molecules are formed we observe enhanced loss of ^{40}K. Beside of sympathetic cooling, another application of the observed stability was that with a small sample of weakly interacting ^{40}K particles one can probe a strongly interacting gas of ^{6}Li. This inspired the Paris group to use the weakly interacting ^{7}Li to measure the temperature of spin-imbalanced ^{6}Li in the unitary limit [Nas10].

The Munich group could demonstrate a degenerate ^{6}Li-^{40}K Fermi-Fermi mixture coexisting with a BEC of ^{87}Rb [Tag08] and they produced heteronuclear molecules on the Li$|1\rangle$K$|3\rangle$ resonance [Voi09]. The molecules are created by magnetic field ramps over the resonance and they obtain 4×10^4 molecules corresponding to 50% molecule creation efficiency. We reached degeneracy as well, see chapter 3, and could generate heteronuclear molecules on the Li$|1\rangle$K$|1\rangle$-resonance with the same method as in Munich, see section 4.6. The Munich group detected the molecules in a Stern-Gerlach type experiment: By applying a magnetic field gradient during expansion the two clouds spatially separate and can be identified on absorption images. This is possible since the molecules and the free atoms have a different magnetic moment, see for example figure 2.3 and the wiggle spectroscopy in appendix C. Our detection method used radio frequency π-pulses to transfer the unbound atoms into another spin state while the molecules are not transferred due to the energy shift caused by the binding energy[25]. Our molecule creation efficiency is similar to the one in Munich but we obtain one order of magnitude less molecules. In an expansion measurement, we could show that the ^{6}Li atoms expand slower when bound into a molecule with ^{40}K.

[24] One example is that only low density regions of neutron matter can be treated as universal since the non-trivial neutron-neutron interactions need to be taken into account for higher densities. This requires to include a non-zero finite range into the calculations which limits the comparability with the so far nearly perfect universal physics of ultracold atoms [Gez08]. Experiments on a non-universal resonance of ultracold atoms could ease this limitation. A comparison of resonances with and without finite range effects could as well be useful to refine theoretical models taking the finite range into account. ^{6}Li has broad and narrow *s*-wave resonances which might allow such a kind of measurement.

[25] The Rabi oscillation frequency for the molecules is also very different from the atoms.

The Amsterdam group published a detailed analysis of the widths of the Feshbach resonances of the system and identified the broadest in the Li$|1\rangle$K$|8\rangle$ state using the asymptotic-bound-state model [Tie10a]. A more favorable mixture is the Li$|1\rangle$K$|10\rangle$ with a comparable width and a cycling transition for imaging. Therefore, they characterized this resonance in detail. They reduce the trap depth and observe atom loss after a certain wait time. By interspecies collisions the mixture can thermalize and preferentially ^{6}Li is lost from the trap since the trap depth of ^{40}K is twice as deep as that of ^{6}Li. The loss rate of ^{6}Li is proportional to the interspecies collisions which they monitor for different magnetic fields across the resonance. By doing so they identify the position of the resonance lying at 114.47(5) G. The observed width is 1.5(5) G making it a promising candidate to reach the strongly interacting regime. Since the resonance is not in the lowest Zeeman state of the system, two-body collisions can lead to atom loss.

This is why we investigated Feshbach resonances in the presence of loss, see chapter 5. The theory part was again provided by NIST, this time from Thomas Hanna and Paul Julienne. We characterized the Li$|1\rangle$K$|3\rangle$ resonance at 155 G thoroughly with respect of elastic and inelastic scattering processes. We excited the axial sloshing oscillation of the ^{6}Li-^{40}K mixture and observed damping due to collisions between the species. As long as this damping can be seen as a small perturbation, we can assume that it is proportional to the interspecies scattering cross section. Using this method we could determine the so-called "Fano-profile" of the resonance; see section 5.3.2. The resonance and the zero-crossing can be observed very well. The shape of the profile agrees very well with numerical calculations giving a width of 880 mG. In another measurement we recorded the loss of ^{40}K atoms across the resonance and calculated the two-body loss coefficient; see section 5.3.2. We could determine with high precision the maximum of the loss at 154.707(5) G which we assume to correspond to the center of the resonance[26]. We compared the measured two-body loss coefficient with theoretical predictions and find again good agreement. In section 5.3.3 we show theoretically that only in a very narrow range of about ±10 mG around the resonance universal behavior is expected. Therefore, to enter the universal regime for the ^{6}Li-^{40}K mixture is challenging.

A survey of the resonances is given in section 5.4 which connects to the work done in Amsterdam [Tie10a]. Note that the width of the resonances as calculated from the asymptotic-bound state model have a tendency towards smaller values. In table 5.2 we give the results obtained from coupled channels calculations which should not suffer from such an effect. The measured width of the Li$|1\rangle$K$|10\rangle$[27] resonance agrees within the uncertainty with our calculated width. The measured position agrees within the width of the resonance. We compare this resonance with the Li$|1\rangle$K$|3\rangle$ resonance which we use for our experiments. Although the width of the resonance used by the Amsterdam group is twice as broad, which gives a good magnetic tunability, the expected losses on this resonance are by a factor of 3.7 larger than on the resonance we use[28]. We suspect that this might limit the versatileness of

[26] Recent results suggest that the atom pairs and molecules have slightly different polarizabilities leading to a small difference in the Stark shift. This effect results in a small shift of the resonance depending on the intensity of the dipole trap laser beam. For the typical intensities in the experiment, this shift amounts to about +10 mG. The resonance position extrapolated to zero light intensity is at about 154.698 G.

[27] Li$|a\rangle$K$|j\rangle$ in the paper.

[28] The parameter a_{res} in table 5.2 is proportional to the loss.

the Li$|1\rangle$K$|10\rangle$ resonance. Already for the Li$|1\rangle$K$|3\rangle$ resonance, we observe typical lifetimes of 10 ms which limits us in the choice of measurements we can perform. However, we believe that the resonances are good for fast measurements which do not rely on thermalization or long sampling times.

Recently, the Munich/Singapore group published their measurements on the scattering cross section of the Li$|1\rangle$K$|3\rangle$ resonance. It is obtained by the method of "cross-dimensional relaxation". They get the resonance position and width [Cos10, Voi09] which agree with our results within the given errors. Their method allows to obtain additional information on the thermalization rate of the individual species which is different due to the mass ratio. They find that ^{40}K needs by a factor of about 2 more collisions than ^{6}Li in order to come into thermal equilibrium with the other species. This deviates from the expected ratio of 3.7 significantly. Since the field where they have observed the molecules in [Voi09] is larger than the field of the resonance, they "conjecture that [they] have demonstrated for the first time a many body effect at the BEC-BCS crossover for a narrow Feshbach resonance" [Cos10].

After we have gained the knowledge of the precise location of the Li$|1\rangle$K$|3\rangle$ resonance, we could start to explore the region around the resonance in detail. Following the footsteps of the groups of John Thomas and Christophe Salomon in their early search for strong interactions in ^{6}Li [O'H02, Bou03], we observe the expansion of ^{6}Li-^{40}K in a similar type of measurements; see chapter 6 [Tre11]. We let the cloud expand from an asymmetric trap and compare the expansion far away from resonance with that on top of the resonance. We see a clear deviation of the two cases. Far away from the resonance the cloud is only weakly interacting and expands "ballistically", i.e. the aspect ratio becomes 1 for long expansion time. On the resonance, the collision rate is high and we see an inversion of the aspect ratio. This can be understood in the hydrodynamic picture, mentioned in section 1.1.3. We observe the inversion of the aspect ratio only in a narrow magnetic field range of about 30 mG around the resonance, which we interpret as the region where the mixture is strongly interacting. When we look on the volume of the cloud, we observe that the volume of ^{6}Li is reduced while that of ^{40}K is slightly increased on resonance. We interpret this in a picture that the lighter lithium is slowed down by the heavier potassium while potassium is accelerated by lithium. To understand this "drag effect" better, we analyze the density profiles of the expanding clouds. While ^{40}K shows no structure, for ^{6}Li we can clearly distinguish different regions: an inner "hydrodynamic core" of slow atoms expanding together with ^{40}K and an outer shell of essentially unperturbed fast atoms. By fitting two Gaussians on the ^{6}Li cloud, we can get a qualitative distinction between the core and the outer shell. From this we estimate a 20% fraction of the ^{6}Li atoms in the core corresponding to about the same atom number as ^{40}K atoms.

We have clearly observed strong interaction effects in the ^{6}Li-^{40}K mixture: the inversion of the aspect ratio and a hydrodynamic core of co-expanding atoms. These effects occur only in a very narrow field range which requires a good field stability and control. Although broader resonances exist, which could widen the universal regime, the inferred lifetime of the molecules might be unfavorable. However, we are sure the ^{6}Li-^{40}K Fermi-Fermi mixture is a wonderful, though challenging system for studying imbalanced Fermi gases.

1.2.3 Status of our experiment

At the moment, we have a well working system after we improved it in several steps from the status as described in [Wil09a]. Already there are mentioned the replacements of the dye laser for ^{6}Li (671 nm) and of the B-field coils. When the new coils were implemented, we encountered problems with the larger size of the Feshbach coils which was unfavorable for loading of ^{40}K. Therefore, we use the Feshbach coils for loading of ^{6}Li and switch then to the smaller curvature coils for loading of ^{40}K. Both coils can be switched from anti-Helmholtz to Helmholtz configuration using relays. The Feshbach coils are already switched into Helmholtz configuration during ^{40}K loading. We upgraded the ^{40}K laser system (767 nm) where we replaced the 3 original diode lasers with one master laser plus tapered amplifier. The two beat-locks were replaced by a cascade of AOMs[29]. We refilled the potassium reservoir about once per year with each filling done with one ampoule[30] of about 10-15 mg enriched ^{40}K. The replacement was working very well as outlined in [Wil09a]. In order to reach a field stability in the mG regime, we had to implement several features: an ultrastable power supply connected to batteries and a passive 50 Hz line noise compensation was implemented, see appendix E. The ultrastable power supply is a Danfysik 858 which we have upgraded with an digital control input and increased the current and optimized the speed. Unfortunately, it is not well compensated for 50 Hz line noise which is induced into the control electronics. Therefore, we had to cancel 50 Hz noise separately.

The optical dipole traps have been changed several times. Originally, we used 2 crossed beams of 25 μm waist to obtain confinement in radial and axial direction, chapter 2. After we exchanged the magnetic field coils, we had another coil system at hand giving us confinement due to the curvature of the magnetic field (26 Hz for ^{6}Li and 10 Hz for ^{40}K at 1180 G). Since then, we use a single-focus optical dipole trap as our first optical dipole trap to be loaded from the MOT. The original 100 W fiber laser was replaced by a 200 W version[31] with which we could increase the waist on the atoms to 38 μm. The second AOM in the beam-path was removed and an additional housing with constant clean air-flow around the laser and AOM was built. Before, we had to clean the optics often to prevent damage coming from dust. The original plan to use a standing-wave optical dipole trap ("resonator") as a first dipole trap was never implemented since the 200 W laser is much easier to handle and gives sufficient atom number. After a first evaporative cooling in this dipole trap (at 1180 G) we load the atoms into another optical dipole trap of lower power. This was originally derived from a 5 W fiber laser[32] intersecting at an angle of 53° as documented in [Wil09a]. Later this low-power trap was replaced by one beam of 41 μm waist which is co-propagating with the 200 W laser. Instead of the cross, another beam intersecting at an angle of 17.5° was implemented which had an exchangeable telescope to adjust the beam waist to either 95 μm or 60 μm. The two low-power beams were derived from two 5 W fiber lasers[32]. We implemented single-mode fibers to deliver the 5 W beams which improved the beam quality.

[29] The master laser for ^{40}K is now a TA100-pro system from Toptica and 3 double-pass AOMs are used for the 1.3 GHz hyperfine splitting. The imaging light is derived with additional AOMs. The two original tapered amplifiers are still in use.

[30] In the last filling at the end of 2009 we inserted 2 ampoules.

[31] YLR-200-SM-LP from IPG, broadband fiber laser at around 1070 nm.

[32] YLD-5-LP from IPG, broadband fiber laser at 1065 nm.

This was important when we did the sloshing measurements discussed in section 5.3.2, where otherwise dephasing due to anharmonicities of the trap made it difficult to observe the zero-crossing. While measuring the data for section 5.3.2, we encountered that the broadband laser sources cause light-induced losses. Therefore, we replaced the two 5 W broadband lasers with beams derived from a single-mode laser[33] and we obtained by a factor of 2 less loss. Recently, we replaced this laser by a more stable single-mode laser[34] without changing the trap.

The vacuum system had to be opened at the end of 2010 because we encountered a leak at the ^{6}Li reservoir of the oven. Both MOTs were not loading anymore because of the bad vacuum in the oven section[35]. We replaced the entire oven, the strontium part was left out and the lithium part was redesigned. The reason for the leak was that the nickel gasket between the reservoir and the oven was corroded by lithium. The flange was covered entirely with a yellow-green alloy. In the new design we welded the reservoir directly onto the oven and used an additional tube for filling the reservoir with a flange outside of the heated region. This design turned out to be unfavorable for filling lithium. The metal easily sticks to the walls and therefore needed to be cut into small pieces and pushed down making the filling procedure long lasting. Another problem during filling was that lithium reacted with nitrogen which we used to flood the chamber. We did not wanted to use argon since it can cause problems with the ion pumps[36]. All lithium was converted into lithium nitride Li_3N in an exothermal reaction. The next time we had to use argon. Another small leak at the first differential pumping stage was tightened and an additional titan-sublimation pump was installed. After baking the oven section, we have now a good vacuum in the oven chamber of $\leq 5 \times 10^{-9}$ mbar when the oven is operating[37]. We do not know the vacuum in the main experimental chamber but the lifetime of the atoms is 50 s after evaporation. After the first bakeout an improper closed valve caused the entire vacuum system to be vented accidentally to air for a few 10 seconds. We decided not to bake the main chamber. We flashed the titan-sublimation pumps several times and it seems that the vacuum in the main experimental chamber has not suffered too much by this accident. The lifetime of the atoms before this accident had been several minutes.

There are still several improvements which could be done in the near future: We have intrinsically less ^{40}K atoms than ^{6}Li atoms, because if we load more ^{40}K, we would deplete ^{6}Li during evaporation. We see a negative influence of the ^{6}Li MOT on the ^{40}K MOT and during loading into the dipole trap we see similar effects. The density of ^{6}Li should be as

[33] Versadisk from ELS, type 1030-50 with single-mode option giving 25 W at 1030 nm.

[34] Mephisto 18 W, 1064 nm from Innolight.

[35] The oven section of the vacuum chamber is located between the oven and the Zeeman slower. Starting from the oven the atoms pass a CF63 cube pumped by two ion pumps and windows for transversal cooling (not used), a first differential pumping stage, a CF40 cross pumped with one ion pump, a "gate valve", a second differential pumping stage and the Zeeman slower. After the Zeeman slower, the atoms enter the main experimental chamber which is made of glass. See [Wil09a].

[36] The so-called "argon instability" causes the current of an ion pump to oscillate slowly. It can even happen that argon is suddenly released from the pump leading to spikes in the pressure.

[37] When the oven is off the pressure in the oven section is $\leq 5 \times 10^{-10}$ mbar. We did not know the pressure before the chamber was opened because the ion gauge was broken. This made finding of the cause of our bad MOT loading difficult. The ion gauge could be fixed later.

low as possible for loading ^{40}K. We see this on the fluorescence during loading of the ^{40}K MOT. For loading from the MOT into the dipole trap, the effect is more involved and not fully investigated. This was not observed in [Wil09a] but now we have always to find a compromise. At the moment we do not know the exact processes but it is related to recent measurements done in Paris [Rid11]. We need to do a spin relaxation to clean the ^{40}K spin states where we loose atoms. This indicates that optical pumping of ^{40}K, see chapter 4, does not work perfectly. The temperature measurement of the oven is influenced probably by grounding problems causing sudden jumps in the temperature. The software used for data taking needs to be updated. The Danfysik power supply and the ^{40}K laser system suffer from 50 Hz line noise. The current of the Danfysik power supply comes from batteries but the control electronics is still connected to line. Additional shielding of the current transducer itself might reduce induced fields. We increased the speed of the power supply by tuning the control electronics but now it starts to oscillate if the current is above 110 A. Since we evaporate at 1180 G, we have to ramp over the broad ^{6}Li resonance at 834 G. To avoid molecule formation, we have to remove one of the spin states of ^{6}Li. But when doing this, we loose about 10^5 of ^{6}Li atoms in the other state because of the strong interactions at this field. Depending on the trap depth this can induce some heating as well. Imaging of the K$|3\rangle$ state is not completely cycling at 155 G such that we do not see all atoms at this field.

Beside of these minor problems, the system works very well with a good stability and fast loading. The obtained temperatures are low and atom numbers are good. We are sure we can enter the BEC-BCS regime for the ^{6}Li-^{40}K mixture soon.

1.2.4 Outlook

After having observed hydrodynamic behavior in the ^{6}Li-^{40}K mixture, we are ready to inspect the strongly interacting regime around the 155-G resonance more closely. The approach is similar to the experiments on the BEC-BCS crossover with homonuclear fermions mentioned above. Methods would include expansion, radio-frequency spectroscopy, Bragg spectroscopy or measurements on collective modes.

We first extracted the interaction energy from absorption images after long expansion time. For long expansion, all interaction energy and potential energy is converted into kinetic energy and one simply obtains the total energy of the cloud from the 2^{nd} moment. The second moment is a summation for each pixel $\langle x^2\rangle = \sum(x-x_c)^2$ with x_c the center of the cloud. The total energy is calculated by $E_{tot} = \frac{m\langle x^2\rangle}{t^2}$. Here $t \gg 2\pi/\omega$ is the expansion time which must be larger than the inverted trap frequencies ω along all axes[38]. The interaction energy is obtained from the difference of the total energies of an interacting state with that of the non-interacting one. We investigated the interaction energy across the resonance and observed the expected dispersive behavior far away from resonance where mean-field shifts are dominating. Close to the resonance, the energy changes smoothly from repulsive (BEC) to attractive (BCS) but the exact transition is difficult to interpret because of the noise in the data. Apart form the averaging over the trap, we believe that the situation is more

[38]Note that for a thermal cloud the density distribution is Gaussian for which the second moment is directly related to the width of the Gaussian $\langle x^2\rangle_{Gauss} = \sigma^2$.

complicated and it would be useful to extract direct information on the different states across the resonance.

Since we expect to see different states, we try to get spectral information using radio frequency transitions. We do two types of experiments: either we transfer the mixture from the strongly interacting regime into the weakly interacting or vice versa. The first probes the ground state properties of the strong interacting Li$|1\rangle$K$|3\rangle$ state which was prepared adiabatically. The second experiment probes all possible states including excited states. We call it "quench" experiment because we switch on interactions within the duration of the rf pulse, which is short. The system is transferred into a non-equilibrium state and starts to relax after the "quench". We probe either immediately after the rf pulse or we probe the relaxation after some time. This type of experiment has several advantages over the adiabatic preparation which is more common. One advantage is that our initial state is weakly-interacting, either Li$|1\rangle$K$|2\rangle$ or Li$|2\rangle$K$|3\rangle$. Therefore, we know very well the initial state and its momentum and density distribution. Another advantage is that we do not spend long time in the lossy region of the resonance which would be needed if the interacting state was prepared adiabatically. The obtained information is different as well. The adiabatic preparation gives us the wave function overlap with the ground state while the "quench" gives us the wave function overlap with all possible states. We can study by this the repulsive polaron close to resonance or for example the "molecule-hole" continuum which is caused by the Fermi-Dirac distribution of the initial state [Mas11].

Another method to get information of the system is by exciting collective oscillations. One example where this was done successfully in the homonuclear case was when the phase transition from the normal to the superfluid state could be observed [Rie11]. For our case, the lossy resonance will only allow to use fast oscillations, like in the radial direction. It would be advantageous to increase the atom number of ^{40}K for such measurements to have a better overlap with the ^{6}Li cloud and to obtain lower temperatures.

Another type of measurement would be to use Bragg spectroscopy to selectively study momentum-dependent damping of one species in a bath of the other species. The Bragg-laser beams for ^{40}K are implemented in our system but have not yet been tested.

To observe a superfluid, either directly by vortices or indirectly by collective oscillations, would be already a great achievement opening the path to investigate the BEC-BCS crossover with our ^{6}Li-^{40}K Fermi-Fermi mixture. We are sure this can be done, although it is challenging.

Chapter 2

Publication: Exploring an Ultracold Fermi-Fermi Mixture: Interspecies Feshbach Resonances and Scattering Properties of ^{6}Li and ^{40}K†

Phys. Rev. Lett. **100**, 053201 (2008)

E. Wille,[1,2] F. M. Spiegelhalder,[1] G. Kerner,[1] D. Naik,[1] A. Trenkwalder,[1] G. Hendl,[1] F. Schreck,[1] R. Grimm,[1,2] T. G. Tiecke,[3] J. T. M. Walraven,[3] S. J. J. M. F. Kokkelmans,[4] E. Tiesinga,[5] and P. S. Julienne[5]

[1] *Institut für Quantenoptik und Quanteninformation, Österreichische Akademie der Wissenschaften, 6020 Innsbruck, Austria*
[2] *Institut für Experimentalphysik und Forschungszentrum für Quantenphysik, Universität Innsbruck, 6020 Innsbruck, Austria*
[3] *Van der Waals-Zeeman Institute, University of Amsterdam, 1018 XE, The Netherlands*
[4] *Eindhoven University of Technology, P.O. Box 513, 5600 MB Eindhoven, The Netherlands*
[5] *Joint Quantum Institute, National Institute of Standards and Technology and University of Maryland, Gaithersburg, Maryland 20899-8423, USA*

We report on the observation of Feshbach resonances in an ultracold mixture of two fermionic species, ^{6}Li and ^{40}K. The experimental data are interpreted using a simple asymptotic bound state model and full coupled channels calculations. This unambiguously assigns the observed resonances in terms of various s- and p-wave molecular states and fully characterizes the ground-state scattering properties in any combination of spin states.

†The contribution of the author was mainly during the initial setup of the experiment: mounting the glass cell, bakeout of the vacuum chamber, lithium and strontium filling and distillation, oven installation and first operation and getting the first ^{6}Li MOT of the experiment. This paper was a collaboration with several groups: Tobias Tiecke, Jook Walraven and Servaas Kokkelmans developed the ABM. Eite Tiesinga and Paul Julienne performed the coupled channels calculations. We had many fruitful discussions with them and acknowledge their great contribution to this paper.

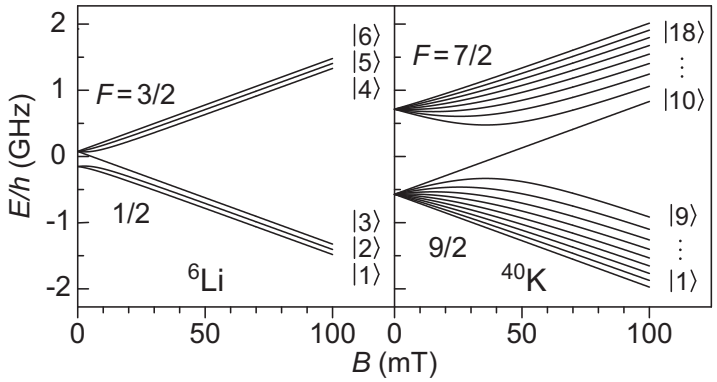

Figure 2.1: Ground-state energies of ^{6}Li and ^{40}K versus magnetic field.

Fermion pairing and Fermi superfluidity are key phenomena in superconductors, liquid ^{3}He, and other fermionic many-body systems. Our understanding of the underlying mechanisms is far from being complete, in particular for technologically relevant high-T_c superconductors. The emerging field of ultracold atomic Fermi gases has opened up unprecedented possibilities to realize versatile and well-defined model systems. The control of interactions, offered in a unique way by Feshbach resonances in ultracold gases, is a particularly important feature. Such resonances have been used to achieve the formation of bosonic molecules in Fermi gases and to control pairing in many-body regimes [Ing08, Gio08, Chi10, Köh06, Blo08].

So far all experiments on strongly interacting Fermi systems have been based on two-component spin mixtures of the same fermionic species, either ^{6}Li or ^{40}K [Ing08, Gio08]. Control of pairing is achieved via a magnetically tunable s-wave interaction between the two states. After a series of experiments on balanced spin mixtures with equal populations of the two states, recent experiments on ^{6}Li have introduced spin imbalance as a new degree of freedom and begun to explore novel superfluid phases [Zwi06b, Par06a]. Mixing two different fermionic species leads to unprecedented versatility and control. Unequal masses and the different responses to external fields lead to a large parameter space for experiments and promise a great variety of new phenomena [Liu03, Pet05, Isk06, Ors08, Pet07]. The combination of the two fermionic alkali species, ^{6}Li and ^{40}K, is a prime candidate to realize strongly interacting Fermi-Fermi systems.

In this Letter, we realize a mixture of ^{6}Li and ^{40}K and identify heteronuclear Feshbach resonances [Sta04, Ino04, Fer06]. This allows us to characterize the basic interaction properties. Figure 2.1 shows the atomic ground-state energy structure. We label the energy levels Li$|i\rangle$ and K$|j\rangle$, counting the states with rising energy. The hyperfine splitting of ^{6}Li is $(3/2)a_{\rm hf}^{\rm Li}/h = 228.2\,$MHz. For ^{40}K, the hyperfine structure is inverted and the splitting amounts to $(9/2)a_{\rm hf}^{\rm K}/h = -1285.8\,$MHz [Ari77]. For the low-lying states with $i \leq 3$ and $j \leq 10$, the projection quantum numbers are given by $m_{\rm Li} = -i+3/2$ and $m_{\rm K} = j-11/2$. A Li$|i\rangle$K$|j\rangle$ mixture can undergo rapid decay via spin relaxation if exoergic two-body processes exist that preserve the total projection quantum number $M_{\rm F} = m_{\rm Li} + m_{\rm K} = -i + j - 4$. Whenever one of the species is in the absolute ground state and the other one is in a low-lying state ($i = 1$ and $j \leq 10$ or $j = 1$ and $i \leq 3$), spin relaxation is strongly suppressed [Sim03].

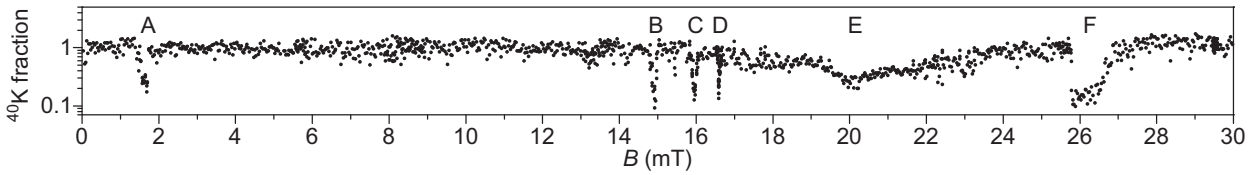

Figure 2.2: Feshbach scan of the Li$|1\rangle$K$|2\rangle$ mixture. The remaining fraction of ^{40}K atoms relative to off-resonant regions after 10 s interaction with ^{6}Li atoms is shown as a function of magnetic field. Loss features A, B, C, D, and F are due to interspecies Feshbach resonances. Loss feature E is caused by a ^{40}K p-wave Feshbach resonance [Reg03c].

We prepare the mixture in an optical dipole trap, which is formed by two 70 W-laser beams (wavelength 1070 nm), crossing at an angle of 12° [Wil09a]. The dipole trap is loaded with about 10^7 ^{6}Li atoms and a few 10^4 ^{40}K atoms from a two-species magneto-optical trap (MOT). At this stage the trap depth for ^{6}Li (^{40}K) is 1.7 mK (3.6 mK) and the trap oscillation frequencies are 13 kHz (7.3 kHz) and 1.7 kHz (1.0 kHz) in radial and axial directions. After preparation of the internal states of the atoms [Spi10], a balanced mixture of Li$|1\rangle$ and Li$|2\rangle$ atoms together with K$|1\rangle$ atoms is obtained. We perform evaporative cooling at a magnetic field of 76 mT close to the 83.4 mT Feshbach resonance between Li$|1\rangle$ and Li$|2\rangle$ [Ing08, Gio08] by reducing the optical dipole trap depth exponentially by a factor of 70 over 2.5 s. We observe that potassium remains thermalized with lithium during the evaporation. This results in 10^5 Li$|1\rangle$ and 10^5 Li$|2\rangle$ atoms together with 10^4 K$|1\rangle$ atoms at a temperature of 4 μK. This three-component Fermi mixture serves as a starting point to prepare several different stable two-component mixtures, namely Li$|2\rangle$K$|1\rangle$, Li$|1\rangle$K$|1\rangle$, Li$|1\rangle$K$|2\rangle$, or Li$|1\rangle$K$|3\rangle$ with $M_{\mathrm{F}} = -5, -4, -3, -2$, respectively. Atoms in the K$|1\rangle$ state are transferred to the desired state with adiabatic radio-frequency sweeps. Population in unwanted states is pushed out of the trap by pulses of resonant light [Spi10]. Finally, to increase the collision rate, the sample is compressed by increasing the power of the optical trap. The temperature rises to 12 μK and the peak density of lithium (potassium) increases to about $10^{12}\,\mathrm{cm}^{-3}$ (few $10^{11}\,\mathrm{cm}^{-3}$).

We detect Feshbach resonances by observing enhanced atom loss at specific values of the magnetic field [Chi10], which is caused by three-body decay. For each mixture we perform a magnetic field scan with a resolution of 0.03 mT between 0 and 74 mT (0 to 40 mT for the Li$|1\rangle$K$|3\rangle$ mixture). A scan consists of many experimental cycles, each with a total duration of about 1 min during which the mixture is submitted for ten seconds to a specific magnetic field value. The quantity of remaining atoms is measured by recapturing the atoms into the MOTs and recording their fluorescence light.

In Fig. 2.2, we show a loss spectrum of Li$|1\rangle$K$|2\rangle$. A striking feature is that the potassium atom number decreases by an order of magnitude at specific values of the magnetic field. Since the mixture contains an order of magnitude more lithium than potassium atoms, the lithium atom number does not change significantly by interspecies inelastic processes. Therefore, the potassium loss is exponential and near complete. In order to distinguish loss mechanisms involving only one species from those involving two species, we perform additional loss measurements, using samples of either pure ^{6}Li or pure ^{40}K. Loss features A,

Table 2.1: Feshbach resonances in collisions between ^{6}Li and ^{40}K in a range from 0 to 76 mT. For their positions B_0, we give the center of the measured loss features and the results from both the ABM and coupled channels calculations. The first columns give the ^{6}Li and ^{40}K channel indices i and j and the projection quantum number $M_\mathrm{F} = -i + j - 4$. Note that the experimental width of a loss feature, ΔB, is not the same thing as the width ΔB_s related to the scattering length singularity. The latter is only defined for s-wave resonances, and not for the observed p-wave resonances. The typical statistical and systematic error in the experimental B_0 is about 0.05 mT for s-wave resonances.

		Experiment		ABM	Coupled channels	
i, j	M_F	$B_0(mT)$	$\Delta B(mT)$	$B_0(mT)$	$B_0(mT)$	$\Delta B_\mathrm{s}(mT)$
2, 1	-5	21.56[a]	0.17	21.67	21.56	0.025
1, 1	-4	15.76	0.17	15.84	15.82	0.015
1, 1	-4	16.82	0.12	16.92	16.82	0.010
1, 1	-4	24.9	1.1	24.43	24.95	p wave
1, 2	-3	1.61	0.38	1.39	1.05	p wave
1, 2	-3	14.92	0.12	14.97	15.02	0.028
1, 2	-3	15.95[a]	0.17	15.95	15.96	0.045
1, 2	-3	16.59	0.06	16.68	16.59	0.0001
1, 2	-3	26.3	1.1	26.07	26.20	p wave
1, 3	-2	Not observed		1.75	1.35	p wave
1, 3	-2	14.17	0.14	14.25	14.30	0.036
1, 3	-2	15.49	0.20	15.46	15.51	0.081
1, 3	-2	16.27	0.17	16.33	16.29	0.060
1, 3	-2	27.1	1.4	27.40	27.15	p wave

[a]Near coincidences with lithium p-wave resonances [Zha04, Sch05].

B, C, D, and F only appear using a two-species mixture. Loss feature E persists in a pure ^{40}K sample and can be attributed to a potassium p-wave Feshbach resonance [Reg03c]. On the basis of the experimental data only, we can not unambiguously attribute loss feature C to an interspecies Feshbach resonance, since it coincides with a known ^{6}Li p-wave resonance [Zha04, Sch05].

Our main findings on positions and widths ΔB of the observed loss features are summarized in Table 2.1, together with the results of two theoretical models described in the following.

Our analysis of the data requires finding the solutions for the Hamiltonian $H = H_\alpha^\mathrm{hf} + H_\beta^\mathrm{hf} + H^\mathrm{rel}$. To underline the generality of our model, we refer to Li as α and to K as β. The first two terms represent the hyperfine and Zeeman energies of each atom, $H^\mathrm{hf} = (a_\mathrm{hf}/\hbar^2)\,\mathbf{s}\cdot\mathbf{i} + \gamma_e\,\mathbf{s}\cdot\mathbf{B} - \gamma_n\,\mathbf{i}\cdot\mathbf{B}$, where $\mathbf{s}$ and $\mathbf{i}$ are the single-atom electron and nuclear spin, respectively, and γ_e and γ_n are the respective gyromagnetic ratios. The Hamiltonian

of relative motion is

$$H^{\rm rel} = \frac{\hbar^2}{2\mu}\left(-\frac{d^2}{dr^2} + \frac{l(l+1)}{r^2}\right) + \sum_{S=0,1} V_S(r) P_S, \tag{2.1}$$

where μ is the reduced mass, r is the interatomic separation, and l is the angular momentum quantum number for the relative motion. Defining the total electron spin as $\mathbf{S} = \mathbf{s}_\alpha + \mathbf{s}_\beta$, the projection operator P_S either projects onto the $S = 0$ singlet or $S = 1$ triplet spin states. The potential $V_S(r)$ is thus either for the singlet $X^1\Sigma$ or triplet $a^3\Sigma$ state. This Hamiltonian H conserves both l and $M_{\rm F}$.

Our first method to locate the Feshbach resonances is inspired by a two-body bound state model for homonuclear [Moe95] and heteronuclear [Sta04] systems. We have expanded this previous work to include the part of the hyperfine interaction that mixes singlet and triplet levels. This mixing is crucial for the present analysis. We refer to this model as the Asymptotic Bound state Model (ABM).

The ABM model expands the bound state solutions $|\Psi^l\rangle$ for each l in terms of $|\psi_S^l\rangle|S, M_S, \mu_\alpha, \mu_\beta\rangle$ where $|\psi_S^l\rangle$ is the asymptotic last bound eigenstate of the potential $V_S(r) + \hbar^2 l(l+1)/(2\mu r^2)$ and $|S, M_S, \mu_\alpha, \mu_\beta\rangle$ are spin functions where M_S, μ_α and μ_β are the magnetic quantum numbers of $\mathbf{S}$, $\mathbf{i}_\alpha$ and $\mathbf{i}_\beta$, respectively. Only spin functions with the same conserved $M_{\rm F} = M_S + \mu_\alpha + \mu_\beta$ are allowed. Note that $S, M_S, \mu_\alpha, \mu_\beta$ are good quantum numbers for large magnetic field. Expanding $|\Psi^l\rangle$ in this basis and assuming that the overlap $\langle\psi_0^l|\psi_1^l\rangle$ is unity[1], the coupled bound state energies are found by diagonalizing the interaction matrix [Tie10b].

The energies E_S^l of the last bound state of the $S = 0$ and 1 potentials are eigenvalues of Eq. (2.1), and serve as free parameters in the ABM model. We can reduce this to only two binding energy parameters $E_0 = -E_0^0$ and $E_1 = -E_1^0$ if we use information about the actual shape of the potential. We can do this using model potentials derived from Refs. [Sal07, Aym05], and the van der Waals coefficient $C_6 = 2322\, E_{\rm h}\, a_0^6$ ($E_{\rm h} = 4.35974 \times 10^{-18}$ J and $a_0 = 0.0529177\,$nm) [Der01]. Each E_S can be varied by making small changes to the short range potential while keeping C_6 fixed. The energy E_S uniquely determines both the s-wave scattering length as well as E_S^l for $l > 0$.

Figure 2.3 shows the bound state energies of the ABM model as a function of magnetic field for $M_{\rm F} = -3$. Feshbach resonances occur at the crossings of bound states and threshold. We find a good fit for the experimental resonance positions for parameters $E_0/h = 716(15)\,$MHz and $E_1/h = 425(5)\,$MHz, where the uncertainty represents 1 standard deviation, see Table 2.1.

For additional analysis we have also used exact, yet much more computationally complex coupled channels calculations [Sto88], varying the short range potential as discussed above. An optimized fit to the measured resonance positions gives E_0/h=721(10) MHz and $E_1/h = 426(3)\,$MHz. This corresponds to a singlet scattering length of $52.1(3)\, a_0$ and a triplet scattering length of $63.5(1)\, a_0$. Thus, within the fitting accuracy to the experimental data, the prediction of the ABM model agrees with the result of the full coupled channels calculation. Table 2.1 shows the coupled channels resonance locations and widths for a representative

[1]The actual values are 0.979 for l=0 and 0.965 for l=1.

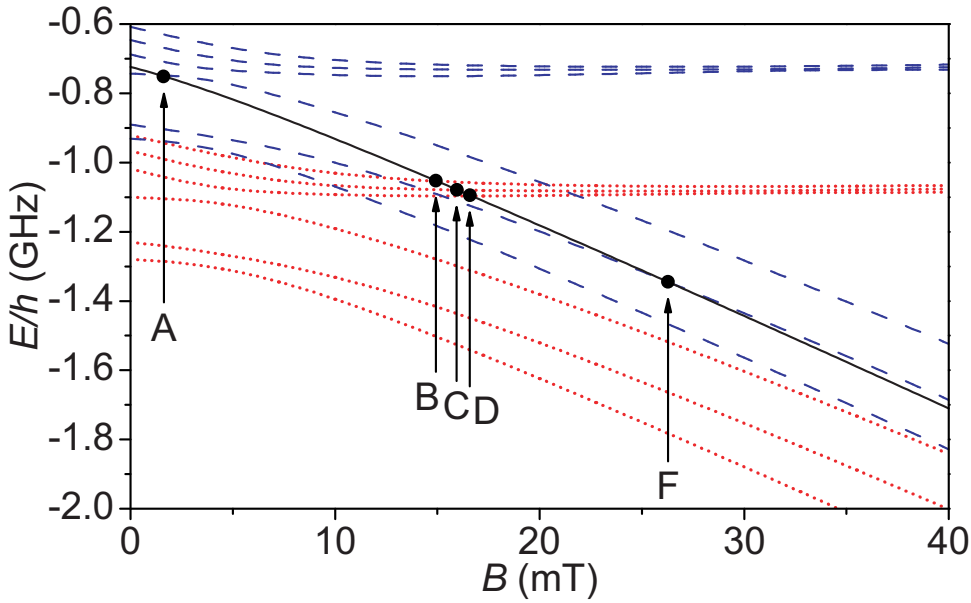

Figure 2.3: Bound state energies versus magnetic field. Dotted (dashed) lines indicate the s-wave (p-wave) states. The two-body threshold for the Li$|1\rangle$K$|2\rangle$ collision channel ($M_\mathrm{F} = -3$) is indicated by the solid line. The dots and the corresponding arrows indicate the measured resonance positions (see Fig. 2.2).

calculation with $E_0/h = 720.76\,\mathrm{MHz}$ and $E_1/h = 427.44\,\mathrm{MHz}$. The s-wave resonance width ΔB_s is defined by $a_\mathrm{s}(B) = a_\mathrm{bg}(1 - \Delta B_\mathrm{s}/(B - B_0))$, where a_bg is the background scattering length near the resonance position B_0. Note that ΔB_s need not be the same as the empirical width ΔB of a loss-feature. All resonances except the $M_\mathrm{F} = -3$ p-wave resonance near 1.6 mT agree with the measured positions within 0.13 mT. Fine-tuning of the long range potential would be needed to fit this resonance to comparable accuracy. Figure 2.4 shows the calculated s-wave scattering lengths and p-wave elastic cross sections versus magnetic field B for this model. The background scattering length a_bg for the s-wave resonances is approximately $63\,a_0$.

The accuracy and computational simplicity of the ABM model make resonance assignments very efficient, allowing rapid feedback between the experiment and theory during the exploratory search for resonances. As the ABM model in its present form does not yield the width of the resonances, the prediction of a resonance position is not expected to be more accurate than the corresponding experimental resonance width. For the ^{6}Li-^{40}K mixture, the ABM model predicts hundreds of further resonances in various s- and p-wave channels up to 0.1 T[2].

A remarkable feature of the ^{6}Li-^{40}K system is the large widths of the p-wave resonances near 25 mT, which by far exceeds the width of the observed s-wave resonances. Naively, one would expect the s-wave resonances to be wider than their p-wave counterparts because of the different threshold behavior. However, in the present case the difference in magnetic

[2]Tobias Tiecke, private communication.

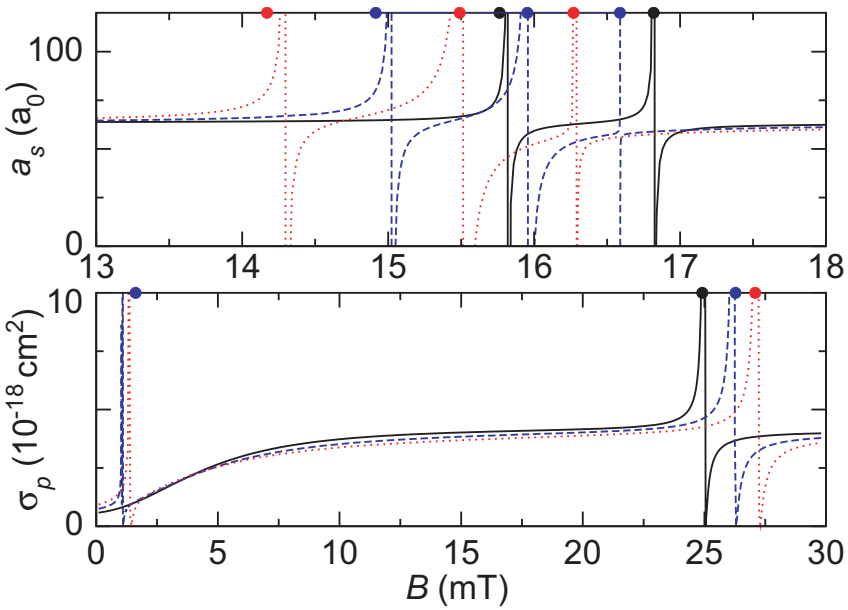

Figure 2.4: Results from coupled channels calculations for the magnetic-field dependence of the s-wave scattering length $a_s(B)$ (upper panel) and the $m_l = 0$ contribution to the p-wave elastic scattering cross section $\sigma_p(E)$ for $E/k_B = 12\,\mu$K (lower panel) for the channels in Table 2.1 with $M_F = -4$ (solid line), -3 (dashed line), and -2 (dotted line). The dots indicate the measured resonance locations.

moments between the atomic threshold and the relevant molecular state is found to be anomalously small, which stretches out the thermally broadened p-wave resonance features over an unusually wide magnetic field range. Also the asymmetry of the loss feature supports its interpretation as a p-wave resonance [Zha04, Sch05, Che05b][3].

An important issue for future experiments is the character of the s-wave resonances, i.e., the question of whether they are entrance-channel or closed-channel dominated [Chi10, Köh06]. All our observed resonances are rather narrow and thus closed-channel dominated. The existence of entrance-channel dominated resonances would be of great interest to experimentally explore BEC-BCS crossover physics [Ing08, Gio08] in mixed Fermi systems. However, our coupled channels calculations for a partial set of predicted resonances have not yet found any such resonances, and their existence seems unlikely in view of the moderate values of the background scattering lengths [Chi10, Köh06].

In conclusion, we have characterized the interaction properties in an ultracold mixture of ^{6}Li and ^{40}K atoms by means of Feshbach spectroscopy and two theoretical models. The results are of fundamental importance for all further experiments in the emerging field of Fermi-Fermi mixtures. Further steps will be the formation of bosonic ^{6}Li^{40}K molecules through a Feshbach resonance and evaporative cooling towards the creation of a heteronuclear molecular Bose-Einstein condensate.

A double-degenerate mixture of ^{6}Li and ^{40}K was recently demonstrated in a magnetic trap [Tag08].

[3]Details of the Li$|1\rangle$K$|1\rangle$ p-wave resonance around 245 G are presented in appendix B.

We thank E. Tiemann for stimulating discussions. The Innsbruck team acknowledges support by the Austrian Science Fund (FWF) and the European Science Foundation (ESF) within the EuroQUAM project. TGT and JTMW acknowledge support by the FOM-Program for Quantum gases. SJJMFK acknowledges support from the Netherlands Organization for Scientific Research (NWO). PSJ acknowledges partial support by the U.S. Office of Naval Research.

Erratum (unpublished)

In table 2.1 the calculated width of the Li$|1\rangle$K$|3\rangle$ resonance at 16.29 mT is wrong. In the publication it is given with 0.060 mT but it should read 0.006 mT.

Chapter 3

Publication: Collisional Stability of ^{40}K Immersed in a Strongly Interacting Fermi Gas of ^{6}Li†

Phys. Rev. Lett. **103**, 223203 (2009)

F. M. Spiegelhalder,[1] A. Trenkwalder,[1] D. Naik,[1] G. Hendl,[1] F. Schreck,[1] and R. Grimm[1,2]

[1]*Institut für Quantenoptik und Quanteninformation, Österreichische Akademie der Wissenschaften, 6020 Innsbruck, Austria*
[2]*Institut für Experimentalphysik und Zentrum für Quantenphysik, Universität Innsbruck, 6020 Innsbruck, Austria*

We investigate the collisional stability of a sample of ^{40}K atoms immersed in a tunable spin mixture of ^{6}Li atoms. In this three-component Fermi-Fermi mixture, we find very low loss rates in a wide range of interactions as long as molecule formation of ^{6}Li is avoided. The stable fermionic mixture with two resonantly interacting spin states of one species together with another species is a promising system for a broad variety of phenomena in few- and many-body quantum physics.

The ground breaking achievements in experiments with ultracold Fermi gases have opened up unprecedented possibilities to study new regimes of strongly interacting quantum matter [Ing08, Gio08, Blo08]. Recent experiments have opened up two important new research frontiers with fermionic atoms that go beyond the two-component spin mixtures so far exploited in the field. Mixtures involving three different spin states [Ott08, Huc09] and mixtures of different fermionic species [Tag08, Wil08, Tie10a] have produced first exciting results like the demonstration of fermionic Efimov states [Wen09, Wil09b] and the creation of Fermi-Fermi molecules [Voi09, Spi10].

†The author performed the thermometry and analyzed the data together with D. N. who mainly analyzed the data for figure 3.3. Data was taken by F. Sp., D. N. and the author.

A key ingredient in the success story of strongly interacting Fermi gases is their collisional stability. In contrast to other systems with large scattering lengths, which usually exhibit very fast collisional decay, a two-component Fermi gas can be extraordinarily stable. This results from Pauli suppression effects in atomic three-body decay [Esr01] and in atom-dimer and dimer-dimer collisions [Pet04b]. Obviously, such a suppression effect is absent when three distinguishable particles interact. This raises general questions concerning collisionally stable regimes and thus the possibilities for experiments on multicomponent Fermi gases with strong interactions. The recent experiments [Ott08, Huc09] on three-component spin mixtures of ^{6}Li have indeed shown very rapid collisional decay in regimes involving large scattering lengths.

In this Letter, we experimentally explore a three-component Fermi gas with strong interactions between two of its components. A single spin state of ^{40}K is immersed in a deeply degenerate two-component spin mixture of ^{6}Li atoms. While the intraspecies interaction between the two ^{6}Li spin states can be tuned to arbitrarily large strength, the interspecies interaction remains weak. We find that a wide stable region exists where elastic collisions dominate over inelastic decay. This opens up a variety of new exciting experimental possibilities. Here we demonstrate two immediate applications, the sympathetic cooling of another species by a strongly interacting Fermi gas and the possibility of precise thermometry in the strongly interacting regime.

The Fermi-Fermi mixture is prepared in an optical dipole trap [Spi10]. Initially about 10^7 Li atoms and a few 10^4 K atoms are loaded from a two-species magneto-optical trap (MOT) into the focus of an intense infrared laser beam (initial power 70 W, wavelength 1070 nm, waist 25 μm). The spin states are prepared such that Li is in an equal mixture of its two lowest energy states, labeled Li$|1\rangle$ and Li$|2\rangle$, and K is in its lowest state, labeled K$|1\rangle$. After a forced evaporative cooling process, which takes typically 10 s, the atoms are trapped in a 75 mW beam (waist $\sim$45μm). In the final evaporation phase, the axial trapping is essentially provided by the magnetic-field curvature of 28 G/cm^2 [Joc03b]. Throughout the whole evaporation process the magnetic field is set to 1190 G, above the broad 834-G Feshbach resonance [Ing08, Gio08], where the scattering length between the two ^{6}Li spin states is $a = -2900\,a_0$ (a_0 is Bohr's radius). Finally, to avoid further evaporative loss, the sample is recompressed by a twofold increase of the trap depth[1]. We obtain a mixture of about 10^5 Li atoms per spin state at a temperature $T^{\mathrm{Li}} \approx 100$ nK together with about 4×10^3 K atoms at a temperature $T^{\mathrm{K}} \approx 140$ nK; note that the two species are not fully thermalized at this point, such that $T^{\mathrm{K}} > T^{\mathrm{Li}}$. In terms of the corresponding Fermi temperatures $T_F^{\mathrm{Li}} = 650$ nK and $T_F^{\mathrm{K}} = 90$ nK, the temperatures can be expressed as $T^{\mathrm{Li}}/T_F^{\mathrm{Li}} \approx 0.15$ and $T^{\mathrm{K}}/T_F^{\mathrm{K}} \approx 1.6$.

This ultracold mixture serves as the starting point for our investigation of collisional loss throughout the crossover of the ^{6}Li gas from molecular Bose-Einstein condensation (BEC) to Bardeen-Cooper-Schrieffer (BCS) type behavior [Ing08, Gio08, Blo08]. This BEC-BCS crossover is controlled by the magnetic field via the broad ^{6}Li Feshbach resonance centered at 834 G. Under our conditions, with a Li Fermi wave number $k_F^{\mathrm{Li}} = 1/(4400\,a_0)$, the strongly interacting regime ($|k_F^{\mathrm{Li}}a| \geq 1$) is realized between 765 and 990 G. Note that

[1]The oscillation frequencies for Li (K) are 26 Hz (10 Hz) axially, and 450 Hz (260 Hz) radially, and the trap depth is 3 μK (6 μK).

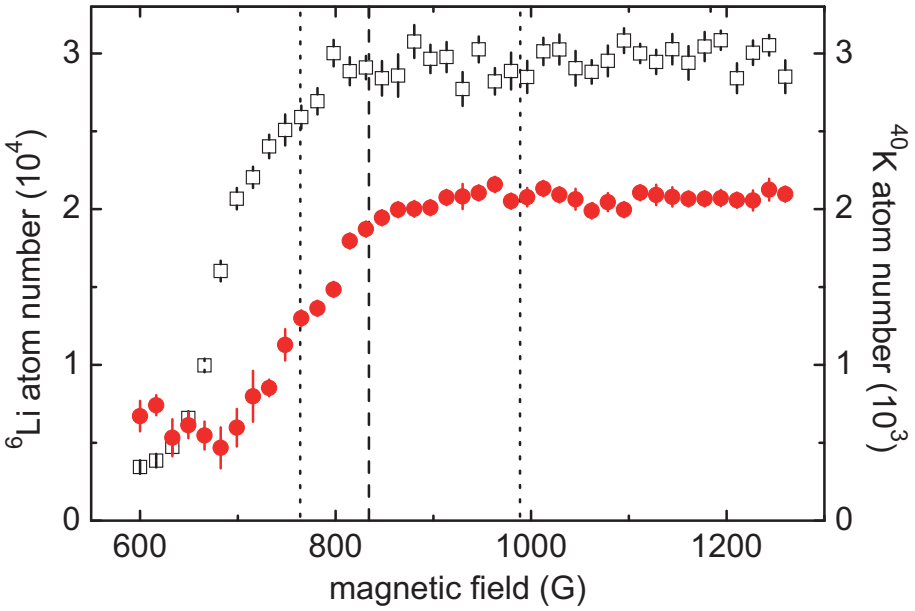

Figure 3.1: Remaining number of ^{6}Li atoms per spin state (open squares) and of ^{40}K atoms (filled circles) after a hold time of 1 s at a variable magnetic field. The dashed line at 834 G marks the center of the broad ^{6}Li Feshbach resonance and the dotted lines at 765 and 990 G indicate the strongly interacting regime, where $|k_F^{\mathrm{Li}} a| \geq 1$. The error bars indicate the statistical error of ten measurements.

there are no interspecies Feshbach resonances in the corresponding magnetic-field range and the interspecies scattering length remains constantly small at about $+60\,a_0$ [Wil08]. Since there are typically 25 times less K atoms in the trap than Li atoms, the Li sample remains essentially unperturbed by K.

In a first set of experiments, we ramp the magnetic field to a variable value and study the loss of atoms during a 1-s hold time. For detection, the remaining atoms are recaptured into the two-species MOT and their fluorescence is recorded. The atom numbers determined from fluorescence are calibrated by absorption images.

The loss of Li and K atoms around the 834-G Li Feshbach resonance is shown in Fig. 3.1. The Li sample, essentially unperturbed by K, shows a pattern observed previously [Die02, Bou03, Joc04]. On the BCS side of the resonance ($\geq$ 834 G), Li loss is very small and the detected signal stays nearly constant. On the BEC side, the observed loss results from the vibrational relaxation of dimers during dimer-dimer and atom-dimer collisions [Pet04b]. The K signal shows a very similar behavior. While loss is very weak on the BCS side of the Li resonance, strong loss is observed on the BEC side with a maximum around 700 G. At even lower fields, where Li decays very quickly, more K atoms are found to remain. This observation already points to the fact that the main source of K loss results from collisions with Li dimers.

In a second set of experiments, we study the loss more quantitatively and record the time evolution of the atom numbers for several magnetic field values. Example decay curves are shown in Fig. 3.2. We describe K loss by the rate equation $\dot{N}_{\mathrm{K}}/N_{\mathrm{K}} = -\Gamma_{\mathrm{bg}} - L_2 \langle n_{\mathrm{Li}} \rangle -$

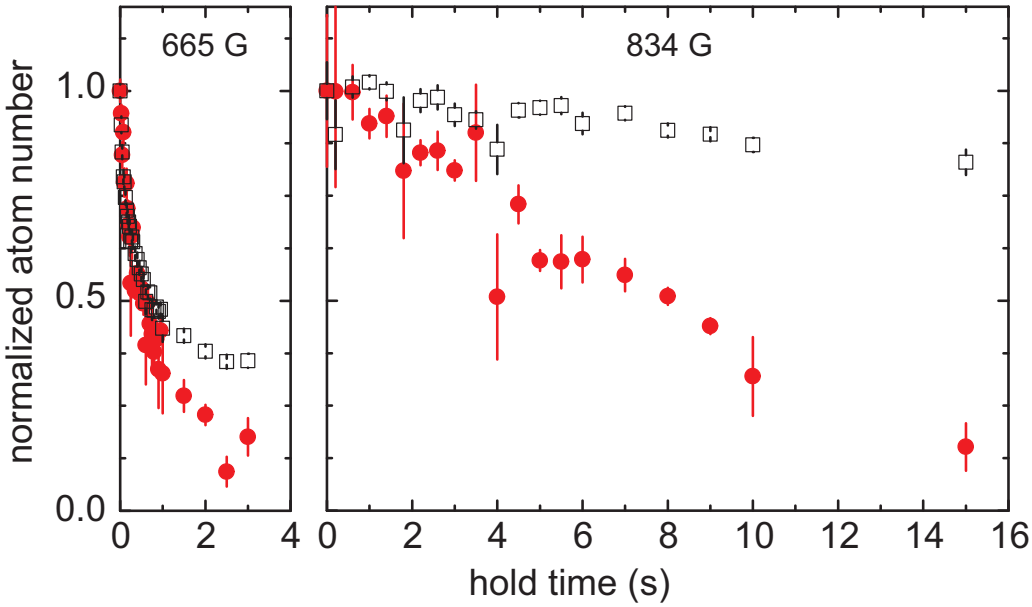

Figure 3.2: ^{6}Li (open squares) and ^{40}K (filled circles) atom number normalized to the respective initial atom number over hold time for 665 G and 834 G.

$L_3 \langle n_{\mathrm{Li}}^2 \rangle$, where the angle brackets denote averages weighted by the K density distribution. N_{K} is the K atom number, n_{Li} the density distribution of a single Li state and Γ_{bg} the background loss rate. The coefficient L_2 describes two-body loss resulting from inelastic collisions of K atoms with Li dimers. The coefficient L_3 takes into account three-body loss that results from collisions of a K atom with two Li atoms in different spin states. Both loss processes involve three distinguishable atoms, for which there is no Pauli suppression effect as in two-component Fermi systems [Esr01, Pet04b].

For short decay times, the Li density and the K temperature do not change significantly and $-\dot{N}_{\mathrm{K}}/N_{\mathrm{K}}$ corresponds to an initial decay rate Γ. We determine Γ as the initial slope of an exponential fit to the first 0.5 s of K decay data (0.3 s for the 665 G data point). K and Li density distributions are calculated from measured atom numbers, temperatures, and trap oscillation frequencies[2]. From unitarity to the BCS region, the K cloud is small compared to the Li cloud and essentially probes the center of the Li sample. On resonance, where the peak Li density is $n_{\mathrm{Li,peak}} = 2.1 \times 10^{12}\,\mathrm{cm}^{-3}$ for each spin state, we find $n_{\mathrm{Li,peak}}/\langle n_{\mathrm{Li}} \rangle = 1.7$ and $n_{\mathrm{Li,peak}}^2/\langle n_{\mathrm{Li}}^2 \rangle = 2.4$. For the data point at the lowest magnetic field (665 G) the Li sample shrinks [Bar04b] to a size smaller than the K sample and it becomes important to consider the averaged Li density, illustrated by the fact that $n_{\mathrm{Li,peak}}/\langle n_{\mathrm{Li}} \rangle = 4$ and $n_{\mathrm{Li,peak}}^2/\langle n_{\mathrm{Li}}^2 \rangle = 6.7$.

Based on our experimental data alone we cannot distinguish between two-body or three-body loss processes. We therefore analyze the data by fully attributing the loss to either one of these two processes, after subtracting the measured background loss. This results in coefficients $\mathcal{L}_2 = (\Gamma - \Gamma_{\mathrm{bg}}) / \langle n_{\mathrm{Li}} \rangle$ and $\mathcal{L}_3 = (\Gamma - \Gamma_{\mathrm{bg}}) / \langle n_{\mathrm{Li}}^2 \rangle$, which in general represent upper limits for the real loss coefficients L_2 and L_3. The background loss rate Γ_{bg}=0.009 s^{-1} is

[2]The K density distribution is approximated as Gaussian. The Li distribution is approximated by a T = 0 Fermi distribution, rescaled in dependence of the magnetic field.

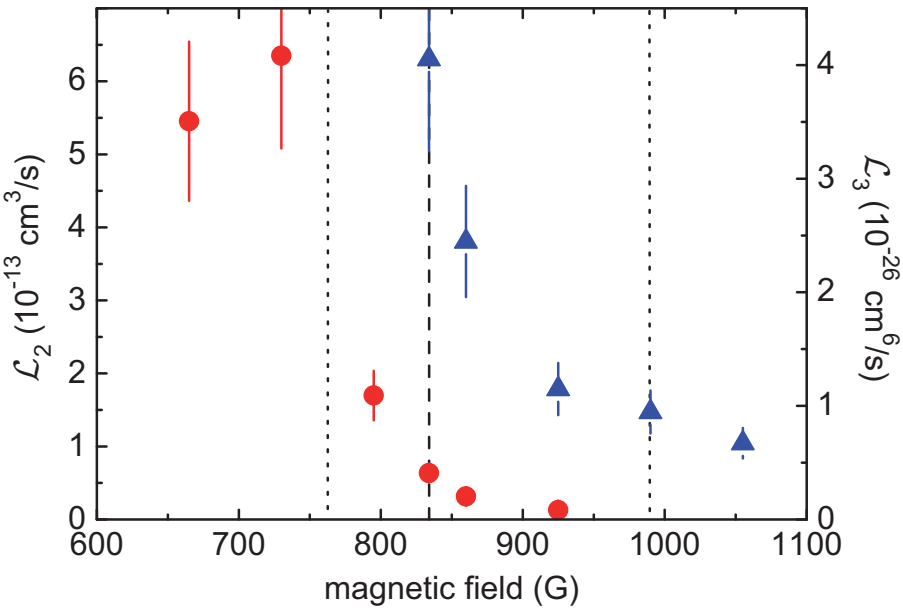

Figure 3.3: Upper bounds $\mathcal{L}_2$ and $\mathcal{L}_3$ (circles and triangles, respectively) for the two- and three-body loss rate coefficients of ^{40}K immersed in a strongly interacting degenerate ^{6}Li sample throughout the ^{6}Li BEC-BCS crossover. The dashed line at 834 G marks the center of the broad ^{6}Li Feshbach resonance and the dotted lines at 765 and 990 G indicate the strongly interacting regime, where $|k_F^{\mathrm{Li}} a| \geq 1$. The error bars represent the statistical errors from fitting the loss curves. Additional uncertainties arise from our limited knowledge of the size of the Li sample. On the BCS side this is negligible in comparison with the shown statistical errors, but on the BEC side it may introduce additional errors of up to a few 10%.

determined by analyzing the decay of a pure K sample. Above fields of 900 G the interspecies loss rate is comparable to this background loss rate.

The upper bounds $\mathcal{L}_2$ and $\mathcal{L}_3$ for the loss coefficients are shown in Fig. 3.3. They peak around 730 G and decrease by more than an order of magnitude for fields of 925 G and above. We expect the dominant loss process to change within the ^{6}Li BEC-BCS crossover. Far on the BEC side, virtually all Li atoms are bound in Li_2 molecules. Potassium is expected to be lost mainly as a result of inelastic two-body collisions with those molecules. At 665 G the real loss rate coefficient L_2 is therefore expected to be very close to $\mathcal{L}_2$, for which we obtain a value of about $6 \times 10^{-13}\,\mathrm{cm}^{-3}/\mathrm{s}$. Closer to resonance on the BEC side, atom-dimer loss is substantially reduced in accordance with the predictions of Ref. [D'I08]. Far on the BCS side, no Li dimers exist and three-body recombination involving a K$|1\rangle$, a Li$|1\rangle$, and a Li$|2\rangle$ atom can be expected to be the dominant interspecies loss process. At 1190 G L_3 is therefore expected to be very close to $\mathcal{L}_3$, for which we obtain a value of $0.7 \times 10^{-26}\,\mathrm{cm}^{-6}/\mathrm{s}$. Near the Feshbach resonance, in the strongly interacting regime, the interpretation of loss is not as straightforward. Three-body loss and an effective two-body loss resulting from collisions with Li pairs may both contribute [Du09]. At the resonance center (834G) we find $\mathcal{L}_2 = 0.6 \times 10^{-13}\,\mathrm{cm}^{-3}/\mathrm{s}$ and $\mathcal{L}_3 = 4 \times 10^{-26}\,\mathrm{cm}^{-6}/\mathrm{s}$.

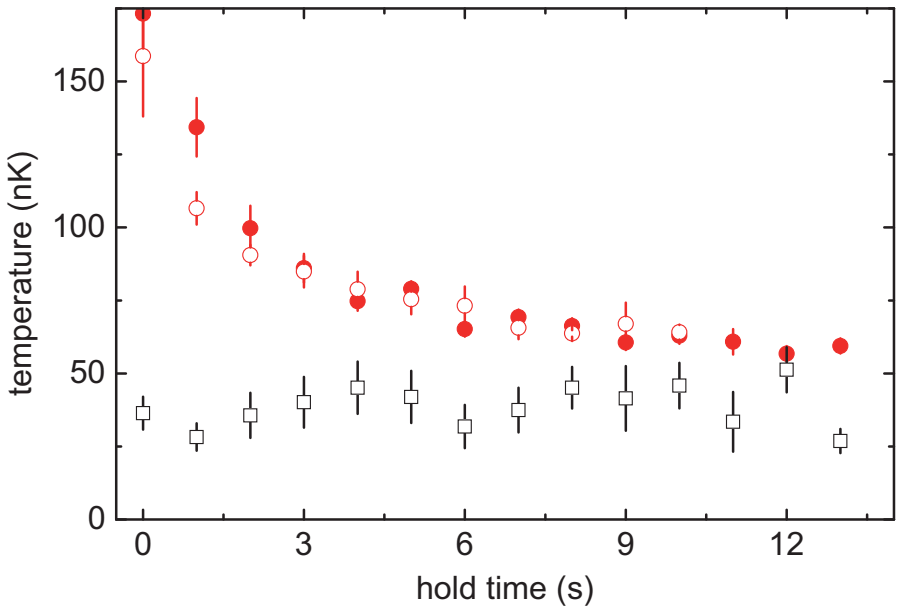

Figure 3.4: Thermalization of ^{40}K in a ^{6}Li bath. The temperature evolution of the ^{40}K probe is shown at 1190 G (filled circles) and at 834 G (open circles). For comparison we also show the temperature of the ^{6}Li bath measured at 1190 G. The error bars represent the fit errors from analyzing time-of-flight images.

Deeper cooling of the Fermi-Fermi mixture leads into the double-degenerate regime [Spi10]. This is achieved by a simple extension of the evaporative cooling process. After completing the forced evaporation ramp (stage I), we hold the sample in the shallow trap for up to 13 s (stage II)[3]; here the Fermi energies are $T_F^{\mathrm{Li}} = 420\,\mathrm{nK}$ and $T_F^{\mathrm{K}} = 95\,\mathrm{nK}$. In this situation, the Li bath undergoes continuous plain evaporation, which can efficiently remove any heat deposited by the K sample or caused by residual heating processes. Initially the bath of Li atoms contains $3.9{\times}10^4$ per spin state and losses throughout stage II remain below 20%. The temperature of the Li bath, as determined by fitting Fermi distributions to absorption images of the cloud after trap release, stays constantly at $T^{\mathrm{Li}} \approx 40\,\mathrm{nK}$.

Figure 3.4 shows how the K component is cooled down sympathetically into the quantum-degenerate regime. The temperature T^{K} is measured by standard time-of-flight absorption imaging. After the evaporation ramp T^{K} starts at about 170 nK, as the ramp in stage I is too fast to establish an interspecies thermal equilibrium. In stage II, with the magnetic field kept at 1190 G (filled circles), the temperature of the 3.4×10^3 K atoms slowly approaches a final value of ∼60 nK, corresponding to $T^{\mathrm{K}}/T_F^{\mathrm{K}} = 0.6$. From an exponential fit to T^{K}, we derive a $1/e$ time constant for the sympathetic cooling process of ∼3 s. For the Li-K mass ratio, thermalization requires about six collisions [Mud02], giving $\sim 2\,\mathrm{s}^{-1}$ for the elastic collision rate. For comparison, we also study the sympathetic cooling when the magnetic field in stage II is set to 834 G. In this case, the Li bath forms a strongly interacting superfluid with unitarity-limited interactions [Ing08, Gio08]. The only difference observed for the two

[3]In stage II, the trap oscillation frequencies for Li (K) are 26 Hz (10 Hz) axially, and 330 Hz (190 Hz) radially. The trap depth is 1.5 μK (3 μK).

settings of the magnetic field in stage II is a loss of about 40% of the K atoms at 834 G in contrast to an essentially lossless situation at 1190 G.

Our data in Fig. 3.4 indicate that the final K temperature stays somewhat above the temperature of the Li bath. This could be readily explained by the presence of a weak heating process of about 5 nK/s for K counteracting the sympathetic cooling. Another possible explanation could be that we underestimate the Li temperature because of systematic problems with thermometry of deeply degenerate Fermi gases, in particular in our shallow trap with considerable anharmonicities. The final temperatures reached in the sympathetic cooling process need further investigations. In any case, the measurement of the K temperature is free from such systematic errors and thus provides a firm upper bound for the true temperature of the Li bath. Also, a comparison of the scatter and error bars of the data in Fig. 3.4 for both species highlights that the K thermometry is much less affected by statistical errors, though performed with an order of magnitude less atoms. These observations point to the great potential of a weakly interacting probe species for precise thermometry in strongly interacting Fermi gases, which in generally is a very difficult task [Ing08, Luo09, Shi08b]. Note that an impurity thermometer relying on basically the same idea was demonstrated for a Fermi gas of ^{40}K atoms in Ref. [Reg05], using a third spin state instead of another species. For stability reasons, however, it was not applied in the strongly interacting regime.

Our ultracold ^{40}K-^{6}Li combination demonstrates the experimental possibility to immerse another species in a strongly interacting Fermi gas without suffering from collisional loss. With the examples of sympathetic cooling and thermometry we have shown two straightforward applications. There are many more experimental options with the potential to break new ground in research with ultracold fermions. The immersed species can in general serve as a weakly interacting probe for the fermionic superfluid with the great advantages that it can be separately addressed, manipulated, and detected by laser and radio-frequency fields. This may be exploited to study interactions in the many-body regime such as atom-pair collisions or to test the viscosity or the superfluid behavior of the system by a controlled motion of the impurity. Moreover, our double-degenerate system represents an excellent starting point to study a rich variety of phenomena related to few-body quantum states [Pet05, Nis09b, Lev09] and the rich many-body quantum phases of multicomponent Fermi mixtures [Paa06, Isk06, Isk07, Pet07, Isk08, Bar08, Bau09, Nis09a, Wan09, Mor09].

We acknowledge support by the Austrian Science Fund (FWF) and the European Science Foundation (ESF) within the EuroQUAM/FerMix project and support by the FWF through the SFB FoQuS.

Chapter 4

Publication: All-optical production of a degenerate mixture of ^{6}Li and ^{40}K and creation of heteronuclear molecules†

Phys. Rev. A **81**, 043637 (2010)

F. M. Spiegelhalder,[1] A. Trenkwalder,[1] D. Naik,[1] G. Kerner,[1] E. Wille,[1,2,*] G. Hendl,[1] F. Schreck,[1] and R. Grimm[1,2]

[1] *Institut für Quantenoptik und Quanteninformation, Österreichische Akademie der Wissenschaften, 6020 Innsbruck, Austria*

[2] *Institut für Experimentalphysik und Zentrum für Quantenphysik, Universität Innsbruck, 6020 Innsbruck, Austria*

We present the essential experimental steps of our all-optical approach to prepare a double-degenerate Fermi-Fermi mixture of ^{6}Li and ^{40}K atoms, which then serves as a starting point for molecule formation. We first describe the optimized trap loading procedures, the internal-state preparation of the sample, and the combined evaporative and sympathetic cooling process. We then discuss the preparation of the sample near an interspecies Feshbach resonance, and we demonstrate the formation of heteronuclear molecules by a magnetic field ramp across the resonance.

†The author contributed the figures in section 4.4 where data was taken in parts by F. Sp. and D. N. The author did the thermometry together with D. N and he performed the magnetic field noise correction and field calibration. He contributed to the optimization of the preparation scheme. He upgraded the dipole trap laser sources and performed the measurements on the Li$|1\rangle$K$|3\rangle$ molecules, briefly mentioned. The spin relaxation was done by F. Sp. and the Li$|1\rangle$K$|1\rangle$ molecules were measured by F. Sch. The author expresses his gratitude to Clarice Aiello who built the magnetic field coils together with Gerhard Hendl.

*Current address: European Space Agency, Noordwijk, The Netherlands.

4.1 Introduction

The ground-breaking achievements in experiments with ultracold Fermi gases [Ing08, Gio08] have opened up unprecedented possibilities to study new regimes of strongly interacting quantum matter. Ultracold gases represent well-controllable model systems for the exploration of many-body regimes in a way not possible in conventional condensed-matter systems [Blo08]. A new frontier in the field is currently being explored in experiments on ultracold Fermi-Fermi mixtures of ^{6}Li and ^{40}K atoms [Tag08, Wil08, Voi09, Spi09, Tie10a]. Because of the mass imbalance and the possibility to apply species-specific optical potentials, such systems promise manifold intriguing applications both in many-body physics [Paa06, Isk06, Isk07, Pet07, Isk08, Bar08, Bau09, Nis09a, Wan09, Mor09] and few-body physics [Pet05, Nis09b, Lev09].

To prepare degenerate Fermi gases, all-optical approaches have proven to be simple and robust and they facilitate highly efficient evaporative cooling. Therefore they are routinely applied in many present experiments; see Ref. [Ing08] for a review of earlier work and Refs. [Fuc07, Ina08, Ott08, Huc09] for more recent examples. Spin mixtures of ^{6}Li atoms near a broad Feshbach resonance are particularly well suited for this cooling approach because of their exceptional collision properties, which offer extremely large cross sections for elastic collisions in combination with very weak inelastic decay. This favorable situation motivates the general idea of using the strongly interacting ^{6}Li gas as a cooling agent for sympathetic cooling of another species. Following this idea in Ref. [Spi09], we recently demonstrated the sympathetic cooling of ^{40}K atoms by an evaporatively cooled, optically trapped spin mixture of ^{6}Li, reaching the double-degenerate regime.

In this article, we first present more details on our all-optical approach of preparing a double-degenerate Fermi-Fermi mixture of ^{6}Li and ^{40}K. We then show new results related to interactions and molecule formation near interspecies Feshbach resonances. In Sec. 4.2, we discuss our dual-species cooling and trapping setup and the special loading procedures used for the optical traps. In Sec. 4.3, we present an important preparation step where spin relaxation in the mixture brings the K atoms into their lowest internal state. In Sec. 4.4, we describe the combined evaporative and sympathetic cooling process. In Sec. 4.5, we show how the mixture can be prepared near interspecies Feshbach resonances. In Sec. 4.6, we finally demonstrate the creation of ultracold heteronuclear Fermi-Fermi molecules by Feshbach association methods.

4.2 Dual-species cooling and trapping setup and procedures

Here, we outline the basic concept of our dual-species setup (Sec. 4.2.1), and we present the special procedures applied to prepare the optically trapped mixture. In Sec. 4.2.2 we describe how we operate a dual-species magneto-optical trap (MOT). In Sec. 4.2.3 we present the optical dipole traps (ODT) used in the experiments. In Sec. 4.2.4 we discuss the special loading procedure for the ODT. The whole scheme is optimized for a large number of ^{6}Li atoms, as this species is used as the cooling agent for sympathetic cooling of ^{40}K into

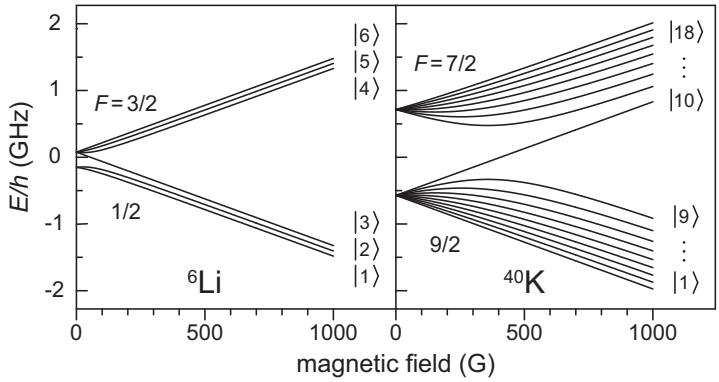

Figure 4.1: Electronic ground-state energies of ^{6}Li and ^{40}K versus magnetic field.

degeneracy [Spi09].

Figure 4.1 shows the atomic ground-state energy structure of ^{6}Li and ^{40}K. We label the energy levels Li$|i\rangle$ and K$|j\rangle$, counting the states with rising energy. The hyperfine splitting of ^{6}Li is 228.2 MHz. For ^{40}K, the hyperfine structure is inverted and the splitting amounts to 1285.8 MHz [Ari77]. For the low-lying states with $i \leq 3$ and $j \leq 10$, the projection quantum numbers are given by $m_{\mathrm{Li}} = -i + 3/2$ and $m_{\mathrm{K}} = j - 11/2$.

4.2.1 Experimental setup

For the cooling and trapping of Li and K we apply standard laser cooling and trapping techniques [Met99] combining a Zeeman-slowed atomic beam and a dual-species MOT for initial collection of atoms in the vacuum chamber. A detailed description of the experimental setup and the laser systems can be found in Ref. [Wil09a]. A dual-species oven, which is connected to the main chamber via a differential pumping section, delivers a well-collimated atomic beam. We operate the oven with isotopically enriched samples containing 80% of ^{6}Li and 7% of ^{40}K. The Zeeman slower can cool both species individually with the respective settings of the magnetic field gradients. The central element of our vacuum chamber is a glass cell that allows for very good optical access. We achieve excellent vacuum conditions with a pressure on the order of 10^{-11} mbar.

For both species we use diode laser systems with one grating stabilized master oscillator in combination with tapered amplifiers. The Li (K) laser system provides 11 mW (12 mW) per MOT beam and 80 mW (100 mW) for the Zeeman slower beam. Figure 4.2 shows a schematic drawing of the atomic energy levels and optical transitions used for cooling and trapping of Li and K. The Li MOT laser beams contain two frequency parts tuned to the cooling ($F = 3/2 \rightarrow F' = 5/2$) and repumping ($F = 1/2 \rightarrow F' = 3/2$) transitions and having equal power. For K the cooling ($F = 9/2 \rightarrow F' = 11/2$) to repumper ($F = 7/2 \rightarrow F' = 9/2$) ratio is three to two.

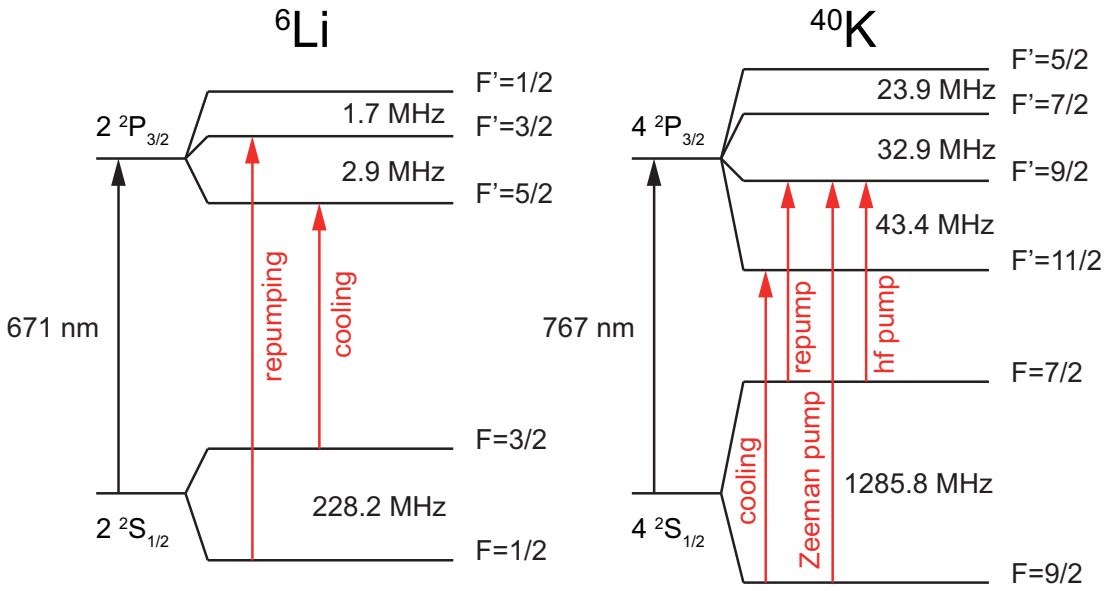

Figure 4.2: Scheme of the atomic energy levels and transitions used to cool and trap Li and K. Also shown are the transitions used for hyperfine (hf) and Zeeman pumping of K.

4.2.2 MOT loading

The initial collection and cooling of ^{6}Li and ^{40}K is achieved by conventional laser-cooling and trapping techniques. As loading of both species requires different settings of the Zeeman slower magnetic field, we use a sequential MOT-loading scheme. The basic idea is to first load Li and then add K in the presence of the Li MOT.

The Li MOT is operated with a field gradient of 26 G/cm along the symmetry axis of the field coils and a laser detuning of -27 MHz, for both cooling and repumping transition. After a loading time of about 15 s, a few 10^9 Li atoms are accumulated in the MOT. At this point we increase the magnetic field gradient to 38 G/cm, where the K MOT works optimally. In 5 s, about 10^7 K atoms are added to the trap. The K MOT is operated with a laser detuning of -34 MHz.

During the K loading phase we operate the Li MOT with a relatively large detuning of -31 MHz in order to compensate for the effect of the higher magnetic field gradient on volume and density. This avoids increased losses by inelastic interspecies collisions, enabling the efficient sequential loading of both species.

In order to reduce shot-to-shot fluctuations of the number of atoms in the trap, we control the Li and K MOT loading by monitoring their fluorescence independently. When the fluorescence of the Li MOT reaches its threshold value, Li loading is stopped and loading of the K MOT is initiated. Once the K MOT fluorescence reaches its threshold, the K loading is turned off. At this point the ODT is ramped on in 100 ms, and the magnetic fields of the Zeeman slower are ramped to zero in 10 ms.

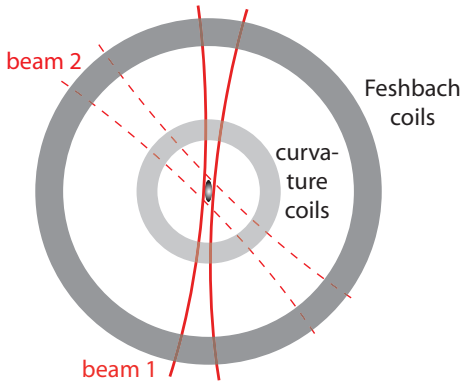

Figure 4.3: Schematic view of the optical trapping beam (beam 1) and the coils for the bias field and magnetic field curvature (shaded areas). Optionally, a second beam (beam 2) can be used for additional axial confinement.

4.2.3 Optical dipole trapping schemes

For further storage and cooling of the atomic cloud, we use a trapping scheme that employs the optical dipole force of an intense infrared laser beam [Gri00] and the magnetic force in the curvature of the magnetic field [Joc03b]. The latter becomes important when the optical trap is operated with low laser power. A schematic drawing of this hybrid trapping scheme is shown in Fig. 4.3.

The principal ODT is formed by a single beam (beam 1) delivered by a 200-W fiber laser that emits light at a central wavelength of 1070 nm (IPG YLR-200SM-LP). The beam is focused down to a waist of 38 μm at the center of the MOT. During loading, the trap is operated with an optical power of 96 W, which results in a depth of 2.6 mK for Li. For K the trap depth is larger by a factor of 2.1 and thus amounts to about 5.5 mK.

Two sets of magnetic field coils are used in our setup to control the bias and curvature field independently; the coil setup is described in more detail in Appendix 4.8. For small bias fields the magnetic confinement is very small in the axial direction; here additional axial confinement can be obtained from another infrared beam (beam 2) delivered by a 5-W fiber laser with a central wavelength of 1065 nm (IPG YLP-5-LP). The single beam is focused to a waist of 97 μm and intersects beam 1 at an angle of 53°.

4.2.4 Dipole trap loading

Loading cold atoms of a single species from a MOT into a dipole trap is a standard procedure in many experiments. Sub-Doppler cooling and MOT compression are common methods to enhance transfer into the optical trap. The optimized loading of two species, however, needs special procedures. Here we describe the sequential loading scheme that gives us excellent starting conditions for the evaporation of Li and K in a common optical trap. A schematic illustration of the loading and transfer sequence is shown in Fig. 4.4. We found that an optimum is achieved by first transferring K into the optical trap while keeping Li stored in the large-volume, low-density MOT and then performing the Li transfer.

After switching on the ODT, in a first step the K MOT is compressed by ramping up the

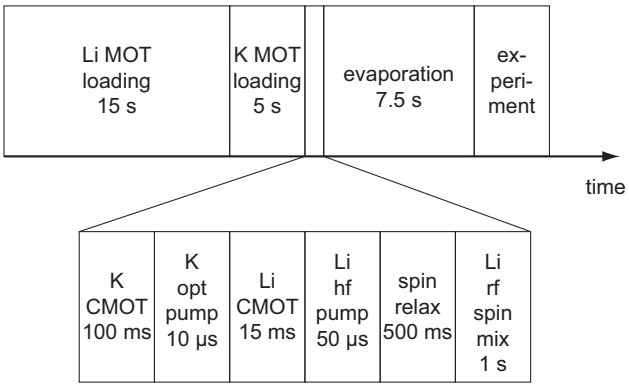

Figure 4.4: Illustration of the loading, transfer, and measurement timing sequence. CMOT stands for compressed MOT.

magnetic field gradient within 50 ms to 96 G/cm and bringing the frequencies of the K lasers closer to resonance to a detuning of a few MHz with an intensity lowered to 70%. At the same time the detuning of the Li MOT is increased to −47 MHz to avoid compression of the Li MOT. At this point the K MOT light is extinguished and the K atoms are confined in the dipole trap while Li is stored practically undisturbed in a MOT at a reduced magnetic field gradient of 64 G/cm. With the K MOT beams off, untrapped atoms are allowed to escape for 50 ms.

Potassium has 10 Zeeman sublevels in the lowest hyperfine ground state; see Fig. 4.1. In order to produce a spin-polarized sample of K in its lowest internal state, we apply an optical pumping scheme that not only transfers the atoms to the lower hyperfine state, but also pumps the atoms to the lowest m_F state.

For optical pumping the quadrupole field is switched off for 2 ms and only a small guiding field is kept on. Parallel to the field we shine in a σ^--polarized laser beam for 10 μs, which optically pumps the K atoms into state $|1\rangle$. The optical pumping beam contains two frequency components, one for Zeeman pumping tuned to the $(F = 9/2 \rightarrow F' = 9/2)$ transition and another one for hyperfine pumping tuned to the $(F = 7/2 \rightarrow F' = 9/2)$ transition as shown in Fig. 4.2. Each frequency component has about 50 times the saturation intensity. During the optical pumping stage, the cloud of Li atoms remains trapped in an optical molasses and can be recaptured without significant losses.

The high-power trapping laser induces a large light-shift on the optical cooling and pumping transitions. Potassium has two optical transitions between the excited $4^2P_{3/2}$ state and the $5^2S_{1/2}$ and $3^2D_{5/2}$ states with wavelengths of 1252 and 1177 nm, respectively. At high intensities of the ODT these two transitions shift the $4^2P_{3/2}$ level by several 100 MHz. Therefore optical pumping cannot be performed in the trap and we have to switch it off for a short time. After the 10-μs off-time of the ODT needed for the optical pumping, essentially all K atoms are recaptured into the ODT.

At this point we have a sample of a few 10^4 polarized ^{40}K atoms in the ODT, surrounded by a magneto-optically trapped cloud of ^{6}Li atoms. We finally apply a compressed MOT stage for Li in order to efficiently load this species into the dipole trap. For this, the quadrupole field is ramped back up to 64 G/cm and the MOT lasers are operated at a very

small detuning of -3 MHz from resonance while the power is lowered to 180 μW per beam for a duration of 15 ms. Hyperfine pumping of Li to the lower state is performed by switching the repumping laser off during the last 50 μs of the pulse. With this sequence we obtain a few 10^5 Li atoms in the lowest two spin states in the ODT at a temperature of about 300 μK.

4.3 Spin relaxation

A Li$|i\rangle$K$|j\rangle$ mixture can undergo rapid decay via spin relaxation if exoergic two-body collisions can take place that preserve the total projection quantum number $m_{\mathrm{tot}} = m_{\mathrm{Li}} + m_{\mathrm{K}} = -i + j - 4$. In such a process,

$$\mathrm{Li}|i\rangle + \mathrm{K}|j\rangle \rightarrow \mathrm{Li}|i-1\rangle + \mathrm{K}|j-1\rangle + E_r,$$

the energy E_r is released. Whenever one of the species is in the absolute ground state, and the other one is in a low-lying state ($i = 1$ and $j \leq 10$ or $j = 1$ and $i \leq 3$), spin relaxation is strongly suppressed [Sim03].

Since optical Zeeman pumping does not lead to a perfect transfer of all K atoms into the lowest spin state, we exploit spin relaxation to fully spin polarize K into state $|1\rangle$. We investigated the conditions under which spin relaxation can be used for this purpose. In these measurements we apply only hyperfine pumping, but no Zeeman pumping. We start with an almost equal mixture of Li in its lowest two hyperfine states, $|1\rangle$ and $|2\rangle$, trapped together with a population of K in all Zeeman substates $j \leq 10$.

We investigate the magnetic field dependence of the spin relaxation by holding the sample for 500 ms at a variable magnetic field. The trap is operated under the same conditions as during trap loading (i.e., with a trap depth of 2.6 mK for Li and 5.5 mK for K). The atom numbers are measured using spin-selective absorption images, which are always taken at a bias field of 1190 G[1]. Figure 4.5 shows the resulting atom numbers of Li in states $|1\rangle$ (open squares) and $|2\rangle$ (solid squares) as well as K in state $|1\rangle$ (solid circles). Two distinct peaks in the K$|1\rangle$ atom number are visible at 40 and 207 G and coincide with dips in the Li$|2\rangle$ atom number. These features are fitted with Lorentzians to determine their positions and widths.

The release energy E_r at 40 G (207 G) corresponds to 2.1 mK (5.8 mK). For an inelastic collision between two atoms with different masses, the resulting kinetic energy contributions are inversely proportional to the mass. For the ^{6}Li-^{40}K combination, 87% of the released energy is transferred to the lighter Li atoms (mass M_{Li}) and only 13% to the heavier K (mass M_{K}). A necessary condition for the trap depth U_{K} under which a K atom stays confined is

$$U_{\mathrm{K}} > \frac{M_{\mathrm{Li}}}{M_{\mathrm{K}} + M_{\mathrm{Li}}} E_r, \tag{4.1}$$

and analogously for U_{Li}. The mass factor along with the about two times larger trap depth for K explains why we observe loss of Li atoms during the spin relaxation while K stays trapped. Furthermore, a K atom in a Zeeman level higher than $|2\rangle$ will need multiple collisions with

[1] We use high-field imaging at 1190 G where the scattering length between Li$|1\rangle$ and $|2\rangle$ is small and negative. The Li cloud can thus be approximated as a weakly interacting Fermi gas which in the degenerate regime allows for easier interpretation of the profiles obtained by absorption images after time-of-flight.

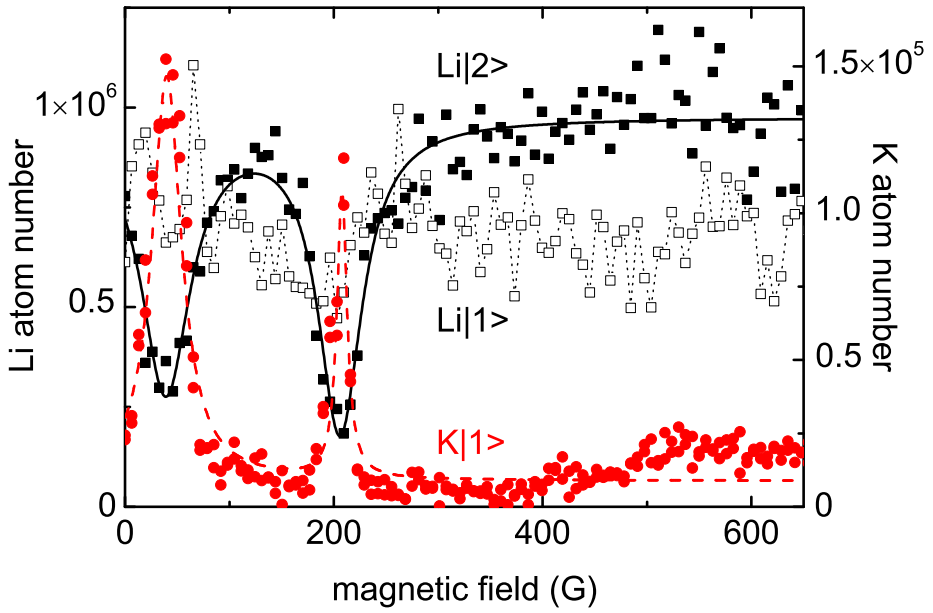

Figure 4.5: Magnetic field dependence of spin relaxation. The numbers of atoms in different spin states are measured by state-selective absorption imaging after a storage time of 500 ms in the dipole trap. The solid (open) squares give the Li$|2\rangle$ ($|1\rangle$) atom number, the solid circles are K$|1\rangle$. The two pronounced features that are visible at 40 and 207 G are fitted by Lorentzians to determine their positions and widths.

Li$|2\rangle$ in order to fully polarize. That explains why much more Li$|2\rangle$ is lost than K$|1\rangle$ is gained during this process.

We interpret our data by comparing the position of the two spin relaxation features with the location of known interspecies Feshbach resonances, since we expect enhanced inelastic loss close to a Feshbach resonance [Chi10]. As Fig. 4.6 shows, there is a series of s-wave Feshbach resonances between Li$|2\rangle$ and K$|2 \leq j \leq 10\rangle$ near the 207-G feature. The distribution of Feshbach resonances coincides with the width of the observed spin relaxation feature. Note that the experiment is performed at relatively high temperature causing considerable broadening of the Feshbach resonances. Therefore individual resonances cannot be resolved.

For the feature of enhanced spin relaxation at 40 G, there are no interspecies s- or p-wave Feshbach resonances and thus we cannot explain it by means of scattering resonances. We speculate that this feature is a result of competition between two effects. At low magnetic fields B the release energy E_r increases $\propto B$. This increase in energy leads to an increase in the density of continuum states in the decay channel, which, according to Fermi's golden rule, increases the loss. The competing effect is that the nuclear spin of Li decouples from the electron spin at a field of a few ten Gauss. This may lead to a reduced probability of spin relaxation during a collision.

In a second set of experiments we investigate the timescale on which spin relaxation occurs at the two relevant magnetic fields 40 and 207 G. For both fields we find that the timescale for the process is 150 ms and a steady state is essentially reached after 500 ms.

Spin relaxation is a very efficient process that allows us to fully polarize our K sample

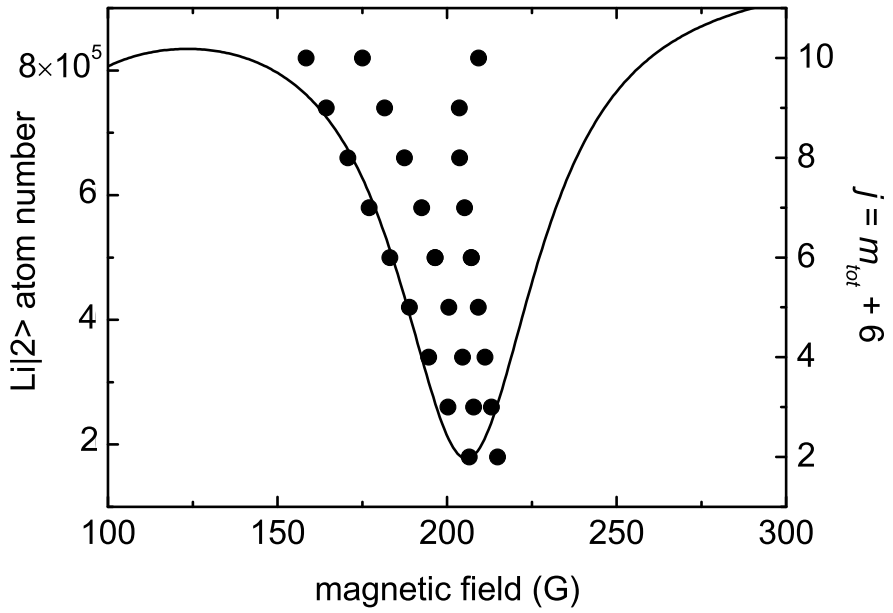

Figure 4.6: Interpretation of the 207-G spin relaxation feature in terms of Feshbach resonances. The dots show the calculated positions of Feshbach resonances between Li$|2\rangle$ and K$|2 \leq j \leq 10\rangle$ [Tie09a]. Also plotted is the Lorentzian fit to the Li$|2\rangle$ loss feature from Fig. 4.5 for comparison.

without loss of K atoms. Since initially much more Li atoms are present in the trap, the Li loss is a minor problem. The resulting imbalance of the two Li spin states can be removed by driving radio-frequency (rf) transitions between the two states.

4.4 Evaporation and sympathetic cooling

A spin mixture of Li$|1\rangle$ and Li$|2\rangle$ near the broad 834-G Feshbach resonance facilitates highly efficient evaporative cooling, as it is well known in the field of strongly interacting Fermi gases [O'H02, Ing08]. The efficiency of the cooling process is due to the very favorable combination of a large elastic scattering cross section with very low losses. In Ref. [Spi09] we have already demonstrated the possibility of using the ^{6}Li spin mixture as an efficient cooling agent to sympathetically cool another species. In this way we have demonstrated the attainment of a double-degenerate Fermi-Fermi mixture of ^{6}Li and ^{40}K. Here we present additional information on the experimental procedures, and the combined evaporative and sympathetic cooling process.

Let us first summarize our main findings of Ref. [Spi09] on the collisional stability of the three-component Fermi gas of Li in the lowest two spin states together with K in the lowest spin state. Interspecies collisional loss is negligible on the BCS side of the broad Li resonance ($B > 900\,\mathrm{G}$) and quite weak even exactly on resonance (834 G). Substantial loss, however, occurs on the BEC side of the resonance in a range between about 650 and 800 G. The latter is a result of inelastic collisions between K atoms with weakly bound Li

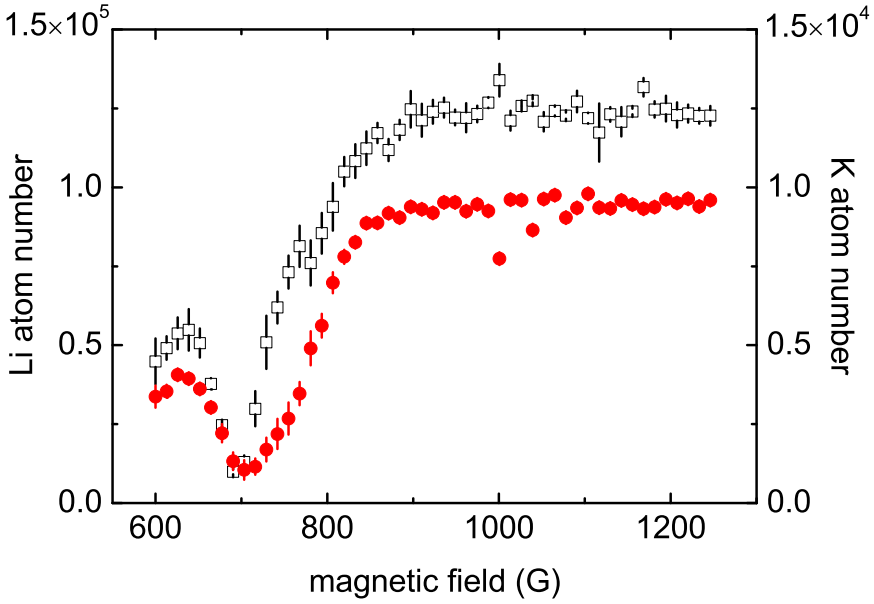

Figure 4.7: Li and K atom numbers after evaporation performed at variable magnetic field. Open squares show the number of Li atoms per state; solid circles show the K atom number.

dimers. Consequently, the combined evaporation and sympathetic cooling process needs to be performed on the BCS side of the Li resonance. For our experiments we choose a field of 1190 G. Here the Li scattering length is $-2900\ a_0$ and the interspecies scattering length is about $+60\ a_0$.

Before starting the evaporation process, we carefully balance the population of the two spin states Li$|1\rangle$ and Li$|2\rangle$. This is particularly important in cases when the spin relaxation stage has caused considerable losses in $|2\rangle$. The spin balance is accomplished by driving the rf transition $|1\rangle \leftrightarrow |2\rangle$ using a series of 20 ramps over 10 kHz with a duration of 50 ms each [Str03]. This procedure is performed at 1190 G, where the Li spin mixture is outside of the strongly interacting regime and interaction-induced rf line shifts are relatively small. Note that the evaporation process is much more sensitive to a spin imbalance on the BCS side of the resonance than on the BEC side of the resonance. The reason is that in the latter case the molecule formation can lead to a self-balancing of the spin population during evaporation [Gri08].

Evaporation of the mixture is performed in the principal ODT, beam 1. The evaporation ramp consists of two stages, technically implemented in different ways. In the first stage, we use a digital input of the laser control unit to reduce the ODT power to about 15 W. This ramp is linear and takes 1.5 s. In a second stage, an acousto-optical modulator (AOM) is used to decrease the power in a nearly exponential ramp. The evaporation ramp is typically stopped after 6 s when the laser power is 60 mW. At this point the trap frequencies in the radial directions are 394 Hz for Li and 219 Hz for K. In the axial direction the trap frequency is dominated by the magnetic confinement and is 27 Hz for Li and 11 Hz for K.

The experimental data in Fig. 4.7 show the number of atoms remaining after the complete evaporation ramp for a magnetic field varied across the full tuning range offered by the

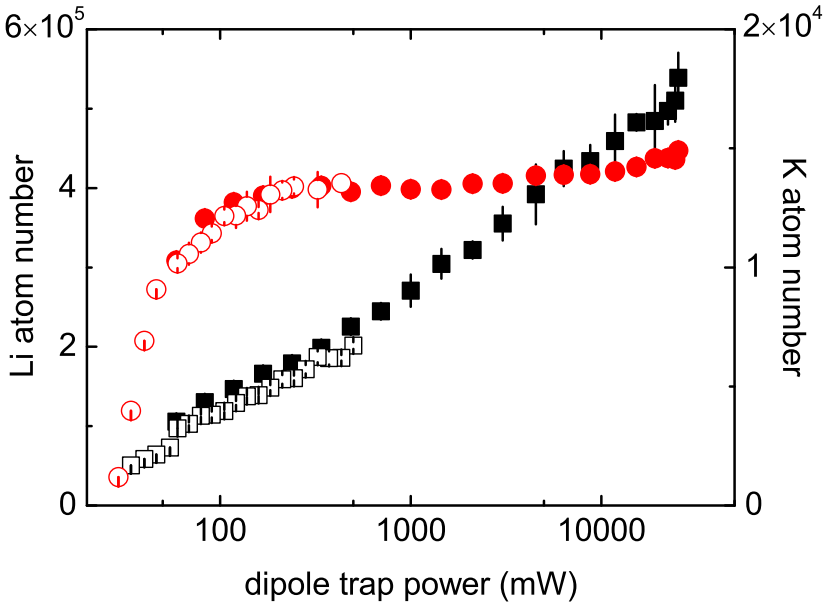

Figure 4.8: Evolution of the atom numbers during the second stage of evaporation. The Li atom number per state is plotted using squares while circles represent the K atom number. Solid (open) symbols represent data from measurements using fluorescence (absorption) imaging.

Li Feshbach resonance. The data correspond to the observations of Ref. [Spi09], showing pronounced loss on the BEC side of the Li Feshbach resonance and large stability on its BCS side. In the high-field region between 950 and 1250 G, where the Li scattering length varies between $-5300\ a_0$ and $-2800\ a_0$, the magnetic field has no significant influence.

In order to analyze the cooling process, we stop the evaporation ramp at a variable endpoint and measure the number of Li and K atoms. The measurements are performed by recapture into the MOT and subsequent detection of the fluorescence intensity or, at lower power, by absorption imaging after release from the ODT into free space. Figure 4.8 shows that the Li atom number steadily decreases while the K cooling proceeds essentially without losses. Note that the trap depth for K is a factor of 2.1 larger than for Li. This changes at about 100 mW, as the gravitational sag of K reduces the trap depth and we begin to see significant loss of K when further lowering the power of the ODT.

Figure 4.9 shows the temperature evolution of Li and K in the last part of the evaporation ramp. We extract the Li temperature by fitting a Thomas-Fermi profile to absorption images of the atomic cloud after time-of-flight. The K temperature is determined using a simple Gaussian fit, as the sample here remains in the nondegenerate regime. Throughout the whole evaporation the temperature of K lags behind the temperature of Li.

At the end of an extended evaporation ramp, at a trap power of 40 mW, the radial trap frequencies for Li (K) amounts to 320 Hz (160 Hz). In the axial direction the trap frequency is dominated by the magnetic confinement and is 27 Hz for Li and 11 Hz for K. The Fermi temperatures are calculated to be $T_F^{\mathrm{Li}} = 390$ nK for Li and $T_F^{\mathrm{K}} = 135$ nK for K. Following the scheme we have presented in Ref. [Spi09], we continue cooling of the mixture by holding it in

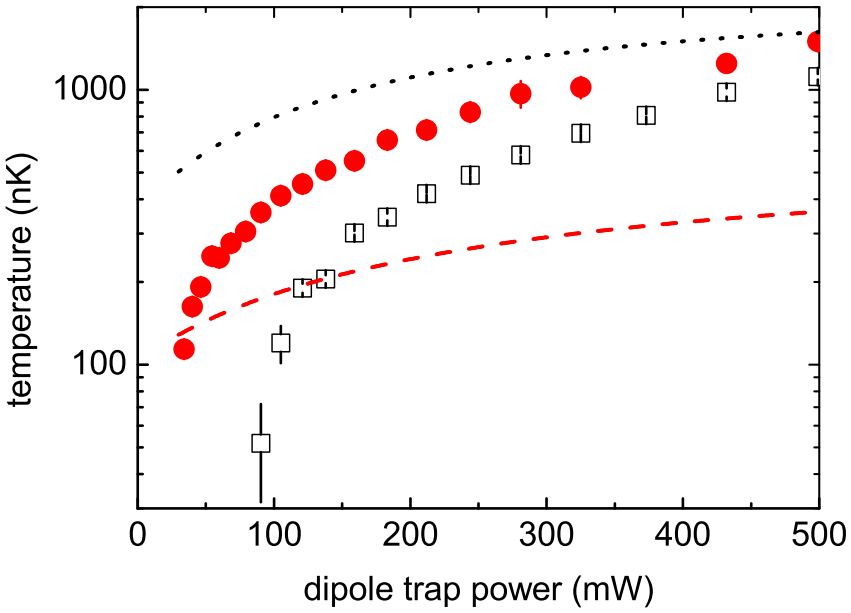

Figure 4.9: Temperature evolution during the last part of the evaporation. Open squares (solid circles) indicate the Li (K) temperature. Also plotted are curves that represent the evolution of the Fermi temperature for Li (dotted line) and K (dashed line).

this shallow trap for 5 s. This way we achieve a final K temperature of 50 nK corresponding to a degeneracy of $T^{\mathrm{K}}/T_F^{\mathrm{K}} \approx 0.6$ while Li is deeply degenerate with $T^{\mathrm{Li}}/T_F^{\mathrm{Li}} < 0.2$.

Since Li is the coolant of our evaporation scheme, we adjust the amount of K with which evaporation starts such that at the end of evaporation we have about 10 times more atoms of Li in each spin state than atoms in K$|1\rangle$. In this situation K can be used as a probe for the Li mixture. One example of this idea has already been presented in Ref. [Spi09]. The measurement of the K temperature was used in order to get a firm upper bound for the temperature of the Li bath even in the strongly interacting regime. This method was recently adopted to using ^{7}Li as a probe in Ref. [Nas10].

4.5 Preparation near interspecies Feshbach resonances

The ^{6}Li-^{40}K mixture offers several s-wave Feshbach resonances in the range between 150 and 200 G [Wil08, Tie10a]. All of them tend to be quite narrow, which is a common situation in cases of moderate values of the background scattering length [Chi10]. The broadest resonances were found for the channels Li$|1\rangle$K$|7...10\rangle$ with widths between 1 and 2 G [Tie09a]. The energetically lowest channel Li$|1\rangle$K$|1\rangle$, which is of particular interest because of the energetic suppression of any two-body decay, features two resonances with calculated widths around 100 mG. In this work, we focus on the resonance near 168 G. We show how a degenerate two-component Li-K mixture can be prepared near this resonance after sympathetic cooling at high magnetic field and present measurements on inelastic and elastic properties of the mixture.

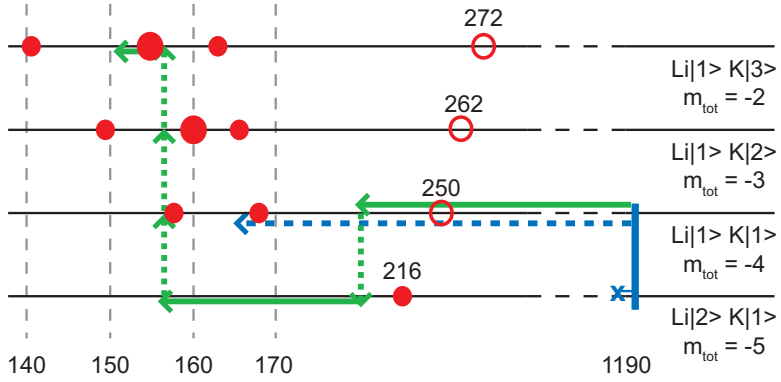

Figure 4.10: Preparation scheme of a two-component mixture near interspecies Feshbach resonances. The horizontal lines indicate four different Li-K spin channels being of particular relevance for our experiments. The numbers give the magnetic field values in Gauss. Solid (open) circles represent s-wave (p-wave) interspecies resonances. The Li$|1\rangle$ and Li$|2\rangle$ intraspecies p-wave resonances (not shown) are located at 160 and 215 G, respectively [Zha04, Sch05], and nearly coincide with interspecies resonances. For the s-wave resonances, the relative widths are indicated by the size of the symbols. State transfer, indicated by vertical dashed lines, is achieved by rf transitions. After the evaporation at 1190 G, the Li$|2\rangle$ population is removed by a resonant laser pulse, as indicated by the **x**.

When ramping down the magnetic field from its evaporation setting (1190 G) to the interspecies resonances, one has to cross the region of the broad 834-G Li$|1\rangle|2\rangle$ Feshbach resonance. If this spin channel is populated, the formation of ^{6}Li dimers inevitably leads to strong losses from the atomic sample. To avoid this problem, we remove one of the Li spin components by the light pressure of a resonant laser pulse [Du08] before starting the ramp. Note that already the momentum kick from one photon is sufficient to push a Li atom out of the shallow trap after evaporation. The pulse is applied for 10 μs with a few times the saturation intensity. We find that at 1190 G the interaction between the two spin components is weak enough to avoid any significant effect on the population in the remaining spin state. In this way, we reduce the three-component Fermi-Fermi gas to a two-component mixture.

To approach a specific interspecies resonance, it is also important to avoid the effect of other inter- and intraspecies resonances. We find that our ramps are fast enough (ramp speed up to 20 G/ms) to cross all the p-wave resonances without any problem. However, we find substantial losses on the interspecies s-wave resonances, even on the weaker ones. This already points to efficient molecule association [Chi10] as we will discuss in Sec. 4.6.

Figure 4.10 illustrates the procedures applied to reach specific interspecies Feshbach resonances. While it is straightforward to reach the 168-G resonance in the Li$|1\rangle$K$|1\rangle$ channel by a fast ramp after removal of the state Li$|2\rangle$, other resonances require more elaborate methods. As an example, we discuss the 155-G resonance in the Li$|1\rangle$K$|3\rangle$ channel, which is of interest as one of the broadest resonances (width between 0.5 and 1 G) in the low-lying spin channels. Here a possible way is to transfer the Li atoms from $|1\rangle$ to $|2\rangle$ after ramping down the field to $\sim$200 G, thus converting the sample into a Li$|2\rangle$K$|1\rangle$ mixture. This can

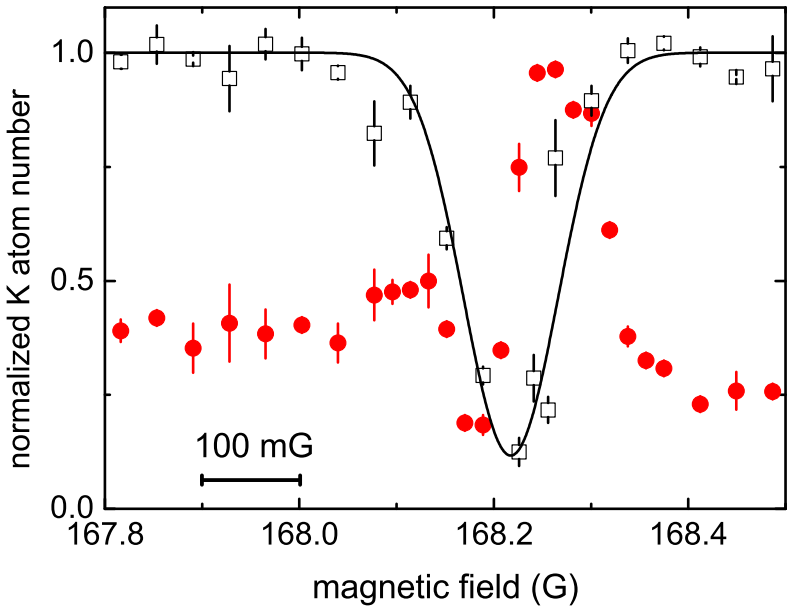

Figure 4.11: Loss measurement and evaporative cooling near an interspecies Feshbach resonance. Plotted is the K atom number normalized to the background value of the loss measurement away from resonance. The open squares show a set of loss measurements holding the sample at variable magnetic field for 5 s. The solid line is a Gaussian fit to the data. The solid circles show a corresponding set of measurements where evaporation was performed by lowering the optical power to one-third of its initial value within 3 s.

be done with very high efficiency using rf transfer methods. Then the ramp is continued down to a value close to 155 G and three subsequent rf transfers are applied to convert the population from Li$|2\rangle$K$|1\rangle$ to Li$|1\rangle$K$|3\rangle$. This procedure avoids all detrimental resonances. Analogous schemes can be applied to reach any other desired resonance.

In a set of experiments performed at the 168-G interspecies Feshbach resonance in the Li$|1\rangle$K$|1\rangle$ channel, we investigate aspects of inelastic and elastic collisions. Initially, we prepare about 2×10^5 Li atoms together with about 1.4×10^4 K atoms at a temperature of about 300 nK. The power of the trapping beam (beam 1) is 170 mW, corresponding to a radial (axial) trap frequency of 660 Hz (14 Hz) for Li. For K the trap frequencies are 375 and 6 Hz, respectively. The peak densities of the clouds are $n_0^{\mathrm{Li}} \approx 2 \times 10^{12}\,\mathrm{cm}^{-3}$ and $n_0^{\mathrm{K}} \approx 4 \times 10^{11}\,\mathrm{cm}^{-3}$ and the degeneracies are $T^{\mathrm{Li}}/T_F^{\mathrm{Li}} \approx 0.3$ and $T^{\mathrm{K}}/T_F^{\mathrm{K}} \approx 1.5$. Note that these conditions are deliberately prepared with an incomplete evaporation ramp, stopped at 170 mW instead of the usual final power of 60 mW (Sec. 4.4).

In the first series of measurements, we ramp the magnetic field to a variable value and study the loss of atoms after a hold time of 5 s. For detection, the remaining atoms are recaptured into the two-species MOT and their fluorescence is recorded. The K atom number, normalized to the background value away from resonance, is plotted in Fig. 4.11 (open squares). We observe a loss feature centered at 168.2 G. Ramping across the Feshbach resonance does not lead to loss, indicating that the phase-space density used in these experiments is insufficient for adiabatic molecule creation during the magnetic field ramp.

In the second series of measurements, we investigate whether an effect of enhanced elastic collisions can be observed in evaporative cooling near the interspecies resonance. Here we lower the power of beam 1 to 55 mW within 3 s, which results in a radial (axial) trap frequency of 375 Hz (14 Hz) for Li and 210 Hz (5 Hz) for K. As before, the number of remaining atoms is determined by recapture into a MOT and fluorescence detection. The corresponding data, plotted in Fig. 4.11 (solid circles), show a pronounced asymmetry and thus a different behavior on the two sides of the Feshbach resonance. On its high-field side, corresponding to large negative scattering length, we observe a maximum in the recaptured atom number at 168.26 G. This signifies evaporative cooling with an enhanced elastic scattering cross section as compared to the background value. At lower fields, however, loss enhanced by the resonance dominates and leads to a minimum in atom number at 168.18 G. The loss properties on the two sides of the Feshbach resonance are thus found to be strikingly different with more favorable conditions on the side of negative scattering length, where no weakly bound molecular state exists.

To determine the resonance position more precisely, we prepare a sample with higher phase-space density than used for the previous sets of experiments. Now both beams of the ODT are used. Beam 2 is held at a constant power of 250 mW, corresponding to a trap depth of 1 μK for Li and 2.1 μK for K. Its purpose is to add confinement along the weak direction of beam 1 at the very end of evaporation. Evaporation at 1190 G and the ramp to low magnetic field proceed as described above. For further cooling, we create a balanced mixture of Li$|1\rangle$ and $|2\rangle$ at 170.5 G, using a sequence of rf sweeps. Afterwards, beam 1 is ramped from a Li trap depth of 1.9–1.5 μK during one second and the sample is left to thermalize for another second. Then Li$|2\rangle$ is removed by a short pulse of resonant light. At this point the sample has a temperature of $\sim$200 nK and contains about 1.3×10^4 K atoms and 8×10^4 Li atoms. With the trap oscillation frequencies of axially 90 Hz (50 Hz), and radially 390 Hz (210 Hz) for Li (K), we calculate Fermi temperatures of about 900 nK for Li and 270 nK for K, corresponding to $T^{\mathrm{Li}}/T_F^{\mathrm{Li}} \approx 0.2$ and $T^{\mathrm{K}}/T_F^{\mathrm{K}} \approx 0.7$. The K cloud has less than half the size of the Li cloud. For both components the density in the center of the trap is about $2 \times 10^{12}\,\mathrm{cm}^{-3}$.

Under these deep cooling conditions, we detect the fast atom loss as a function of the magnetic field. In order to approach the magnetic field value of interest without forming molecules, K is transferred into state $|2\rangle$ by an rf π-pulse prior to the magnetic field ramp. At the final field, K is transferred back to state $|1\rangle$ by another π-pulse. After a hold time of 10 ms, the remaining K atom number is measured. Figure 4.12 shows the corresponding data. We observe maximum loss of atoms centered at 168.217 G, with an estimated calibration uncertainty of 10 mG.

4.6 Creation of ultracold Fermi-Fermi molecules

Here, we describe our basic methodology for molecule creation and detection (Sec. 4.6.1), present experimental results (Sec. 4.6.2), and discuss our findings (Sec. 4.6.3).

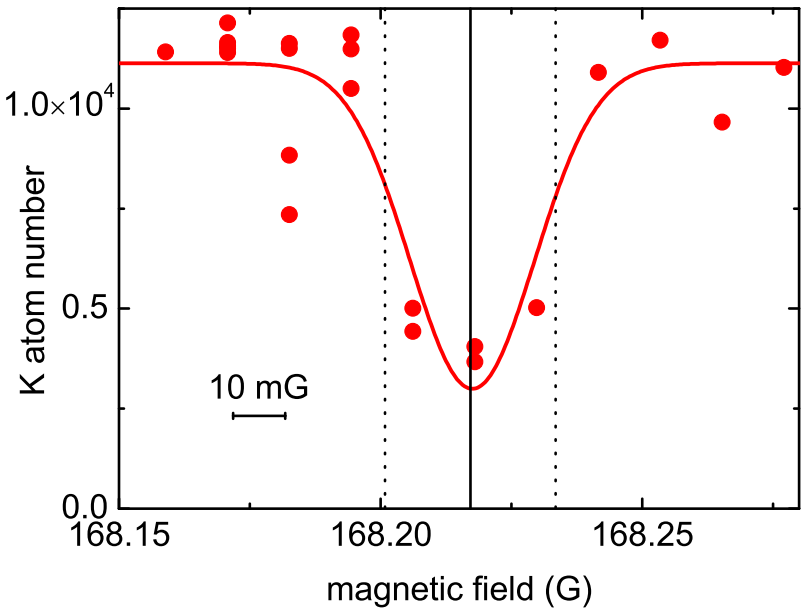

Figure 4.12: Scan of the Li-K Feshbach resonance at 168 G with 10-ms hold time. The $1/e$ width of the loss feature (indicated by the dotted lines) is determined by fitting a Gaussian to the experimental data and amounts to 33 mG.

4.6.1 Creation and detection schemes

The creation of the molecules starts with a Li$|1\rangle$K$|1\rangle$ mixture under the same conditions as prepared for Fig. 4.12. The molecules are associated by a magnetic field ramp from 170.5 G to 168.19 G within 10 ms, crossing the Li$|1\rangle$K$|1\rangle$ 168-G Feshbach resonance (ramp speed 0.23 G/ms). Instantly after the ramp, the sample is released from the ODT.

Selective imaging of molecules and remaining unpaired atoms is possible after transfer of the unpaired atoms to the states Li$|2\rangle$ and K$|2\rangle$. An rf π-pulse, tuned to the atomic $|1\rangle\rightarrow|2\rangle$ transition, is used for this purpose[2]; see Fig. 4.13. Atoms bound in LiK molecules are not transferred to state $|2\rangle$ if the molecular binding energy detunes the transition far enough from the free atom transition to be outside of the Fourier spectrum of the rf pulse. This condition requires a detuning of 23 kHz for K, which is reached 9 mG below resonance according to the relative magnetic moment of the molecular state [Tie09a]. The rf pulses are applied one after the other during the 0.4-ms free expansion of the sample.

State-selective absorption images are taken simultaneously on cycling transitions starting from the Li$|1\rangle$ and K$|1\rangle$ states. This way, molecules are imaged directly. The resulting pictures are shown in the left-hand column of Fig. 4.14[3]. A second pair of images, this time

[2]The rf transition frequencies for Li and K are 39 and 69 MHz, respectively. The π-pulses are approximately rectangular and have a total duration of 43 μs (333 μs) for K (Li). The duration of the Li pulse is much longer than that of the K pulse, because less rf power is available. The full width of the dominant central peak in the Fourier spectrum is 46 kHz for K and 6 kHz for Li. We can achieve transfer efficiencies higher than 99 %.

[3]A slight off-resonant contribution of atoms in the K$|2\rangle$ state is visible on K$|1\rangle$ images. Since this contribution has a much larger spatial extent than the cloud of molecules, it is possible to correct for it

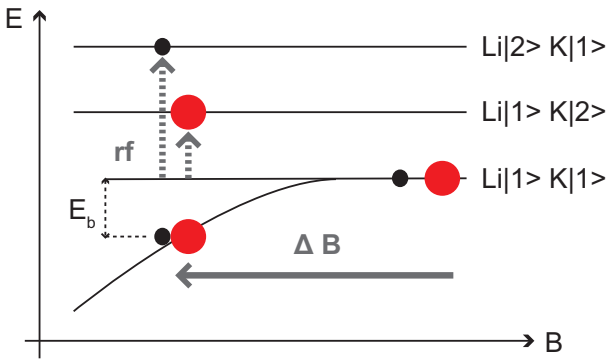

Figure 4.13: Molecules are associated by a magnetic field ramp, indicated by the arrow labeled ΔB, across a Feshbach resonance. Transitions to higher atomic spin states are driven by rf pulses. Atoms bound in a molecule are not affected because of the binding energy E_b.

of the unpaired atoms, which have been transferred to the $|2\rangle$ states, is taken 1 ms later and shown in the right-hand column of Fig. 4.14[4].

Absorption imaging of the molecules gives lower boundaries $\mathcal{N}_{\mathrm{mol}}^{\mathrm{K}}$ and $\mathcal{N}_{\mathrm{mol}}^{\mathrm{Li}}$ for the real molecule numbers $N_{\mathrm{mol}}^{\mathrm{K}}$ and $N_{\mathrm{mol}}^{\mathrm{Li}}$ since the absorption cross section of atoms bound in LiK molecules is somewhat smaller than the one of unpaired atoms [Fer09]. Close to the Feshbach resonance the cross section is similar to the one of free atoms and decreases for increasing binding energy. The number of remaining unpaired atoms $N_{\mathrm{free}}^{\mathrm{K}}$ and $N_{\mathrm{free}}^{\mathrm{Li}}$ can be obtained from the second pair of absorption images.

From K images (top row of Fig. 4.14) we obtain $\mathcal{N}_{\mathrm{mol}}^{\mathrm{K}} = 3 \times 10^3$ and $N_{\mathrm{free}}^{\mathrm{K}} = 9 \times 10^3$ and from Li images (bottom row of Fig. 4.14) $\mathcal{N}_{\mathrm{mol}}^{\mathrm{Li}} = 4 \times 10^3$ and $N_{\mathrm{free}}^{\mathrm{Li}} = 8 \times 10^5$. The small cloud of K is immersed in a much larger degenerate Li bath. The molecule conversion efficiency is therefore best characterized by the K conversion efficiency. A lower bound for the molecule fraction can be determined from K absorption images as $\mathcal{F} = \mathcal{N}_{\mathrm{mol}}^{\mathrm{K}}/(\mathcal{N}_{\mathrm{mol}}^{\mathrm{K}} + N_{\mathrm{free}}^{\mathrm{K}})$. From the images shown in Fig. 4.14 we obtain $\mathcal{F} = 0.25$.

4.6.2 Experimental results

We now examine the molecule creation process and properties of the molecules in more detail. First, we determine the magnetic field value of the onset of molecule creation. For this, we perform experiments as the one just described, but we vary the endpoint of the magnetic field ramp, keeping the ramp duration fixed. The frequency of the rf pulse for the

when extracting data from the image. We also account for unpaired atoms not transferred by the rf pulse by independently measuring the π-pulse transfer efficiency.

[4] ^{6}Li$|2\rangle$ atoms are directly imaged using a probe beam of appropriate frequency. Since we do not have a probe beam with the correct frequency to image K$|2\rangle$ atoms, we first transfer those atoms back to state $|1\rangle$ using another π-pulse and then take the image using the same K$|1\rangle$ probe beam as before. Atoms imaged on the first set of pictures have been accelerated and heated by the probe beam flash and have dispersed enough at the time the second image is taken to not influence it.

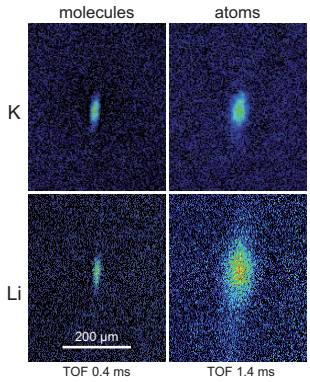

Figure 4.14: Absorption images of LiK Feshbach molecules and unpaired atoms taken at a magnetic field of 168.19 G. The upper row shows images of molecules and atoms taken with light resonant to the K transition whereas the lower row shows images taken with light resonant to the Li transition. The left column shows molecules imaged after 0.4-ms time-of-flight (TOF) expansion and the right column unpaired atoms imaged 1 ms later.

separation of free K atoms and LiK molecules and the probe beam frequencies are adapted accordingly. The Li rf pulse was not used in these experiments.

Figure 4.15 shows the lower bound for the molecule fraction $\mathcal{F}$. Imperfect rf pulses lead to a 3% systematic offset in the data, indicated by the horizontal dashed line[5]. It is found that the detected molecule fraction depends strongly on the endpoint of the magnetic field ramp. No molecules are detected down to a final field of 168.217 G. Only 13 mG lower the maximum molecule fraction is observed. This magnetic field range corresponds well to the required detuning from resonance for our atom-molecule separation method to work, as discussed above. For lower fields the molecular signal drops again, first steeply down to about 168.19 G and then much slower. At about 167.5 G (outside the range of the plotted data) it becomes indiscernible from the background noise. The dependence of the detected molecule fraction on the field may have several reasons. It might be caused by the change in absorption cross section of the molecules with the magnetic field. The slow decrease away from resonance comes from loss of molecules as more time is spent between molecule association and detection.

Within the measurement precision of a few mG the onset of molecule detection coincides with the center of the loss feature from Fig. 4.12, marked by the solid vertical line in Fig. 4.15. This observation is in accordance with the standard picture of molecule formation close to a Feshbach resonance [Köh06].

The maximum K molecule conversion efficiency extracted from this data is reached at 168.204 G and amounts to about 40%. A different method to determine the K molecule conversion efficiency is to examine the number of free K atoms at a magnetic field just above the onset of molecule production and just below 168.19 G. Assuming all missing atoms have

[5]The offset in dependence of the magnetic field originates from imperfect frequency adjustment of the K π-pulse and was determined by experiments during which molecule formation was inhibited by removing Li$|1\rangle$ from the sample with a short flash of resonant light before the molecule association magnetic field ramp. The offset is 1 % at 168.9 G and rises to 10 % 1.5 G away from that position.

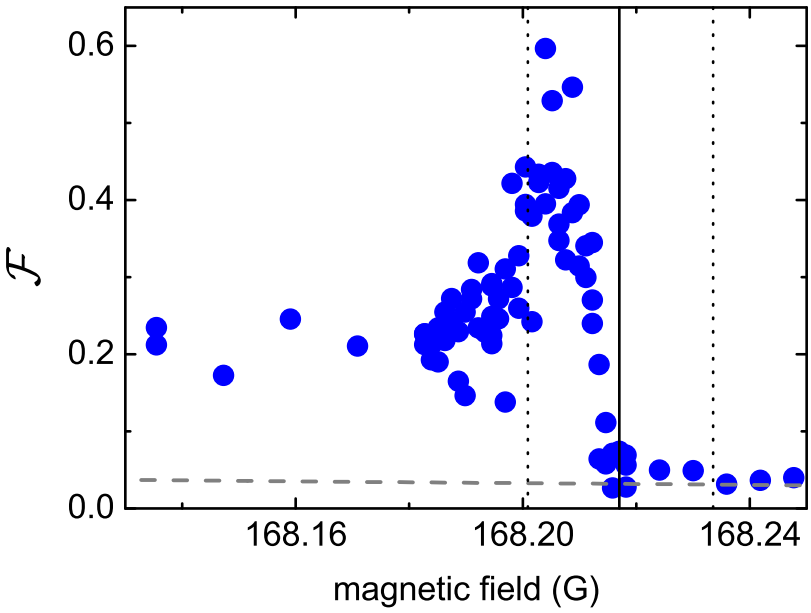

Figure 4.15: Lower bound of molecule fraction $\mathcal{F}$ in dependence of the final magnetic field value of the molecule association magnetic field ramp. Molecules are detected for fields below 168.218 G. This field corresponds to the center of the loss feature shown in Fig. 4.12, which is marked by the vertical solid line here. The dashed vertical lines mark the $1/e$ width of the loss feature and the horizontal dashed line marks a systematic offset.

formed molecules, the molecule conversion efficiency is also determined to be 40%. The assumption that no molecules are lost is well justified since the time spent in the Feshbach resonance region during the magnetic field ramp to 168.19 G (120 μs) is short compared to the lifetime of the molecules.

The lifetime of the LiK molecules is determined by holding the sample after molecule creation for a varying time in the ODT at a constant magnetic field of 168.204 G and measuring the molecule number afterwards. A fit to the decay of the molecule number gives a lifetime of 1.7 ms; see Fig. 4.16. This lifetime does not change if the remaining free Li atoms are removed just after molecule creation by a resonant flash of light, indicating that the dominant loss mechanism does not involve free Li atoms. We did not investigate the effect of unpaired K atoms on the molecule lifetime.

A striking manifestation of molecule formation can be observed by comparing the expansion behavior of clouds of LiK molecules with the one of clouds of unpaired Li atoms in imaging with Li light. For this comparison, we record the expansion of the molecules and the remaining unpaired Li atoms after a molecule association magnetic field ramp to 168.196 G; see Fig. 4.17. We find the average expansion velocity of molecules to be slower by a factor of 3.3, as determined by fits to the expansion. We interpret this difference mainly as a result of the higher mass of the molecules compared to unpaired Li atoms. It corresponds well to the expected velocity ratio of $v_{\mathrm{Li}}/v_{\mathrm{LiK}} = \sqrt{M_{\mathrm{LiK}}/M_{\mathrm{Li}}} = \sqrt{46/6} = 2.8$ in the approximation of thermal clouds of equal temperature. This observation tells us that Li atoms that remain in state $|1\rangle$ after the π-pulse are bound to K atoms.

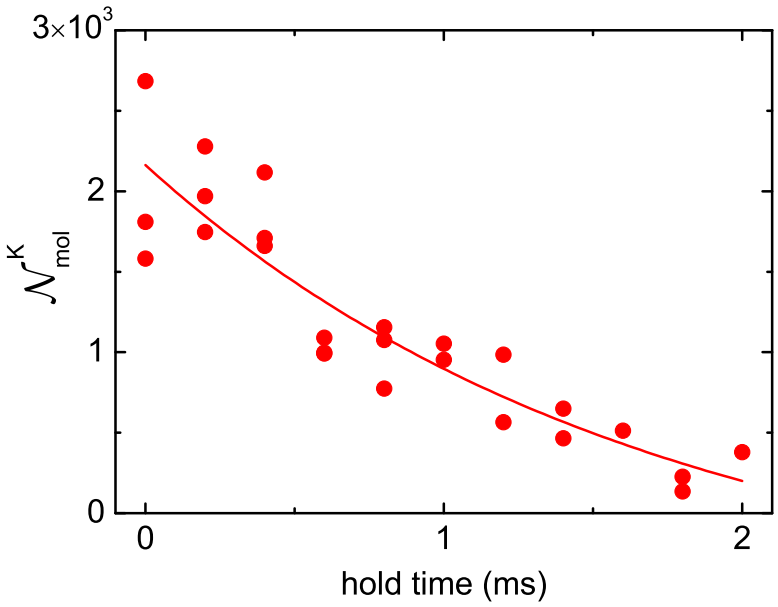

Figure 4.16: Decay of LiK molecules at 168.204 G. Plotted is the number of molecules $\mathcal{N}_{\mathrm{mol}}^{\mathrm{K}}$ in dependence on the hold time after the fast magnetic field ramp. The solid line is an exponential fit to the data, yielding a lifetime of 1.7 ms.

4.6.3 Discussion

In our experiment, molecule association is achieved in basically the same way as demonstrated in many other cold atom experiments before [Chi10, Köh06] and our results agree well with the standard picture of molecule formation close to a Feshbach resonance [Köh06]. We observe that molecule association is most efficient in samples of high phase-space density and obtain a maximum molecular conversion efficiency for K of 40%. This conversion efficiency is typical for experiments employing the Feshbach ramp technique. A Monte Carlo simulation based on the method presented in Ref. [Hod05] agrees with our results, giving a conversion efficiency of about 50% for K.

The lifetime of our molecules is quite short, only 1.7 ms. Because of this, it would be technically challenging to observe the standard signature of molecule association, which is the reduction of the absorption imaging signal when ramping to the molecular side of the Feshbach resonance and the recovery of the signal after ramping back. Our rf state separation detection technique, which allows one to obtain images of molecules less than 0.1 ms after molecule association, overcomes this detection problem.

The Li$|1\rangle$K$|1\rangle$ molecule lifetime that we measure is much shorter than typical lifetimes of Li$|1\rangle$K$|3\rangle$ molecules that were measured by the Munich group [Voi09]. Presently, we do not know whether the different spin channels and therefore the different Feshbach resonances used for molecule association can explain the different lifetimes. There are also other possible, more technical reasons, which we presently cannot rule out. One possibility, which needs further investigation, is the loss of molecules because of the absorption of photons from the

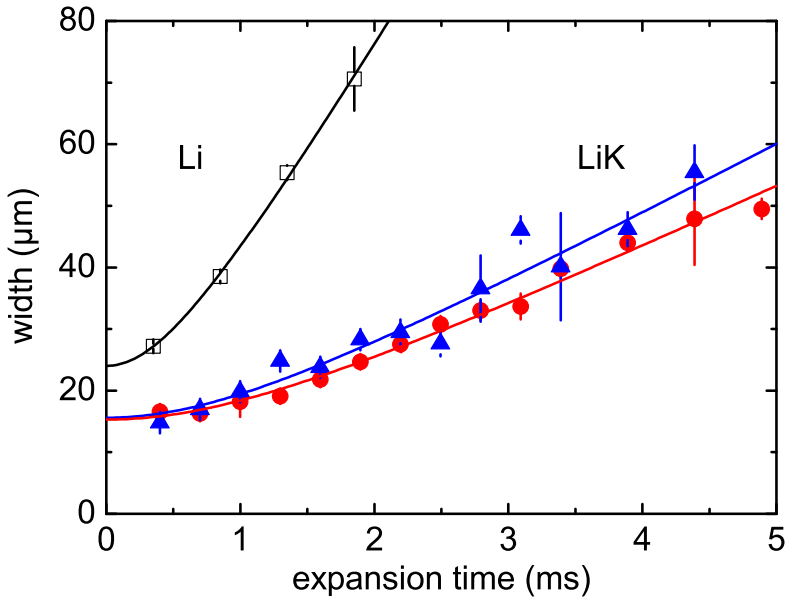

Figure 4.17: Comparison of the free expansion of LiK Feshbach molecules (circles, detection of the bound K atoms; triangles, detection of the bound Li atoms) and unpaired Li atoms (open squares) at 168.196 G. Shown is the radial $1/\sqrt{e}$ width of Gaussian fits to integrated density profiles.

broad spectrum of the multimode fiber laser used for the ODT[6].

4.7 Conclusion and Outlook

We have presented an all-optical evaporative and sympathetic cooling scheme for the preparation of a double degenerate ^{6}Li-^{40}K Fermi-Fermi mixture. We have also shown the general methodology to prepare the sample close to specific interspecies Feshbach resonances. As a first application, we have demonstrated the formation of Fermi-Fermi heteronuclear molecules and we have examined the molecule association process and some properties of the molecules.

With the basic tools at hand, we are now in the position for the next steps toward our main goal of realizing strongly interacting regimes in the Fermi-Fermi mixture. Since the available Feshbach resonances are quite narrow this requires precise knowledge of the exact resonance position and the magnetic-field-dependent elastic and inelastic interaction properties. We are currently inspecting the relatively broad 155-G resonance in the Li$|1\rangle$-K$|3\rangle$ channel as a promising candidate, for which we experimentally find a width of about 800 mG [Nai11]. Strongly interacting conditions generally require a scattering length exceeding the interparticle spacing. Under our typical experimental conditions this would be realized with

[6] A strong influence of broadband laser light on the lifetime of molecules was observed in experiments on cesium Feshbach molecules in Innsbruck. The lifetime substantially increased when the trapping light was provided by a single-frequency infrared laser.

a magnetic detuning below 10 mG, which is experimentally feasible.

Acknowledgments

We thank Paul Julienne for fruitful discussions and support on the theoretical understanding of the interspecies scattering properties, Tobias Tiecke for the calculated Feshbach resonance positions displayed in Fig. 4.6, Christoph Kohstall for useful comments on the manuscript, and Clarice Aiello for contributions to the experimental setup. This work is supported by the Austrian Science Fund (FWF) and the European Science Foundation (ESF) within the EuroQUAM/FerMix project and by the FWF through the SFB FoQuS.

4.8 Appendix: Magnetic field coils

Three pairs of magnetic field coils are present in the setup: a pair of high-current, large-diameter coils, which we call Feshbach coils, a smaller-diameter pair of high-current coils, which we call curvature coils, and a third, low-current, low inductance pair of coils, which we call fast coils. Normally, the currents in all coils circulate in the same direction. To achieve a quadrupole field configuration for MOT operation, the direction of current in one coil of the Feshbach coil pair and one coil of the curvature coil pair can be reversed using mechanical relays. In the normal configuration, the Feshbach coils are in Helmholtz configuration and give a very homogeneous bias field near the trap center of up to 3000 G. The curvature coils exhibit a magnetic field curvature, which gives rise to an additional contribution to the trapping potential [Joc03b]. With the current used during evaporation, the curvature coils give a homogeneous bias field of 600 G and a magnetic field curvature of 27 G/cm^2 along the axial direction of the dipole trap beams (perpendicular to the symmetry axis of the coils). This curvature gives rise to a magnetic confinement corresponding to trap frequencies of 27 Hz for Li and 10 Hz for K. When working at bias fields between 150 G and 170 G, where the interspecies Feshbach resonances are, the curvature coils provide a magnetic confinement corresponding to 13 Hz for Li and 5 Hz for K.

When high magnetic field stability is needed, we make use of a battery-powered current supply. Since the interspecies Feshbach resonances are very narrow, it is necessary to control the magnetic field with very high precision. Passive stabilization methods, not employing any shielding, lead to a stability of about 10 mG peak-to-peak over a 50-Hz cycle. By synchronizing the experimental sequence to line, we achieve a magnetic field stability of a few mG for times on the order of 1 ms, which is much larger than the typical duration of rf π-pulses we use for internal state transfer. Magnetic field values are calibrated using rf transitions.

For probing the interspecies resonances we make use of the fast coils, which have Helmholtz configuration. Using these coils we make precise magnetic field ramps with ramp rates of up to 300 G/s. At these ramp rates eddy currents change the magnetic field by less than 10 mG compared to the steady state value.

Erratum (unpublished)

Because of a calibration error the magnetic field values given in this paper in the vicinity of the 168 G resonance in the $|1\rangle|1\rangle$ channel need to be corrected by -47 mG.

Chapter 5

Publication: Feshbach resonances in the ^{6}Li-^{40}K Fermi-Fermi mixture: Elastic versus inelastic interactions[†]

Eur. Phys. J. D (2011)[a]

D. Naik,[1] A. Trenkwalder,[1] C. Kohstall,[1,2] F.M. Spiegelhalder,[1] M. Zaccanti,[1,3] G. Hendl,[1] F. Schreck,[1] R. Grimm,[1,2] T.M. Hanna,[4] and P.S. Julienne[4]

[1] *Institut für Quantenoptik und Quanteninformation, Österreichische Akademie der Wissenschaften, 6020 Innsbruck, Austria*
[2] *Institut für Experimentalphysik, Universität Innsbruck, 6020 Innsbruck, Austria*
[3] *LENS, Physics Department, University of Florence and INO-CNR, 50019 Sesto Fiorentino, Italy*
[4] *Joint Quantum Institute, NIST and University of Maryland, 100 Bureau Drive, Stop 8423, Gaithersburg MD 20899-8423, USA*

We present a detailed theoretical and experimental study of Feshbach resonances in the ^{6}Li-^{40}K mixture. Particular attention is given to the inelastic scattering properties, which have not been considered before. As an important example, we thoroughly investigate both elastic and inelastic scattering properties of a resonance that occurs near 155 G. Our theoretical predictions based on a coupled channels calculation are found in excellent agreement with the experimental results. We also present theoretical results on the molecular state that underlies the 155 G resonance, in particular concerning its lifetime against spontaneous dissociation. We then present a survey of resonances in the system, fully characterizing the corresponding elastic and inelastic scattering properties. This provides the essential information to identify optimum resonances for applications relying on interaction control in this Fermi-Fermi mixture.

[a] Published online, DOI: 10.1140/epjd/e2010-10591-2

[†] The author contributed equally with D. N. in taking and analyzing the experimental data. The author performed the magnetic field stabilization and field calibration. He solved a major problem on the bus system and improved the imaging setup of ^{6}Li and ^{40}K. He setup the dipole traps together with D. N. and F. Sp. Tom Hanna and Paul Julienne provided the coupled channels calculations and the theory part of the paper. We thank Bo Gao for stimulating discussions.

5.1 Introduction

A new frontier in the research field of strongly interacting Fermi gases [Ing08, Gio08] has been approached by the recent realizations of ultracold Fermi-Fermi mixtures of ^{6}Li and ^{40}K [Tag08, Wil08, Voi09, Spi09, Tie10a, Spi10, Cos10]. Degenerate Fermi-Fermi mixtures represent a starting point to experimentally explore a rich variety of intriguing phenomena, such as many-body quantum phases of fermionic mixtures [Liu03, For05, Paa06, Isk06, Isk07, Pet07, Isk08, Bar08, Bau09, Nis09a, Wan09, Mor09, Gez09, Die10, Baa10] and few-body quantum states [Pet05, Nis09b, Lev09, Nis10].

The possibility to precisely tune the interspecies interaction via Feshbach resonances [Chi10] is an important prerequisite for many experiments. This has motivated theoretical and experimental work on Feshbach resonances in the ^{6}Li-^{40}K mixture [Wil08, Tie09c, Tie10a]. It turned out that all resonances for s-wave scattering in this system are quite narrow, the broadest ones exhibiting a width of $\lesssim 2\,\mathrm{G}$[1], and their character is closed-channel dominated [Chi10]. This causes both practical and fundamental limitations for experimental applications. Interaction control is practically limited by magnetic field uncertainties and, on more fundamental grounds, the universal range [Chi10] near the center of the resonance is quite narrow.

Our work is motivated by identifying the Feshbach resonances in the ^{6}Li-^{40}K system that are best suited for realizing Fermi-Fermi mixtures in the strongly interacting regime. In a previous study [Tie10a], Tiecke *et al.* approached this question by calculating the widths of the different resonances[2], and they studied elastic scattering for one of the widest resonances in the system. Another important criterion is stability against inelastic two-body decay. For the ^{6}Li-^{40}K mixture, inelastic spin-exchange collisions do not occur when at least one of the species is in its lowest spin state [Wil08]. When one of the species is in a higher state, decay is energetically possible, but rather weak as it requires spin-dipole coupling to outgoing higher partial waves. The wider resonances in the ^{6}Li-^{40}K system are found in higher spin channels. This raises the important issue of possible inelastic two-body losses. The question of which is the optimum resonance for a particular application can only be answered if both width and decay are considered.

In this Article, we present a detailed study of Feshbach resonances in the ^{6}Li-^{40}K system, characterizing their influence on both elastic and inelastic scattering properties. In Sec. 5.2 we briefly review a general formalism to describe decaying resonances. In Sec. 5.3 we present a case study of a particularly interesting resonance. In theory and experiment, we investigate its elastic and inelastic scattering properties and the properties of the underlying molecular state. In Sec. 5.4 we present a survey of all resonances, summarizing their essential properties. In Sec. 5.5 we conclude by discussing the consequences of our insights for ongoing experiments towards strongly interacting Fermi-Fermi mixtures.

[1] Here, $\mathrm{G} = 0.1\,\mathrm{mT}$.

[2] Resonance positions and widths have also been calculated by E. Tiemann using a coupled channels approach similar to our theoretical work, private communication.

5.2 Feshbach resonances with decay

A Feshbach resonance results from the coupling of a colliding atom pair to a near-degenerate bound state. If this molecular state can decay into open channels other than that in which the colliding pair is initially prepared, the situation is referred to as a decaying resonance [Chi10]. A formalism for describing such resonances has been developed for optical coupling [Fed96, Boh99], and has also been applied to the magnetically tunable case [Hut07]. A well known example of a decaying resonance exists in the collision of two ^{85}Rb atoms [Rob98], for which molecular lifetimes have been studied [Tho05a, Köh05].

The scattering properties in the zero-energy limit can be expressed through a complex s-wave scattering length, $\tilde{a} = a - ib$, where a and b are real. The relation of these two parameters to the two experimentally relevant quantities, the elastic scattering cross section σ and the loss rate coefficient K_2 for inelastic decay, is for non-identical particles given by

$$\sigma = 4\pi(a^2 + b^2) \tag{5.1}$$

and

$$K_2 = \frac{2h}{\mu} b\,. \tag{5.2}$$

Here, h is Planck's constant and μ is the reduced mass.

The complex scattering length can be parametrized by

$$a(B) = a_{\rm bg} - a_{\rm res}\frac{\gamma_{\rm B}(B - B_0)}{(B - B_0)^2 + (\gamma_{\rm B}/2)^2}\,, \tag{5.3}$$

$$b(B) = 2a_{\rm res}\frac{(\gamma_{\rm B}/2)^2}{(B - B_0)^2 + (\gamma_{\rm B}/2)^2}\,. \tag{5.4}$$

Here, B is the magnetic field strength, the resonance occurs at $B = B_0$, and $a_{\rm bg}$ is the background scattering length. The decay of the "bare" molecular state that causes the resonance is characterized by a rate γ [Köh05], which we conveniently express in magnetic field units, $\gamma_{\rm B} = \hbar\gamma/\delta\mu$, where $\delta\mu$ is the difference in magnetic moment between the entrance channel and the bare molecular state. The resonance length parameter $a_{\rm res}$ is related to the resonance width Δ by

$$a_{\rm res} = \frac{a_{\rm bg}\Delta}{\gamma_{\rm B}}\,, \tag{5.5}$$

and gives the range $a_{\rm bg} \pm a_{\rm res}$ within which the real part of the scattering length can vary, thus providing an indication of the possible control. A common figure of merit for the coherent control of an ultracold gas is the ratio a/b. For $|B - B_0| \gg \gamma_{\rm B}$, and a change in scattering length much larger than $a_{\rm bg}$, this can be shown from Eqs. (5.3) and (5.4) to be

$$\frac{a}{b} \approx -2\frac{(B - B_0)}{\gamma_{\rm B}} \approx 2\frac{a_{\rm res}}{a}\,. \tag{5.6}$$

A larger $a_{\rm res}$ therefore gives better coherent control and lower losses for a given change in scattering length. Combining Eqs. (5.2) and (5.6) gives a simple expression for the loss rate coefficient

$$K_2 \approx \frac{h}{\mu}\frac{a^2}{a_{\rm res}}\,, \tag{5.7}$$

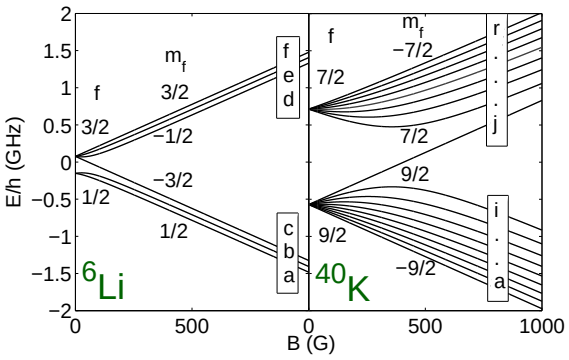

Figure 5.1: Zeeman sub-levels in the electronic ground state of ^{6}Li and ^{40}K, giving the total angular momentum f and its projection m_f along the quantization axis. We label Zeeman states alphabetically in order of increasing energy, as shown.

which shows a general a^2-scaling of two-body loss near a decaying Feshbach resonance.

5.3 Case study of the 155 G resonance

In this Section, we present a thorough study of the 155 G Feshbach resonance, which serves as our main tool for interaction tuning in strongly interacting Fermi-Fermi mixtures. It was first observed in Ref. [Wil08] and used for molecule formation in Ref. [Voi09]. We first (Sec. 5.3.1) present theoretical predictions for the elastic and inelastic scattering properties near this resonance based on coupled channels calculations. We then (Sec. 5.3.2) present our corresponding experimental results, providing a full confirmation of the expected resonance properties. We finally (Sec. 5.3.3) discuss the properties of the molecular state that causes the resonance.

Figure 5.1 shows different magnetic and hyperfine sub-levels of the electronic ground states of ^{6}Li and ^{40}K. Here we follow the notation of Ref. [Chi10] and label the sub-states alphabetically in increasing order of energy. The 155 G resonance occurs in the *ac* channel, i.e. for a ^{6}Li atom in state a colliding with a ^{40}K atom in state c.

5.3.1 Scattering properties: Theory

We have carried out coupled channels studies [Mie96] of the scattering properties in the *ac* $s-$wave channel. The potentials used were taken from Ref. [Tie09c] and, to make this paper self-contained, we have summarized the important parameters in Table 5.1.

The resonance is created by spin-exchange coupling [Chi10] of the colliding pair to a bound state of the same $M_F = m_1 + m_2$. Here $m_{1,2}$ are the projections along the magnetic field quantization axis of the total angular momenta of atoms 1 and 2, $\vec{f}_{1,2}$, and M_F is that of the total spin angular momentum, $\vec{F} = \vec{f}_1 + \vec{f}_2$. We note that f and F are only good quantum numbers at zero magnetic field.

For a pair of atoms in an excited Zeeman channel, there are two processes that can cause

singlet scattering length a_s	$52.61\,a_0$
triplet scattering length a_t	$64.41\,a_0$
vdW coefficient C_6	$2322\,E_h$
vdW length $R_\mathrm{vdW} = \frac{1}{2}(2\mu C_6/\hbar^2)^{1/4}$	$40.8\,a_0$
vdW energy $E_\mathrm{vdW} = \hbar^2/(2\mu R_\mathrm{vdW}^2)$	$h \times 207.6\,\mathrm{MHz}$

Table 5.1: Important parameters of the interaction potentials of ^{6}Li–^{40}K, taken from the potentials of Ref. [Tie09c]. The van der Waals (vdW) parameters describe the long range part of the potential, $-C_6/r^6$, where r is the interparticle distance. Here, $a_0 = 0.529177 \times 10^{-10}\,\mathrm{m}$ is the Bohr radius and $E_h = 4.359744 \times 10^{-18}\,\mathrm{J}$ represents a hartree.

two-body collisional loss. Spin-exchange coupling can lead to inelastic spin relaxation (ISR), in which the colliding pair is coupled into an energetically lower channel of the same M_F and the same partial wave ℓ. Since each resonance considered in this work is in the energetically lowest $s-$wave channel of the relevant M_F, ISR does not occur. Spin dipole coupling [Chi10], however, can couple a colliding pair to channels of a different M_F or ℓ, under the constraints that $M_\mathrm{tot} = M_F + m_\ell$ is conserved, and the change in partial wave is given by $\Delta\ell = \pm 2$. Here, m_ℓ is the projection of $\vec{\ell}$ along the magnetic field quantization axis. For the resonances considered here, spin dipole coupling links s- and d-waves, d- and g-waves, etc., with odd partial waves excluded by symmetry requirements. For the ac channel, the two main decay pathways are the aa and ab $d-$wave channels. Consequently, a basis including all $s-$ and $d-$wave channels with $M_\mathrm{tot} = -2$ is sufficient.

Scattering properties in the vicinity of the 155 G resonance are shown in Fig. 5.2, along with the fit from Eqs. (5.2)-(5.4). The calculation used a collision energy of $k_\mathrm{B} \times 1\,\mathrm{pK}$, while the fit assumes zero temperature. The fit gives excellent agreement, with only small deviations visible outside the core of the resonance, and at the very center, where effects related to finite collision energies become important. The background scattering length near the resonance is $63.0\,a_0$, a suitable value for evaporative cooling, while the resonance width of 0.88 G makes it easily accessible experimentally. The calculation places the center of the resonance at $B_0 = 154.75\,\mathrm{G}$, with an uncertainty on the order of 100 mG resulting from the limited knowledge of the spectroscopically derived potentials.

Suppression of collisional losses is provided by the $k_\mathrm{B} \times 14\,\mathrm{mK}$ height of the d-wave barrier being greater than the Zeeman splitting ($k_\mathrm{B} \times 1.8\,\mathrm{mK}$ for ab, $k_\mathrm{B} \times 3.6\,\mathrm{mK}$ for aa) between the entrance and exit channels. Consequently, decaying pairs must tunnel through the centrifugal barrier. The resulting resonance length is $4.0 \times 10^6\,a_0$. This is comparable to results we have found for much broader, entrance-channel dominated resonances, such as the ee resonance of ^{85}Rb at $B_0 = 155\,\mathrm{G}$, which has $a_\mathrm{res} = 2.5 \times 10^6 a_0$. We note that three-body effects, not included in our calculations, are also of significance for experiments.

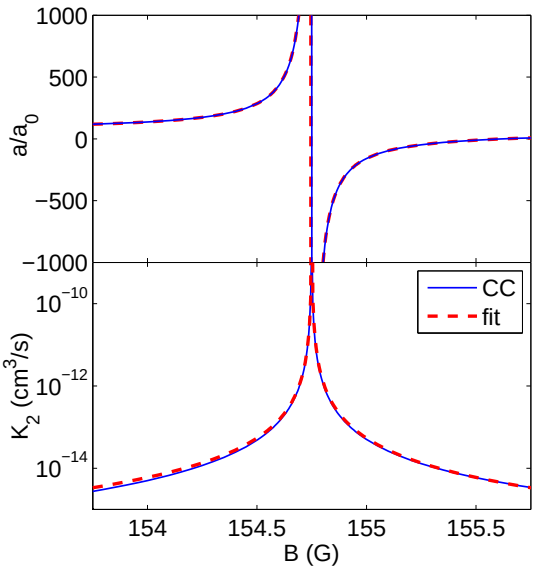

Figure 5.2: *s*-wave scattering properties of the *ac* channel, as a function of magnetic field. A coupled channels calculation (CC, solid line) is compared to a fit using Eqs. (5.2)–(5.4) (dashed line). The top panel shows the real part of the scattering length, while the two-body loss rate coefficient is shown in the lower panel.

5.3.2 Scattering properties: Experiment

Experimental conditions

The basic procedures to prepare the Fermi-Fermi mixture near the 155 G Feshbach resonance are described in Ref. [Spi10]. Here we briefly summarize the main experimental parameters, and mention some issues of particular relevance for the present experiments.

Our optical dipole trapping scheme employs two stages. In the first stage, we use a high-power laser source (200 W fiber laser) to load and evaporatively cool the mixture [Spi09, Spi10]. As the quality of this high-power beam suffers from thermally induced effects such as spatial shifts and thermal lensing effects, we transfer the mixture into a second trapping beam that uses less laser power and is optimized for beam quality. This beam serves as the trapping beam in the second stage where all the measurements are performed. As the laser source we either use a broadband 5 W fiber laser (IPG YLD-5-1064-LP, central wavelength 1065 nm) or a 25 W single-mode laser (ELS VersaDisk 1030-50, central wavelength 1030 nm)[3]. In both cases the trapping potential (Gaussian beam waist 41 μm) is essentially the same, but

[3]Specific product citations are for the purpose of clarification only, and are not an endorsement by the authors, JQI or NIST.

we found that the broadband fiber laser can induce inelastic losses[4]. For our measurements on elastic interactions (Sec. 5.3.2) we used the broadband laser, and we later switched to the single-mode laser for the measurements of inelastic decay (Sec. 5.3.2). At a laser power of 70 mW the trapping frequencies for Li (K) are 13 Hz (4.5 Hz) axially[5] and 365 Hz (210 Hz) radially, and the trap depth is 1.6 μK (3.6 μK).

The mixture contains about 10^5 Li atoms at a temperature $T^{\mathrm{Li}} \approx 140$ nK together with about 2×10^4 K atoms at a temperature $T^{\mathrm{K}} \approx 160$ nK; the temperatures are measured by time-of-flight imaging. Note that the two species are not fully thermalized at this point, such that $T^{\mathrm{K}} > T^{\mathrm{Li}}$. In terms of the corresponding Fermi temperatures $T_F^{\mathrm{Li}} = 490$ nK and $T_F^{\mathrm{K}} = 140$ nK, the temperatures can be expressed as $T^{\mathrm{Li}}/T_F^{\mathrm{Li}} \approx 0.3$ and $T^{\mathrm{K}}/T_F^{\mathrm{K}} \approx 1.1$.

The magnetic field was calibrated by driving RF transitions between the b and the c state of K and using the Breit-Rabi formula[6]. In our set of measurements on the elastic scattering properties (Sec. 5.3.2) the magnetic-field uncertainty was about 20 mG, with a substantial contribution from magnetic field ripples connected with the 50-Hz power line. In the later experiments on inelastic decay (Sec. 5.3.2) we could reduce this uncertainty down to about 5 mG.

Elastic Scattering

Our measurements on elastic scattering are based on the observation of sloshing motion, serving as a simple and sensitive probe for interspecies interactions [Gen01, Mad00a, Fer02, Fer03]. Without interaction both components would oscillate independently with their different sloshing frequencies. The interaction induces friction between the two components and thus leads to damping. In the regime of weak interactions with up to a few scattering events per oscillation period, the damping rate can be assumed to be proportional to the elastic scattering cross section. Note that an alternative approach, based on cross-dimensional relaxation, was followed in Ref. [Cos10].

Here we restrict our attention to the slow axial sloshing motion. We excite this motion by an additional infrared beam intersecting our trapping beam[7]. The magnetic field is quickly ramped to the final setting that is applied in the measurements. After a variable hold time in the trap, we image both clouds to record their damped oscillatory motions. Our data analysis is based on the position of the K cloud, which is completely immersed in the much

[4] When using the fiber laser (bandwidth 0.5 nm) we found inelastic loss near the 155 G Feshbach resonance to be enhanced by roughly a factor of four. We attribute this effect to light-induced collisional decay [Chi10], which we confirmed by measuring its dependence on the intensity of the trapping light. When using the single-mode laser this loss contribution was absent. Consequently, all measurements on inelastic decay were performed with the single-mode laser.

[5] The axial confinement predominantly results from the curvature of the magnetic field.

[6] In the vicinity of the resonance the transition frequency between the b and the c state of ^{40}K can be expressed as $\nu_{\mathrm{RF}} = 38.5756\,\mathrm{MHz} + 195.5\,\mathrm{kHz/G} \times (B - 154.707\,\mathrm{G})$.

[7] The displacement beam is derived from the same laser source as the trapping beam. It has a power of 25 mW and a waist of 60 μm, and it intersects the trapping beam at an angle of 17.5° about 120 μm away from the focus of the trapping beam. By adiabatically turning on the displacement beam we shift the centers of the two trapped species in the axial direction. Then, by suddenly extinguishing the displacement beam, the clouds are released into the unperturbed trap potential and they start their oscillations.

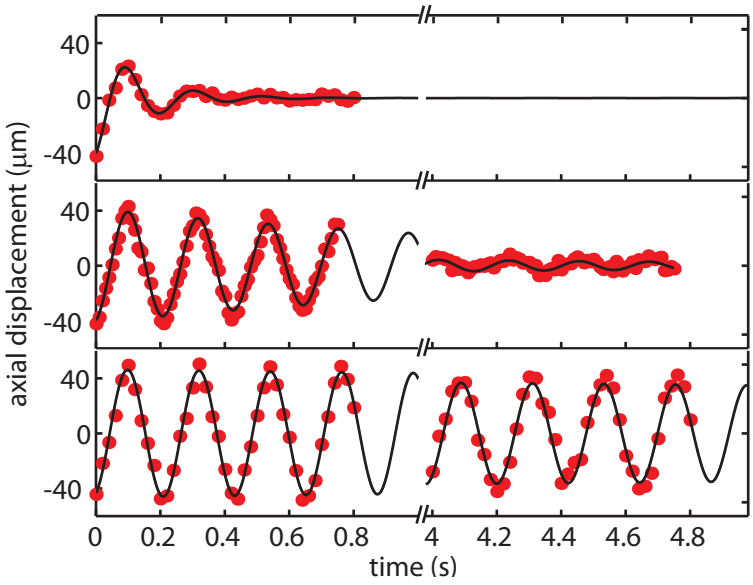

Figure 5.3: Samples of the damped sloshing motion of ^{40}K for three different settings of the magnetic field (upper panel 154.60 G, middle panel 154.96 G, lower panel 155.66 G). The solid circles represent the experimental data, with uncertainties smaller than the size of the symbols. The solid lines are fits under the assumption of a simple damped harmonic oscillation.

larger Li cloud. Its motion is analyzed by fitting a simple damped harmonic oscillation,

$$z(t) = Ae^{-\zeta t}\sin(\omega t + \phi) + z_0\,, \tag{5.8}$$

to the observed axial center-of-mass position. Here A is the oscillation amplitude, ζ represents the damping rate, ω is the oscillation frequency, and z_0 the equilibrium position.

Near the Feshbach resonance, the observed damping strongly depends on the magnetic field, as demonstrated by the three sample oscillations displayed in Fig. 5.3. The measured damping rate as a function of the magnetic field, shown in Fig. 5.4, reflects the characteristic Fano profile of the elastic scattering cross section. The measured rates vary over three orders of magnitude, prominently showing both the pole of the resonance and its zero crossing.

We analyze the observed magnetic-field dependence of the damping under the basic assumption that the rate ζ is proportional to the elastic scattering cross section, which itself is proportional to a^2. Moreover, we take a background damping[8] into account which is independent of the interspecies interaction and express the total magnetic-field dependent damping rate as

$$\zeta(B) = Aa(B)^2 + \zeta_0\,. \tag{5.9}$$

For the scattering length $a(B)$ we use the result of the coupled-channels calculation as presented in Sec. 5.3.1. The theory has an uncertainty in the resonance position of the order

[8]Weak damping of K sloshing with a rate of $\sim$0.04 s^{-1} is also observed when the Li component is absent. We attribute this residual damping to imperfections of the trapping potential such as corrugations and anharmonicities.

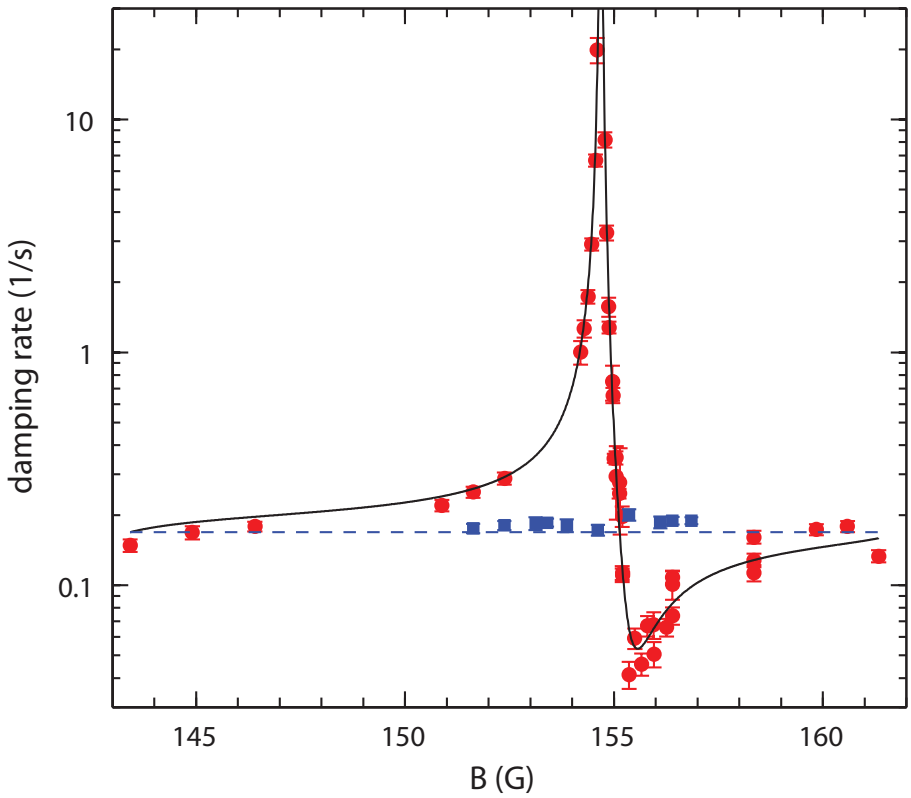

Figure 5.4: Elastic scattering near the 155 G interspecies Feshbach resonance. The measured rates for the ^{40}K sloshing motion are shown (filled red circles) together with a fit based on a coupled-channels calculation of the scattering length (solid black line). For comparison we also plot damping rates measured for the non-resonant *ab* channel (solid blue squares) together with a theoretical line derived from the corresponding non-resonant scattering length (dashed blue line). The error bars shown for the experimental data indicate the fit errors of the damping rate.

of 100 mG, limited by the accuracy of the spectroscopically derived potentials. We therefore allow for a magnetic-field offset by setting

$$a(B) = a_{cc}(B + \delta)\,, \tag{5.10}$$

where $a_{cc}(B)$ refers to the scattering length resulting from the coupled-channels calculation (Sec. 5.3.1) and δ is used as a free parameter. Based on Eqs. (5.9) and (5.10) we fit the experimental damping data with the three free parameters A, ζ_0, and δ.

The fit result, shown by the solid line in Fig. 5.4, shows excellent agreement with the experimental data. For the background damping of the non-interacting mixture, the fit yields $\zeta_0 = 0.0053(3)\,\mathrm{s}^{-1}$, which is consistent with independent measurements on K without Li^8. For the magnetic field offset parameter, the fit yields $\delta = +69(3)\,\mathrm{mG}$. Based on the theoretical results of Sec. 5.3.1 and this shift, we obtain a resonance position of 154.69(2) G with the 20 mG calibration uncertainty being the dominant error source.

The experimental data can also be analyzed independently of the coupled-channels calculations by using the standard Feshbach resonance expression (Eq. (5.3) in the limit $\gamma_\mathrm{B} \to 0$) for a fit in which the width Δ is kept as a free parameter. Our corresponding result $\Delta = 920(50)\,\mathrm{mG}$ is consistent with the prediction $\Delta = 880\,\mathrm{mG}$ resulting from the coupled-channels calculation.

For comparison, we have also investigated elastic scattering in a Li-K mixture in the *ab* channel (solid squares in Fig. 5.4), which near 155 G is weakly interacting. Our measurements show a damping of the sloshing motion that is consistent with the predicted non-resonant scattering length of $68\,a_0$ for this channel (solid line).

Inelastic Scattering

To probe inelastic decay, we first prepare a weakly interacting, long-lived Li-K mixture in the *ab* channel at a variable magnetic field near 155 G. We then apply a short RF π-pulse (duration $90\,\mu$s) to quickly transfer the mixture into the *ac* channel. This transfer method avoids fast magnetic field ramps and thus any waiting time for the magnetic field to be settled to a constant value before measurements can be taken.

Figure 5.5 shows example decay curves. The K loss is essentially exponential, which results from the fact that the K cloud is immersed in a much larger Li sample [Spi09]. In this regime, the Li cloud serves as a large bath with essentially constant density. Here the loss curves do not allow us to distinguish between two-body losses where one K atom interacts with one Li atom and such three-body losses, where one K atom interacts with two Li atoms. Three-body losses resulting from two K atoms interacting with one Li atom would not lead to exponential loss.

We analyze the decay under the hypothesis of dominant two-body loss, which is motivated by the decaying character of the Feshbach resonance as discussed in Sec. 5.3.1. The total K decay rate can be approximated by $\Gamma = K_2\langle n_\mathrm{Li}\rangle + \Gamma_\mathrm{bg}$, where Γ_bg is a small background loss rate[9]. The mean Li number density is given by $\langle n_\mathrm{Li}\rangle$, where the angle brackets denote

[9]The background loss results mainly from rest gas collisions. We use $\Gamma_\mathrm{bg} = 0.009\,\mathrm{s}^{-1}$, which we obtained by analyzing the decay of a pure K sample [Spi09]. Regardless, the influence of this weak loss contribution on our data analysis remains very small.

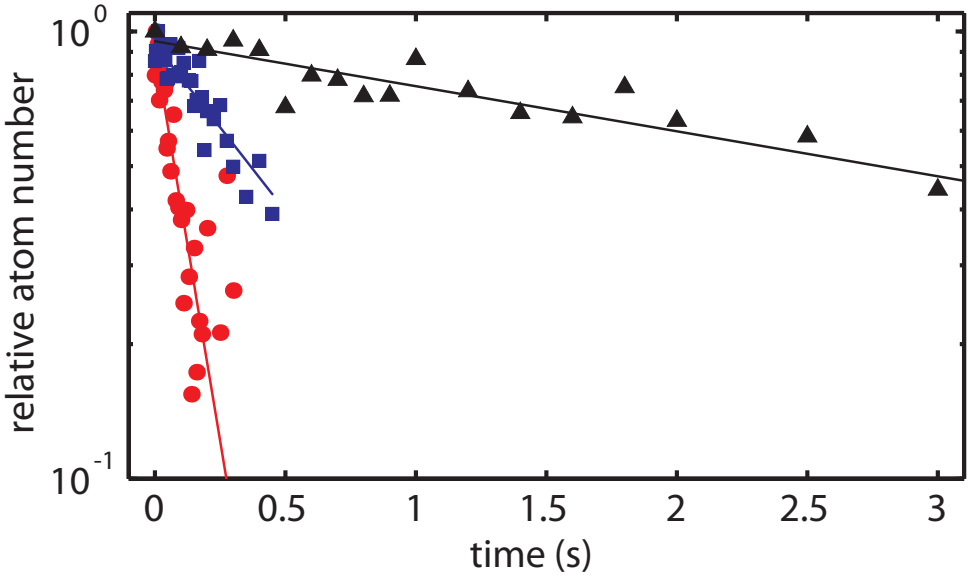

Figure 5.5: Decay of K immersed in the Li cloud for different magnetic fields, far away from resonance at 154.770 G (triangles), very close to resonance at 154.716 G (circles), and for a setting in between at 154.731 G (squares). The scatter of the data indicates the shot-to-shot variations of the measurements. As the lifetimes are plotted on a logarithmic scale, the good linear fits indicate pure exponential decay.

averages weighted by the K density distribution. For our experimental parameters we obtain $\langle n_{\mathrm{Li}} \rangle = 5.9 \times 10^{11}\,\mathrm{cm}^{-3}$, which is about 75 % of the peak density in the center of the Li cloud.

Figure 5.6 shows the measured values for the loss rate coefficient K_2. The data show the expected resonance behavior (Sec. 5.3.1). The values peak at the center of the Feshbach resonance and strongly decrease within a few 10 mG away from the center. For large scattering lengths, the data follow the scaling $K_2 \propto a^2$ according to Eq. (5.7). The observed resonance behavior thus confirms our assumption of the dominant two-body nature of loss. Three-body losses in a two-component Fermi mixture would show a much stronger dependence on a [D'I05], not consistent with this observed behavior. However, significant three-body loss contributions may be present very near to the resonance center.

The figure also shows three theoretical curves, calculated for three different values of the collision energy ($k_{\mathrm{B}} \times 1\,\mathrm{pK}$, representing the zero energy limit, $k_{\mathrm{B}} \times 100\,\mathrm{nK}$, and $k_{\mathrm{B}} \times 300\,\mathrm{nK}$) in a range relevant for our experiments. As a typical value for the collision energy, we can consider an estimate of 200 nK[10]. Very close to the resonance the theory curves illustrate how K_2 increases in the zero temperature limit up to a value corresponding to $b = 2a_{\mathrm{res}}$. In the case of non-zero collision energies it is limited to lower values. For magnetic detunings exceeding about 20 mG, the effect of the finite collision energies can be neglected in the interpretation of the experimental data, which makes the comparison between theory and

[10]The main contribution to the mean collision energy in our trapped sample stems from the kinetic energy of the degenerate Li component. In the trap center, where the K cloud overlaps with the Li, the mean kinetic energy of the Li atoms is given by $(3/10)T_F^{\mathrm{Li}} \approx 200\,\mathrm{nK}$.

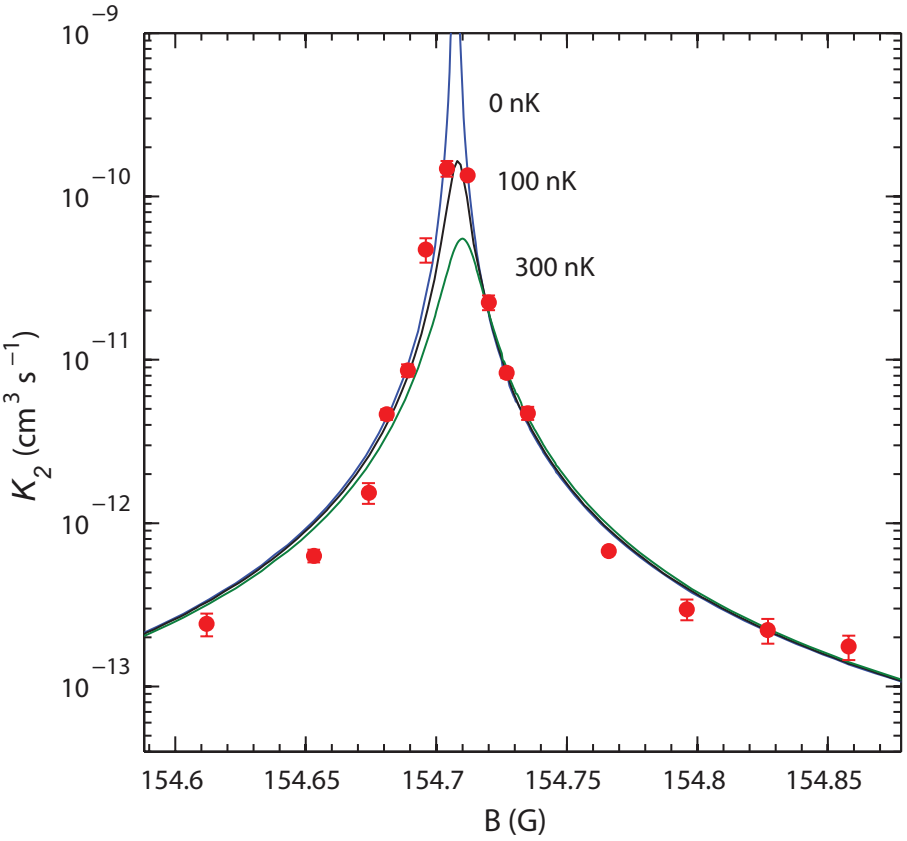

Figure 5.6: Inelastic loss near the 155 G interspecies Feshbach resonance. The measured values for the two-body loss rate coefficient K_2 (solid circles) are compared with theory. The three theoretical curves (solid lines) represent three different collision energies E/k_B (1 pK, labelled 0 to indicate the zero energy limit, 100 nK, and 300 nK), showing the limiting effect of finite collision energy. The error bars represent the statistical errors from fitting the loss curves.

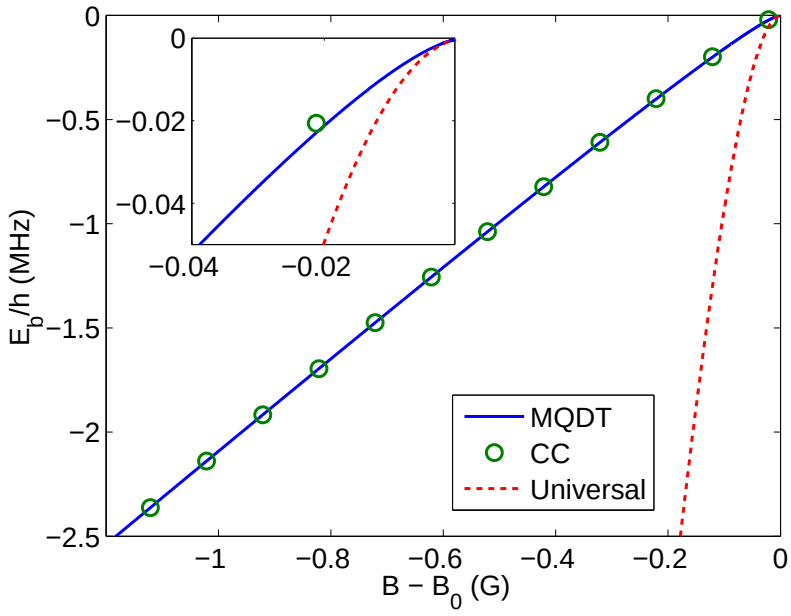

Figure 5.7: Molecular binding energy as a function of magnetic field. MQDT (blue line) refers to the three-parameter model of Ref. [Han09], while CC (green points) indicates a coupled channels calculation. Sufficiently close to the resonance the binding energy converges to the universal result of Eq. (5.11) (red dashed line).

experiment straightforward. Here we find excellent quantitative agreement, confirming two-body decay as the dominant loss mechanism. Very close to the center of the resonance the situation is more complicated. If one completely attributes loss to two-body decay, the 100 nK curve provides an excellent fit to the experimental data. This, however, is somewhat below our estimate of 200 nK for an effective collision energy, which may point to additional three-body losses at the very center of the resonance.

To extract the precise resonance position we proceed in an analogous way as for analyzing the elastic scattering data, allowing for a small magnetic field shift δ between theory and experiment. We write the actual loss coefficient as $K_2(B) = K_{2,cc}(B + \delta)$, where $K_{2,cc}$ refers to the coupled-channels result for K_2 as discussed in Sec. 5.3.1. In the fit, we exclude the three experimental data points that exceed $3 \times 10^{-11}\,\mathrm{cm}^3/s$ to avoid the region where finite collision energies become important. This also makes sure that the loss data are dominated by two-body decay. The shift δ is the only free parameter, and we obtain a small value of $\delta = +38(1)\,\mathrm{mG}$, well in the range of the theoretical uncertainty. We finally obtain a resonance position of $B_0 = 154.707(5)\,\mathrm{G}$, where the main uncertainty results from the magnetic field calibration. Within the experimental uncertainties this value is consistent with the less precise resonance position obtained from elastic scattering measurements.

5.3.3 Bound state properties

In the context of Feshbach molecules, universality refers to the range of magnetic fields sufficiently close to resonance within which the molecular and scattering properties can be

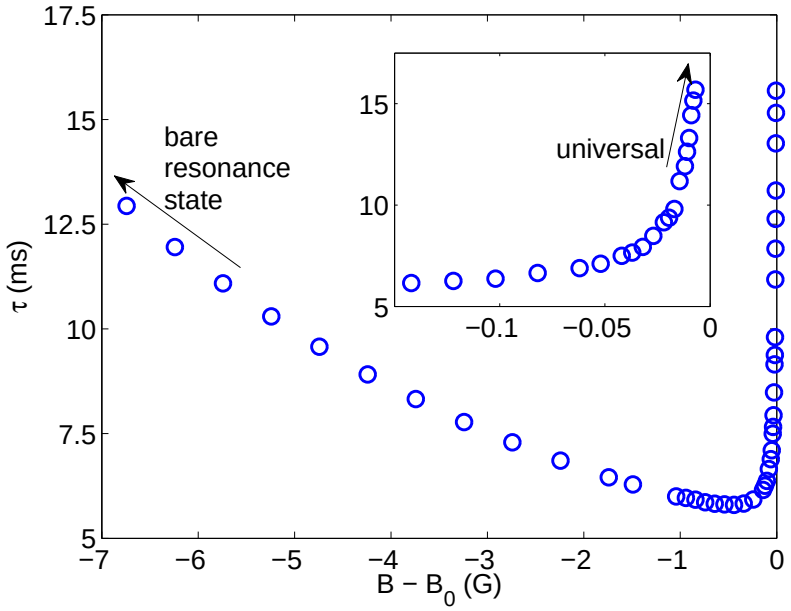

Figure 5.8: Calculated molecular lifetime as a function of magnetic field. The molecular lifetime varies at lower field according to its tunnelling rate through the d-wave centrifugal barrier into the exit channels. The arrows indicate the sharp increase in lifetime as the universal regime is entered, and the region away from resonance where the molecular lifetime converges to that of the bare resonance state.

described solely by the atomic masses and the scattering length $a(B)$. Within this region, the molecule has the form of a halo state, in which a significant part of the wavefunction lies beyond the classically allowed outer turning point of the potential. This results in a strong enhancement of the lifetime of a decaying bound state [Tho05a, Köh05]. The universal binding energy is given by

$$E_{\mathrm{B}} = \frac{\hbar^2}{2\mu a(B)^2}\,. \tag{5.11}$$

Calculations of the relevant bound state energy using the coupled channels method and the simplified three-parameter model of Ref. [Han09] are shown in Fig. 5.7. We note that the three-parameter model, while useful for bound state and resonance characterisation, does not couple partial waves and so can not be used for calculating decay properties in the present case. The energy variation is linear for binding energies greater than a few tens of kHz, having a relative magnetic moment of $\delta\mu/h = 2.3\,\mathrm{MHz/G}$ with respect to the ac threshold. The universal region, as can be seen from the inset of Fig. 5.7, covers a magnetic field range of order mG. This makes it hard to access experimentally. The universal region is wider for broad, entrance channel dominated resonances [Chi10]. However, in the present case, the suppression of decay by the centrifugal barrier allows the molecules to have a long lifetime in the nonuniversal regime.

We now consider the lifetime of ^{6}Li-^{40}K molecules close to the ac resonance at 155 G. Outside the very narrow universal region, the analytic approach of Ref. [Köh05] does not apply. We therefore derive the molecular lifetime from a coupled channels scattering calculation

including the two open d-wave channels into which it decays. The spin-dipole induced decay discussed in the previous section is mediated by the bound state causing the resonance. For collisions at an energy E near the energy E_b of this bound state, the off-diagonal $|T_{12}(E)|^2$ matrix element for the transition probability from one decay channel to the other follows the standard form [Mot65]

$$|T_{12}(E)|^2 = \frac{\hbar^2\gamma_1\gamma_2}{(E-E_\mathrm{b})^2 + \frac{\hbar^2}{4}\Gamma^2}\,. \tag{5.12}$$

Here, γ_1 and γ_2 are the decay rate of the molecule into the ab and aa channels, respectively. The total decay rate is given by $\Gamma = (\gamma_1+\gamma_2)$, and the molecular lifetime by $\tau = 1/\Gamma$. Fitting our calculated $|T_{12}(E)|^2$ to the form of Eq. (5.12) determines the magnitude of Γ for a given B. This calculation includes the entrance channel component and so reproduces the increase in lifetime as the Feshbach molecule takes on a halo form. This should be distinguished from the decay rate of the bare resonance state which appears in Eqs. (5.3) and (5.4).

Our calculated lifetimes are shown in Fig. 5.8. As discussed above, a sharp increase in lifetime occurs as the universal region near B_0 is approached. Above the maximum lifetime shown in the Fig. 5.8, the decay peak described by Eq. (5.12) narrows to the point where we can no longer resolve it in our calculations. The slower increase as B is moved away from B_0 occurs because the bound state moves further behind the centrifugal barrier. Decay from tunnelling through the barrier is then further suppressed. The lifetime of molecules in the vicinity of the 155 G resonance was measured by Voigt *et al.* [Voi09]. They observed a sharp increase in lifetime near the resonance, with which our results qualitatively agree. Their measured background lifetime of ~ 3 ms away from resonance is lower than our calculated minimum of 6 ms. However, our calculations do not include relevant atom-dimer and dimer-dimer collisions, and so may be considered as an upper bound to experimentally observable lifetimes. A lifetime of several ms will permit measurements and manipulation of the Feshbach molecules.

5.4 Survey of resonances

In this section we discuss resonances occurring in various channels of the ^{6}Li-^{40}K mixture. We focus on channels with ^{6}Li in the a state and ^{40}K in the lower ($f = 9/2$) manifold, for which inelastic spin-exchange collisions do not occur. At zero magnetic field, there are three bound states of $F = 4$, 5 and 6 in the range 200 MHz to 300 MHz below these thresholds, as shown in Fig. 5.9. At nonzero magnetic field, these states are projected into their Zeeman sublevels, which give rise to Feshbach resonances when degenerate with the collision threshold of a channel of the same M_tot. Consequently, three proximate resonances are found in channels of $-3 \leq M_\mathrm{tot} \leq 4$. The bound state underlying each resonance adiabatically correlates with one of the zero field F states. We note that the bound state energies shown in Fig. 5.9 were produced with the three-parameter model of Ref. [Han09], which produces slightly different resonance locations to the coupled channels calculations that follow.

We have performed a coupled channels analysis of each resonance, analogous to that performed with the asymptotic bound state model in Ref. [Tie10a]. With our more rigorous

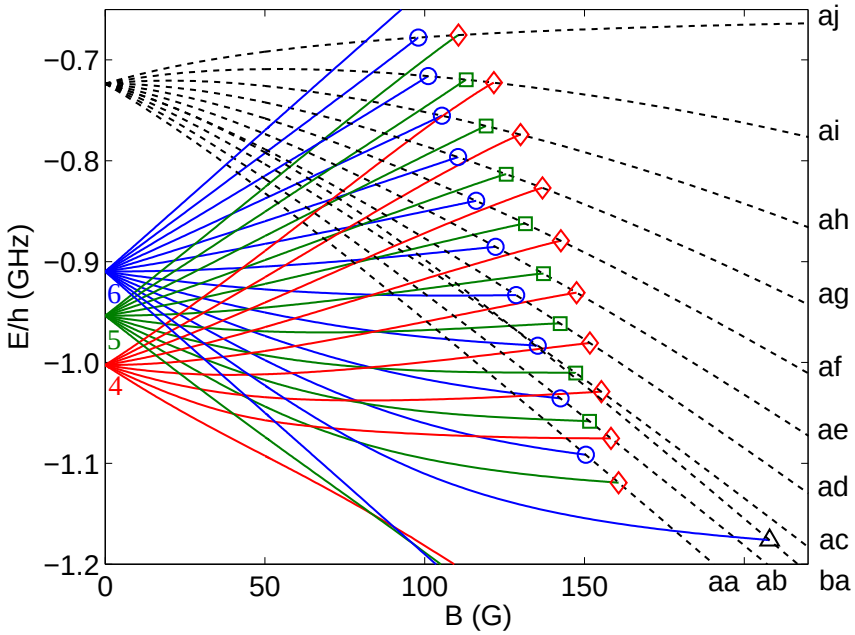

Figure 5.9: Energies of the bound states underlying the resonances studied in this paper, as a function of magnetic field. Collision thresholds of relevant channels are shown as dotted lines, labelled at the right of the figure. The resonances arise from three zero-field bound states of $F = 4, 5$ and 6 (labelled at the left of the figure), which are projected into channels of $|M_{\mathrm{tot}}| \leq F$ at non-zero field. Deeper bound states are not shown for reasons of clarity. Avoided crossings between bound states of the same M_{tot} give rise to three identifiable groups of resonances, indicated by the same symbols used in Fig. 5.10 and Table 5.2. Within each group, resonance parameters vary smoothly (see Fig. 5.10 and text).

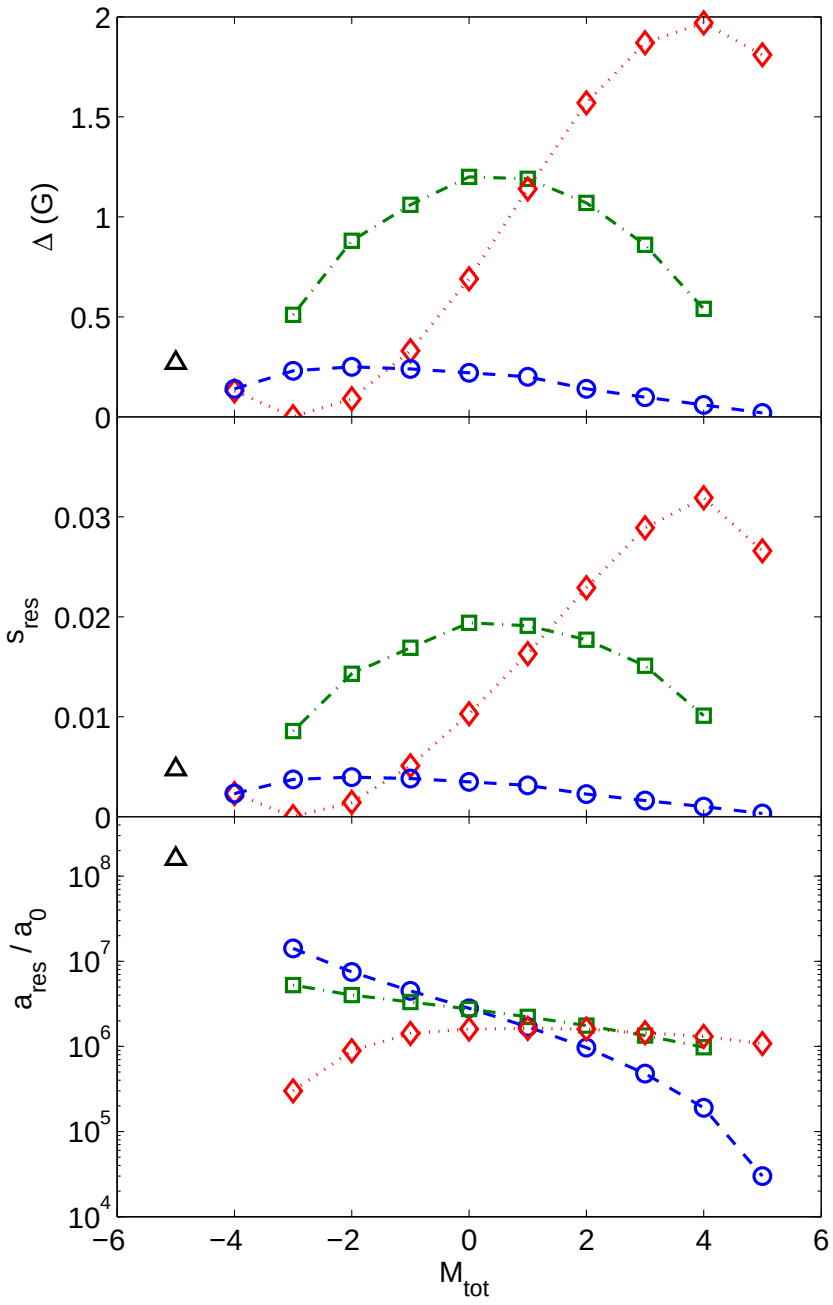

Figure 5.10: Theoretical survey of ^{6}Li–^{40}K s-wave resonances. Each panel shows a resonance parameter as a function of $M_{\rm tot}$: the width Δ (top), strength $s_{\rm res}$ (middle), and length $a_{\rm res}$ (bottom). The ^{6}Li atom is in the a state, except for $M_{\rm tot} = -5$ for which it is in b. The ^{40}K atom is in the lowest Zeeman state producing the relevant $M_{\rm tot}$. The symbols, also used in Fig. 5.9 and Table 5.2, correspond to the resonance groups discussed in the text.

			Experiment			Coupled channels						
Channel	M_{tot}	Group	B_0 (G)	Δ (G)	Ref.	B_0 (G)	Δ (G)	a_{bg}/a_0	$\delta\mu/h$ (MHz/G)	a_{res} ($10^6\,a_0$)	s_{res}	γ_B (μG)
ba	-5	△	215.6		[Wil08]	215.52	0.27	64.3	2.4	160	0.0048	0.11
aa	-4	○	157.6		[Wil08]	157.50	0.14	65.0	2.3		0.0023	0
		◊	168.170(10)		[Spi10]	168.04	0.13	63.4	2.5		0.0023	0
ab	-3	○	149.2		[Wil08]	149.18	0.23	67.0	2.1	14	0.0037	1.1
		□	159.5		[Wil08]	159.60	0.51	62.5	2.4	5.3	0.0086	6.1
		◊	165.9		[Wil08]	165.928	2×10^{-4}	58	2.5	0.3	3.3×10^{-6}	0.04
ac	-2	○	141.7		[Wil08]	141.46	0.25	67.6	2.1	7.5	0.0040	2.3
		□	154.707(5)	0.92(5)	this work	154.75	0.88	63.0	2.3	4.0	0.014	14
		◊	162.7		[Wil08]	162.89	0.09	56.4	2.5	0.89	0.0014	5.7
ad	-1	○				134.08	0.24	68.7	2.0	4.5	0.0038	3.7
		□				149.40	1.06	63.8	2.2	3.3	0.017	20
		◊				159.20	0.33	55.8	2.45	1.4	0.0051	13
ae	0	○				127.01	0.22	68.5	2.05	2.8	0.0035	5.4
		□				143.55	1.20	65.7	2.2	2.8	0.020	29
		◊				154.81	0.69	55.1	2.4	1.6	0.010	24
af	1	○				120.33	0.20	66.8	2.1	1.7	0.0031	7.9
		□				137.23	1.19	65.3	2.2	2.2	0.019	35
		◊				149.59	1.14	53.6	2.4	1.6	0.016	37
ag	2	○				114.18	0.14	67.4	2.1	0.97	0.0023	9.7
		□				130.49	1.07	66.4	2.2	1.8	0.018	40
		◊				143.39	1.57	54.4	2.4	1.6	0.023	53
ah	3	○				108.67	0.098	66.6	2.2	0.48	0.0016	14
		□				123.45	0.86	68.4	2.3	1.3	0.015	44
		◊				135.90	1.87	55.9	2.45	1.5	0.029	72
ai	4	○				104.08	0.06	65.9	2.25	0.19	0.0010	21
		□				116.38	0.54	68.6	2.4	0.98	0.010	38
		◊				126.62	1.97	54.7	2.6	1.3	0.032	83
aj	5	○				100.90	0.02	64.3	2.3	0.03	3.2×10^{-4}	43
		◊	114.47(5)	1.5(5)	[Tie10a]	114.78	1.81	57.3	2.3	1.08	0.027	96

Table 5.2: Survey of s-wave resonances in ^{6}Li-^{40}K. The first two columns give the channel $\alpha\beta$ and total angular momentum projection M_{tot}, with α and β representing the Zeeman state of Li and K, respectively. The third column gives the symbol for the corresponding group of resonances that is used in Figs. 5.9 and 5.10. The next three columns give experimental values of the resonance location B_0 and width Δ, where available, with references. The remaining columns give the results of the coupled channels calculations performed for the current work - B_0 and Δ, as well as the background scattering length a_{bg}, relative magnetic moment $\delta\mu$, resonance length a_{res}, resonance strength s_{res}, and decay rate in magnetic field units, γ_B. Note that a_{res} is not defined for the stable *aa* channel. Note also that the experimental values for B_0 from Ref. [Wil08] are subject to typical uncertainties of about 0.5 G.

approach[2], we obtain good agreement with all experimental data, including the new set of measurements on the 155 G resonance presented in Sec. 5.3.2. The simplified approach of Ref. [Tie10a] seems to underestimate the widths of the resonances by almost a factor of two. With the coupled channels approach, we can also study the decay properties of the resonances. The resonance parameters are shown in Fig. 5.10, and tabulated in Table 5.2. We group the resonances of each channel that are lowest (◯), middle (□) and highest (◊) in B_0, using the indicated symbols to distinguish the resonance groups in Figs. 5.9 and 5.10, and Table 5.2. Within each of these groups, resonance properties vary smoothly as a function of M_{tot}. The resonances with $M_{\mathrm{tot}} = -4$ and 5 have properties consistent with the lowest and highest group, while the *ba* resonance with $M_{\mathrm{tot}} = -5$ has substantially different properties. This is due to F being a good quantum number only at zero magnetic field, and several bound states having avoided crossings in the relevant range of magnetic field. There are several resonances with $\Delta \gtrsim 1\,\mathrm{G}$, offering good opportunities for control of collisional properties. However, several other factors are also useful for deciding the suitability of a resonance for a given application.

One parameter used for quantifying the extent to which a resonance is entrance-channel dominated is the resonance strength parameter [Chi10], defined by

$$s_{\mathrm{res}} = \frac{a_{\mathrm{bg}}}{\bar{a}} \frac{\delta\mu\Delta}{\bar{E}} \,. \tag{5.13}$$

Here, $\bar{a} = [4\pi/\Gamma(1/4)^2]R_{\mathrm{vdw}} \approx 0.956 R_{\mathrm{vdW}}$ is the mean scattering length [Gri93], and $\bar{E} = \hbar^2/(2\mu\bar{a}^2) \approx 1.094 E_{\mathrm{vdW}}$ is the associated energy. If $s_{\mathrm{res}} \geq 1$, the bound state and near-threshold scattering states are concentrated in the entrance channel over a magnetic field range comparable to Δ. In the present case, all resonances are closed-channel dominated, as shown in the middle panel of Fig. 5.10. The background scattering lengths of the resonances are all in the range $55\,a_0$ to $70\,a_0$, and the relative magnetic moments are in the range 2 MHz/G to 2.6 MHz/G. Consequently, the resonance strength follows trends similar to the resonance widths. For the *ac* 155 G resonance we have $s_{\mathrm{res}} = 0.014$. This is reflected in the universal region being only a few mG wide, as discussed above.

Calculated resonance lengths are shown in the lower panel of Fig. 5.10. The range in a_{res} is approximately 3 orders of magnitude, with better stability in channels of lower M_{tot}. This occurs because the energy gaps between higher channels are larger, reducing the height of the centrifugal barrier through which the decaying atoms tunnel. However, all the resonance lengths are sufficiently high that we expect each resonance with $\Delta \gtrsim 1\,\mathrm{G}$ to be very useful.

In view of interaction control in a strongly interacting gas, we now discuss three selected resonances that have received particular attention in experiments: the 168 G resonance in the *aa* channel [Spi10], the 155 G resonance in the *ac* channel [Voi09] (see Sec. 5.3), and the 114 G resonance in the *aj* channel [Tie10a]. In practice, the possible degree of control is limited by uncertainties (drifts and fluctuations) of the magnetic field. A corresponding figure of merit is the maximum controllable scattering length $a_{\mathrm{ctrl}} = a_{\mathrm{bg}}\Delta/\delta_B$, where δ_B stands for the magnetic field uncertainty. Assuming a realistic value of $\delta_B = 5\,\mathrm{mG}$ one obtains $a_{\mathrm{ctrl}} \approx 1600\,a_0$, $11\,000\,a_0$, and $21\,000\,a_0$ for the three resonances considered (168 G, 155 G, and 114 G, respectively). On one hand, this can be compared with the typical requirement of $|a| \gtrsim 5000\,a_0$ for attaining strongly interacting conditions. On the other hand, it can be

compared with the condition for universal behavior $|a| \gg \bar{a}/s_{\mathrm{res}}$[11], which requires $a_{\mathrm{ctrl}} \gg 17\,000\,a_0$, $2800\,a_0$, and $1450\,a_0$. This shows that the resonance at 168 G is too narrow for controlling a strongly interacting Fermi-Fermi mixture, but the other resonances at 155 G and 114 G are broad enough. Although the 114 G resonance is wider than the 155 G resonance by a factor of 2.1, inelastic loss is 3.7 times faster. The higher collisional stability is an important advantage of the 155 G resonance.

5.5 Conclusions

We have characterized elastic and inelastic scattering near Feshbach resonances in the ^{6}Li-^{40}K mixtures. The presence of open decay channels for all broader resonances has two important consequences. Atomic two-body collisions acquire a resonantly enhanced inelastic component, which unavoidably limits the stability of an atomic Fermi-Fermi mixture with resonantly tuned interactions. When Feshbach molecules are created via these decaying resonances, they will undergo spontaneous dissociation.

The intrinsic decay has important consequences for present experiments towards strongly interacting Fermi-Fermi mixtures. Under typical experimental conditions, the lifetime of a Fermi-Fermi mixture with resonantly tuned interactions ($a \to \pm\infty$) will be limited to $\sim$10 ms. This in general means a limitation of possible experiments to short time scales, such as the observation of the expansion of the mixture after trap release [O'H02, Bou03] or measurements of fast collective oscillation modes [Kin04a, Bar04a, Alt07a]. Experiments that require long time scales, such as precise studies of equilibrium states [Zwi06a, Nas10], may be problematic in this decaying mixture.

The short lifetime of the Feshbach molecules, also being of the order of 10 ms, excludes the production of a long-lived molecular Bose-Einstein condensate (mBEC) such as formed in ^{6}Li [Joc03b, Zwi03]. Transient ways to form mBECs, as demonstrated for ^{40}K [Gre03], will still be possible. The detection of fermionic condensates by rapid conversion of many-body pairs into molecules [Reg04b] also seems to be a realistic possibility. Moreover, the predicted increase of the molecular lifetime for larger binding energies can be of general interest for the coherent manipulation of Feshbach molecules [Fer09] and in particular for optimizing the starting conditions for a transfer to the ro-vibrational ground state [Ni08, Lan08, Dan10].

Finally, the question of which Feshbach resonance provides optimum conditions for interaction tuning in ^{6}Li-^{40}K has no straightforward answer. All the broad resonances occurring in the channels ac-aj (widths 0.88 G - 1.97 G) seem to be well suited for controlled interaction tuning. Because of the tradeoff between width and stability, the best choice will depend on the particular application.

We thank Bo Gao for stimulating discussions. We acknowledge support by the Austrian Science Fund (FWF) and the European Science Foundation (ESF) within the EuroQUAM/FerMix project and support by the FWF through the SFB FoQuS. T.M.H. and P.S.J. acknowledge support from an AFOSR MURI on Ultracold Molecules.

[11] $\bar{a}/s_{\mathrm{res}} = R^*$ with R^* being defined in reference [Pet04a].

Note

Recent results at the 155-G resonance suggest that the atom pairs and molecules have slightly different polarizabilities leading to a small difference in the Stark shift. This effect results in a small shift of the resonance depending on the intensity of the dipole trap laser beam. For the typical intensities in the experiment, this shift amounts to about +10 mG. The resonance position extrapolated to zero light intensity is at about 154.698 G.

Chapter 6

Publication: Hydrodynamic Expansion of a Strongly Interacting Fermi-Fermi Mixture†

Phys. Rev. Lett **106**, 115304 (2011)

A. Trenkwalder,[1] C. Kohstall,[1,2] M. Zaccanti,[1,3] D. Naik,[1] A. I. Sidorov,[1,4] F. Schreck,[1] and R. Grimm[1,2]

[1]*Institut für Quantenoptik und Quanteninformation, Österreichische Akademie der Wissenschaften, 6020 Innsbruck, Austria*
[2]*Institut für Experimentalphysik, Universität Innsbruck, 6020 Innsbruck, Austria*
[3]*LENS, Physics Department, University of Florence and INO-CNR, 50019 Sesto Fiorentino, Italy*
[4]*Centre for Atom Optics and Ultrafast Spectroscopy and ARC Centre of Excellence for Quantum-Atom Optics, Swinburne University of Technology, Melbourne, Australia*

We report on the expansion of an ultracold Fermi-Fermi mixture of ^{6}Li and ^{40}K under conditions of strong interactions controlled via an interspecies Feshbach resonance. We study the expansion of the mixture after release from the trap and, in a narrow magnetic field range, we observe two phenomena related to hydrodynamic behavior. The common inversion of the aspect ratio is found to be accompanied by a collective effect where both species stick together and expand jointly despite of their widely different masses. Our work constitutes a major experimental step for a controlled investigation of the many-body physics of this novel strongly interacting quantum system.

Since the first observations of strongly interacting Fermi gases [O'H02, Bou03] the field has produced many exciting results and provided important new insights into the many-body

†The data was taken by the author together with C. K. Thermometry and analysis of the data of figure 6.2 and in parts of figure 6.3 was performed by the author. Analysis of the other figures were performed by C. K. The dipole traps were several times changed by the author, C. K. and M. Z. The author performed the 50 Hz noise compensation and B-field calibration. He exchanged the oven and baked the oven section of the vacuum system. We thank Andrei Sidorov for stimulating discussions.

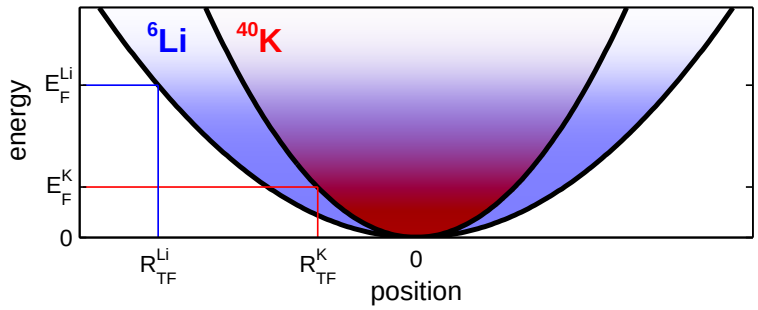

Figure 6.1: Illustration of the optically trapped Fermi-Fermi mixture. A small, moderately degenerate ^{40}K cloud resides in the center of the larger Fermi sea of ^{6}Li. The optical trapping potential of ^{40}K is about 2.1 times deeper than the one for ^{6}Li (solid lines). The Thomas-Fermi radii $R_{\mathrm{TF}}^{\mathrm{Li}}$ and $R_{\mathrm{TF}}^{\mathrm{K}}$ of both species differ by a factor of about two.

behavior of strongly interacting quantum matter [Ing08, Blo08, Gio08]. The general interest cuts across different branches of physics, ranging from strongly correlated condensed-matter systems to neutron stars and the quark-gluon plasma.

Experimental realizations of strongly interacting Fermi gases rely on ultracold mixtures of two components with magnetically tunable *s*-wave interaction. First experiments focused on spin mixtures of a single fermionic species with equal populations in two different Zeeman states [Ing08]. The introduction of population imbalance [Zwi06b, Par06a] then paved the way to the rich physics of polarized Fermi gases [Rad10, Che10]. The recent experimental efforts to create ultracold mixtures of two different fermionic species [Tag08, Wil08, Voi09, Spi09, Spi10, Tie10a, Cos10, Nai11] have brought the field close to a new research frontier with intriguing new possibilities, e.g., related to novel types of superfluids and quantum phases [Liu03, Isk07] and to new few-body states [Lev09, Nis08].

In this Letter, we report on the creation of an ultracold Fermi-Fermi mixture of ^{6}Li and ^{40}K atoms, featuring the high degree of interaction control that is necessary to explore the strongly interacting regime. As a first experimental benchmark, we demonstrate the hydrodynamic expansion after release from the trap. Near the center of an interspecies Feshbach resonance, we observe two different hydrodynamic phenomena with a pronounced dependence on the interactions strength. The first one is the well-known inversion of the aspect ratio [O'H02]. The second one is a hydrodynamic drag between both species, causing their flow velocities to be equal.

We point out that both hydrodynamic phenomena find close analogies in experiments aiming at the creation of a quark-gluon plasma [Bra07, Jac10]. Experiments of this kind study the high-energy collisions of heavy nuclei and detect the expanding collision products. In this context "elliptic flow" refers to an anisotropy of the expansion, which is understood as a consequence of the hydrodynamic interaction between the various collision products. The second analogy becomes evident in the transverse energy spectra of the collision products. Here it is found that heavier particles carry larger energies than the lighter ones [Bea97]. Such a mass-dependence is interpreted as a result of "collective flow" (see, e.g., [Yag05]), which provides another signature of the hydrodynamic nature of the expansion. The analogy between elliptic flow and the expansion of a strongly interacting Fermi gas has been pointed

out already in context with early experiments on ultracold Fermi gases [O'H02, Tho10, Sch09a]. The collective flow analogy is another striking example for the fascinating relation between two fields of physics at energies differing by more than 20 orders of magnitude.

The starting point of our experiments is a weakly interacting mixture of 7.5×10^4 ^{6}Li atoms and 2.0×10^4 ^{40}K atoms in an optical dipole trap[1]; see the illustration in Fig. 6.1. The anisotropy of the trapping potential leads to a cigar-shaped sample with an aspect ratio of about 6.5. The preparation procedures are described in detail in Ref. [Spi10]. At a temperature $T \approx 300\,\mathrm{nK}$ the Li component forms a degenerate Fermi sea with $T/T_F^{\mathrm{Li}} \approx 0.3$ and the K component is moderately degenerate with $T/T_F^{\mathrm{K}} \approx 0.7$; here the Fermi temperatures of both species are given by $T_F^{\mathrm{Li}} = 1.1\,\mu\mathrm{K}$ and $T_F^{\mathrm{K}} = 500\,\mathrm{nK}$. The K cloud is concentrated in the center of the bigger Li cloud, with approximately equal peak densities.

Interaction control is achieved by the 155 G interspecies Feshbach resonance, which occurs for Li in its lowest internal state ($m_f^{\mathrm{Li}} = +1/2$) and K in its third to lowest state ($m_f^{\mathrm{K}} = -5/2$) [Wil08, Voi09, Nai11]. The s-wave scattering length a can be tuned according to the standard resonance expression $a = a_{\mathrm{bg}}(1 - \Delta/(B - B_0))$ with $a_{\mathrm{bg}} = 63.0\,a_0$ (a_0 is Bohr's radius), $\Delta = 880\,\mathrm{mG}$, and $B_0 = 154.707(5)\,\mathrm{G}$ [Nai11].

The Li Fermi energy $E_F^{\mathrm{Li}} = k_B T_F^{\mathrm{Li}}$ represents the leading energy scale in our system. Therefore, a natural condition for strong interactions of the K minority component in the degenerate Fermi sea of Li is given by $k_F^{\mathrm{Li}}|a| > 1$, where $k_F^{\mathrm{Li}} = (2m_{\mathrm{Li}}E_F^{\mathrm{Li}})^{1/2}/\hbar = 1/(3600\,a_0)$. In terms of magnetic detuning, this condition translates to $|B - B_0| < 15\,\mathrm{mG}$. The character of the Feshbach resonance is closed-channel dominated [Chi10], but near-universal behavior can be expected throughout the strongly interacting regime [Nai11].

We create the strongly interacting mixture in a transient scheme, which minimizes the time spent near resonance and thus avoids the detrimental effect of inelastic losses [Nai11]. We start with a weakly interacting combination of spin states with $m_f^{\mathrm{Li}} = +1/2$ and $m_f^{\mathrm{K}} = -7/2$. The magnetic field is set to the target field near B_0 with an estimated uncertainty as low as 3 mG. Then we quickly convert the mixture into a strongly interacting one by flipping the spins of the K atoms to $m_f^{\mathrm{K}} = -5/2$ using a $60\,\mu\mathrm{s}$ radio-frequency π-pulse. We immediately turn off the optical trap, releasing the sample into free space. This procedure provides well-defined initial conditions for the expansion, with the density distributions being the ones of the noninteracting system.

In a first set of experiments, we study the expansion dynamics for a magnetic field very close to resonance ($B = 154.709\,\mathrm{G}$). After a variable time of flight t_{TOF}, absorption images are taken for both species and analyzed by simple two-dimensional Gaussian fits to determine their radial and axial widths, σ_r and σ_z. In Fig. 6.2 we present the resulting data in terms of the aspect ratios $A_i = \sigma_r^i/\sigma_z^i$ and volume parameters $V_i = (\sigma_r^i)^2\sigma_z^i$, where $i = \mathrm{Li}, \mathrm{K}$. For comparison, we also show corresponding measurements performed on a noninteracting sample, where the expansion proceeds ballistically and the aspect ratios asymptotically approach unity[2]. For resonant interactions, the aspect ratios of both species, A_{Li} and A_{K}, undergo an inversion, thus showing the expected hallmark of hydrodynamic behavior. Also, the volume

[1] The trap is realized with two crossed beams derived from a 1030 nm single-mode laser source. The measured trap frequencies for Li (K) are 560 Hz (390 Hz) radially and 90 Hz (57 Hz) axially.

[2] We compared the expansion of a weakly interacting mixture ($a \approx a_{\mathrm{bg}}$) with the noninteracting case realized near the zero crossing of the scattering length ($a = 0$), and found no significant difference.

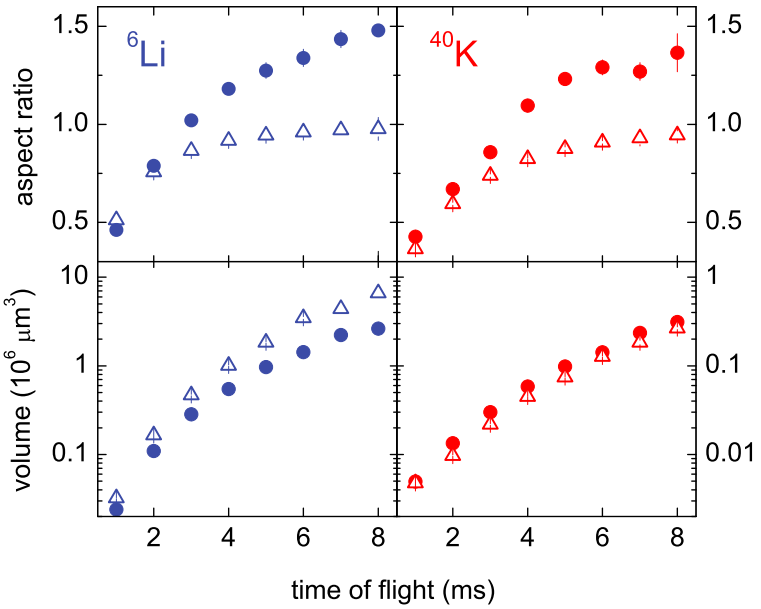

Figure 6.2: Expansion dynamics of the strongly interacting ^{6}Li-^{40}K mixture. The upper two panels show the aspect ratios A_{Li} and A_{K}, while the lower two panels display the volume parameters V_{Li} and V_{K}. The closed symbols refer to the resonant case (154.709 G), while the open symbols refer to noninteracting conditions (155.508 G). The error bars show the statistical uncertainties of the measurements.

parameters V_{Li} and V_{K} reveal striking interaction effects. While V_{Li} is substantially reduced by the interaction, V_{K} shows a small but significant increase. This observation fits to the expectation of collective flow as resulting from the hydrodynamic drag effect.

In a second set of experiments, we observe the expansion at a fixed $t_{\mathrm{TOF}} = 4\,\mathrm{ms}$ for variable interaction strength. Figure 6.3 shows the experimental data obtained for the aspect ratios and volume parameters of both species as a function of the magnetic field. Interaction effects are observed in a range with a total width of the order of 100 mG. Deep hydrodynamic behavior, however, shows up only in a narrow range within the 30 mG wide regime of strong interactions where $k_F^{\mathrm{Li}}|a| > 1$. The observed magnetic-field dependence also points to interaction effects beyond elastic scattering. In the mean-field regime, the interaction is repulsive below resonance and attractive above resonance, which leads to a respective increase or decrease of the cloud size. The corresponding dispersive behavior indeed shows up in our measurements of V_{Li}. As another interaction effect, the maximum of the volume parameter V_{K} displays a shift towards lower magnetic fields with respect to both the resonance position and the maximum observed for the aspect ratio. We speculate that this shift may be related to the magnetic-field dependence of the interaction energy in the strongly interacting regime.

Let us now turn our attention to another striking manifestation of the hydrodynamic drag effect, a bimodality in the spatial distribution of the expanding Li cloud. In the trap center, the Li atoms spatially overlap with the K cloud (see Fig. 6.1). This inner part can, together with the K atoms, form a hydrodynamic core, which is surrounded by a large noninteracting cloud of excess Li atoms. In this core, multiple elastic collisions prevent the two species from

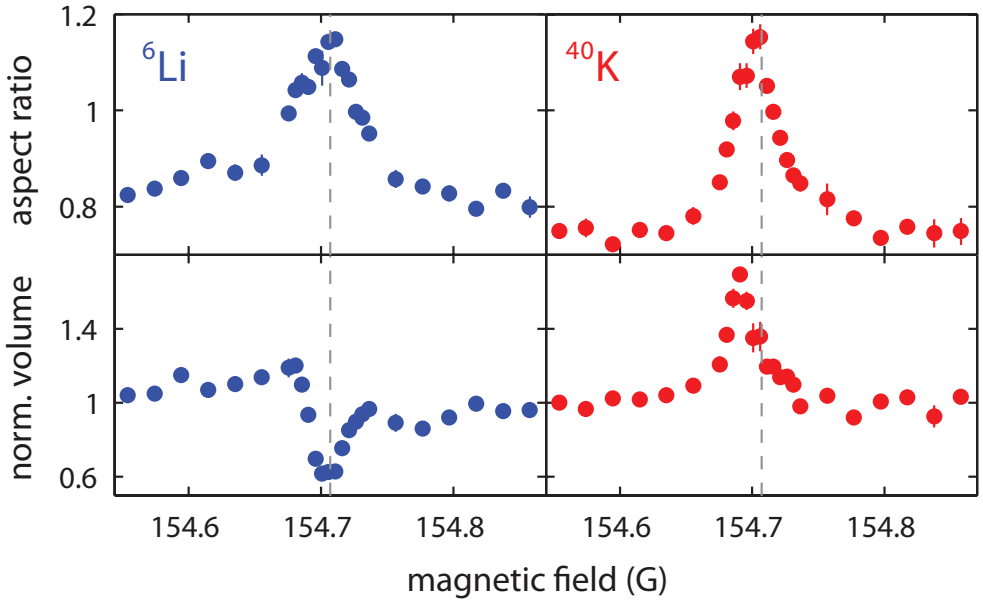

Figure 6.3: Magnetic-field dependence of the hydrodynamic expansion observed at $t_{\mathrm{TOF}} = 4\,\mathrm{ms}$. The upper panels show the aspect ratios A_{Li} and A_{K}. The lower panels show the volume parameters V_{Li} and V_{K}, normalized to their values measured for the noninteracting case. The dashed vertical lines indicate the resonance position B_0. The statistical uncertainties are on the order of the size of the symbols.

separating. This leads to a slow collective expansion of the light Li atoms sticking together with the much heavier K atoms. In contrast, the expansion of the outer part of the cloud is fast and proceeds in an essentially ballistic way[3].

Figure 6.4 shows images of the hydrodynamic core. To increase its visibility on the background of the ballistically expanding particles we show a differential Li image, where a reference image taken under noninteracting conditions is subtracted from the image of the strongly interacting cloud. This Li image is compared with a standard absorption image of the K cloud, as all K atoms are expected to contribute to the hydrodynamic core. The inner distribution detected for the Li component closely resembles the shape and size of the K cloud, supporting our interpretation of a jointly expanding Li-K cloud. The formation of this hydrodynamic core implies that particles are missing in the outer part, which undergoes a near-ballistic expansion[3]. Consequently, the differential Li image shows a negative signal in the outer region.

We analyze the bimodal distribution of the Li cloud by two-dimensional double-Gaussian fits. Two examples for the corresponding spatial profiles are shown in the upper panels of Fig. 6.5. The lower panel displays the fraction of Li atoms in the hydrodynamic core that we find from such fits as a function of the magnetic field. The maximum core fraction near 20% contains about 1.5×10^4 Li atoms, which corresponds to essentially all Li atoms in the overlap region. The maximum in the core fraction of Li near 154.7 G may be interpreted in

[3]During the expansion some atoms in the outer cloud can interact with the hydrodynamic core, which also makes their distribution anisotropic.

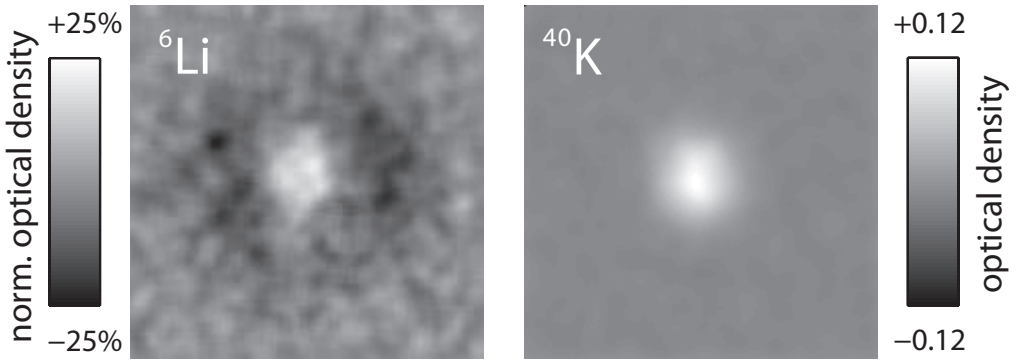

Figure 6.4: Images of the hydrodynamic core of the cloud ($t_{\mathrm{TOF}} = 4\,\mathrm{ms}$) in the regime of resonantly tuned interactions (154.706 G), where ^{6}Li and ^{40}K expand collectively. The image on the left-hand side is a differential image of the Li atoms, where we subtracted a reference image of the noninteracting cloud. The corresponding greyscale refers to the optical density as normalized to the maximum in the noninteracting distribution. The image on the right-hand side shows the K atoms in the strongly interacting cloud. Here the greyscale gives the optical density. The field of view of both images is $500\,\mu\mathrm{m} \times 500\,\mu\mathrm{m}$. The images are averaged over seven individual shots.

terms of a maximum collision cross section, thus marking the exact resonance position B_0, but it may also point to interaction phenomena beyond elastic scattering.

The physics of interactions in the strongly interacting regime can be very rich, and more detailed investigations on the hydrodynamic core will unravel the complex many-body interactions of the system. Besides mean-field shifts, for which we have already observed indications, strong polaronic interactions [Sch09b] or a substantial influence of pairing may be expected at sufficiently low temperatures. On the $a > 0$ side, weakly bound dimers [Voi09, Spi10] may be formed either directly by radio-frequency association or indirectly by three-body recombination. We may speculate that on resonance, already at the moderate degeneracies realized in our present experiments, many-body pairs may contribute. Superfluidity may be expected at lower temperatures. All these phenomena need further detailed investigations and represent exciting future research topics.

In conclusion, we have explored a strongly interacting Fermi-Fermi mixture by studying its expansion dynamics. Our results show pronounced effects of hydrodynamic behavior, manifested in both an anisotropic expansion and in collective flow as resulting from interspecies drag. Our near-future work will be dedicated to a better understanding of the role of interaction effects, in particular, to the equation of state at unitarity [Gez09], and to the equilibrium and dynamics in the trap [Ors08]. The novel system offers many more intriguing possibilities to explore its quantum many-body physics. Already the experiments on strongly interacting spin mixtures [Ing08, Gio08] suggest a rich tool box of different experimental methods, such as measurements on *in situ* spatial profiles, studies of collective modes, the application of radio-frequency or Bragg spectroscopy, and detection of molecular condensates and fermionic pair condensates. Moreover, the Fermi-Fermi mixture offers conceptually new possibilities through the application of species-selective optical potentials, which will allow

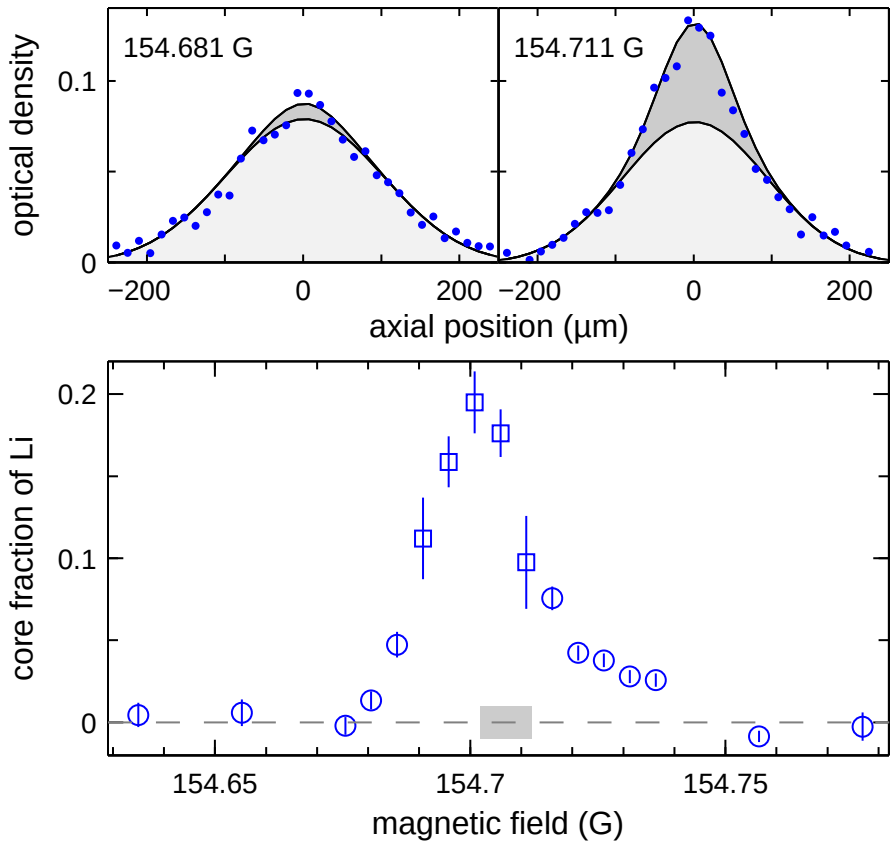

Figure 6.5: Bimodal distributions of ^{6}Li observed at $t_{\mathrm{TOF}} = 4\,\mathrm{ms}$. The upper panels show two example profiles representing axial cuts through the two-dimensional distribution, obtained from a narrow strip of 15 μm width in radial direction. The solid lines show double-Gaussian fits. The lower panel shows the corresponding fraction of atoms in the hydrodynamic core as a function of the magnetic field. The central five points (open squares) are based on fits where the widths of the core were kept as free parameters. Further away from resonance (open circles) the bimodality is much less pronounced and such a multiparameter fit is not applicable. Here the widths were fixed to corresponding widths of the K distribution. The error bars indicate the statistical uncertainties resulting form seven individual measurements at a given magnetic field. The grey shaded area indicates the uncertainty range for the resonance center according to Ref. [Nai11].

for independent control of both components, e.g., for an independent manipulation of the Fermi surfaces in optical lattices [Fei09] or for the creation of mixed-dimensional fermionic systems [Nis08].

We thank A. Recati, S. Giorgini, and S. Stringari for stimulating discussions and G. Hendl for technical assistance. We acknowledge support by the Austrian Science Fund (FWF) and the European Science Foundation (ESF) within the EuroQUAM/FerMix project and support by the FWF through the SFB FoQuS.

Note

Recent results suggest that the atom pairs and molecules have slightly different polarizabilities leading to a small difference in the Stark shift. This effect results in a small shift of the resonance depending on the intensity of the dipole trap laser beam. For the typical intensities in the experiment, this shift amounts to about +10 mG. The resonance position extrapolated to zero light intensity is at about 154.698 G.

Appendix A

High-field Resonance

Anyone who has never made a mistake has never tried anything new.

Albert Einstein

When we worked on the Feshbach spectroscopy paper, see chapter 2, Tobias Tiecke provided tables of possible resonances calculated with an early version of the ABM [Tie10b]. Included was the prediction of a high-field resonance at 2365 G for Li$|1\rangle$K$|1\rangle$. After the paper was finished we searched for this resonance and could indeed find one resonance at 2335 G. However, the ABM as was used in the publication would give a resonance position at much higher fields. Inclusion of the observed resonance would fit less well for the low-field resonances. In the meantime the ABM was extended [Tie10b] and successfully applied to other systems, including a high-field resonance at 2054 G for sodium [Kno11]. Therefore, it might be useful to reconsider this resonance in the extended ABM or other theoretical models. This could provide better knowledge of the energy structure of the ^{6}Li-^{40}K mixture which might be helpful for future experiments.

The filled (black) squares in figure A.1 show the relative atom number of K$|1\rangle$ and of Li$|1\rangle$ after 610 ms hold time at this magnetic field. A clear loss feature can be observed for both species. From a Gaussian fit, solid curve (blue), on the K$|1\rangle$ loss we obtain the field of maximum loss at (2335.2 ± 0.3) G. The maximum of the lithium loss is at the same position. A Lorentzian fit was also performed but did not match as good with the observed loss as the Gaussian fit (the χ^2 was clearly larger).

The field was calibrated using a radio-frequency π-pulse on the Li$|1\rangle$-Li$|2\rangle$ transition without K present. From the frequency the field was calculated using the Breit-Rabi formula presented in appendix D. The pulse had a length of 13 ms. The width of the rf-pulse of about 200 Hz gives the 0.3 G error in the determination of the field. The $e^{-1/2}$-width of the fitted Gaussian of the loss feature is (0.15 ± 0.01) G. But we suspect that it is broadened by magnetic field fluctuations, since we have to use less stable power supplies to reach the field of the resonance.

The mixture is prepared at 1181 G in a single-focus optical dipole trap, derived from

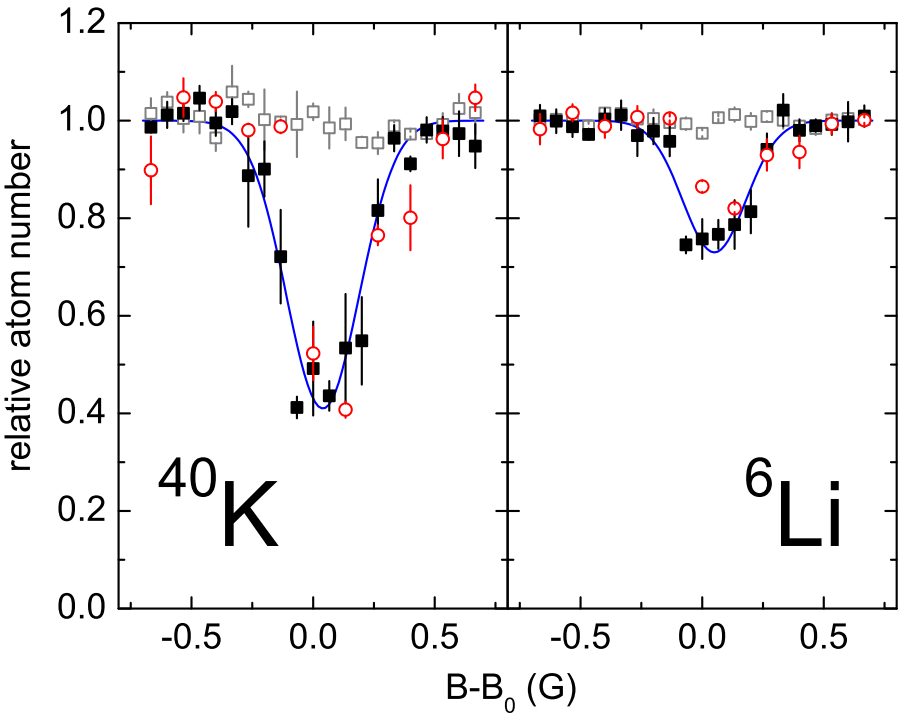

Figure A.1: Li$|1\rangle$-K$|1\rangle$ high field resonance at B_0=2335.2(3) G. Relative atom number for K$|1\rangle$ (left) and Li$|1\rangle$ (right) after 610 ms hold time at the specified magnetic field. Atom number is given relative to the atom number far away from resonance. Filled squares (black) are with both species present. Open squares (gray) are with only one species present. Rings (red) are for higher temperature (for details see text). Solid curves (blue) are Gaussian fits indicating the position and width of the resonance.

a single-mode 1064 nm laser with a waist of 41 μm, operated at 38 mW. A magnetic field curvature of 29 G/cm^2 provides additional confinement in the axial direction. For ^{6}Li (^{40}K) the trap depth is 850 nK (1900 nK) and the trap frequencies are 270 Hz (150 Hz) radially and 26 Hz (10 Hz) axially. After evaporation at 1181 G, Li$|2\rangle$ was removed with resonant light and the atom number of the remaining spin mixture was 1.5×10^5 Li$|1\rangle$ and 1.7×10^4 K$|1\rangle$. This gives a Fermi temperature of 560 nK for ^{6}Li and 210 nK for ^{40}K. Both species were thermalized at a temperature of less than 70 nK which corresponds to $0.1\,T_F$ for Li and $0.3\,T_F$ for K. Thermometry was performed at 1181 G with Fermi fits on both species and was checked with Gaussian fits on K$|1\rangle$. The given temperature is the result obtained by the Gaussian fit. This temperature is an upper bound. The Fermi fits give about 40 nK for both species but can not entirely be trusted due to the difficulty in obtaining the temperature for a degenerate Fermi sea (see for example [Ket08]). The magnetic field was ramped to 2341 G within 200 ms and held there for another 200 ms to wait for stabilization. The ramp afterwards to the (lower) destination field was performed within 100 ms at which the sample was held for 610 ms. There the atoms can collide and form bound molecules. The released energy is sufficiently high such that the atoms leave the trap. After the waiting time the magnetic field was ramped within 100 ms back to 1181 G where the remaining atoms in the trap were recorded by absorbtion imaging of Li$|1\rangle$ and K$|1\rangle$ simultaneously.

The atom loss shown in Figure A.1 corresponds to 4×10^4 lithium atoms and 1×10^4 potassium atoms. The unequal loss could be explained by heating and the less deep trap for lithium. We observe indeed a small increase of temperature of the remaining atoms which is about 100 nK for K (obtained by Gauss fits; Fermi fits on ^{6}Li give 80 nK). To check that the observed loss is not a homonuclear feature (like a p-wave resonance) we performed the same measurement as described but with either lithium or potassium removed by resonant light. Note that the temperature and atom number of one species is not affected by removing the other one. This measurement was performed with slightly more atoms than before and the hold time was 500 ms. However, no loss is observed as can be seen by the open symbols in figure A.1. This gives us confidence that the loss feature is a heteronuclear resonance.

To see the temperature dependence of the loss feature, we stopped the evaporation at 96 mW infrared power, giving a trap depth of 2.2 μK and 4.9 μK for ^{6}Li and ^{40}K, respectively. The corresponding trap frequencies for ^{6}Li (^{40}K) are 430 Hz (250 Hz) radially and 26 Hz (10 Hz) axially. The atom number was different to previous measurements: 2.6×10^5 for Li$|1\rangle$ and 1.5×10^4 for K$|1\rangle$ which gives a Fermi temperature of 940 nK and and 190 nK for ^{6}Li and ^{40}K, respectively. The temperature was 200 nK (obtained by Gauss fits on ^{40}K; Fermi fits on ^{6}Li give 180 nK), which corresponds to $0.2\,T_F$ for ^{6}Li and T_F for ^{40}K. The loss feature was measured as described above, only the waiting time was 500 ms at the destination field. The resulting loss feature is shown as rings (red) in figure A.1. No significant change in the loss feature can be seen. We suspect that the temperature change might have been too small to come into effect or the B-field noise is still dominating over thermal broadening. The position of the resonance shows a small upshift by 0.1 G with respect to previous measurements but this can be understood by the 0.3 G uncertainty in the determination of the B-field.

About the nature of the resonance we can only speculate. It might come from a different scattering potential or a lower bound molecular state. Also the partial wave of the resonance is unknown. We only observe that the loss feature does not show a significant asymmetry

and temperature dependence, at least at the temperature range of the measurement. These observations indicate an *s*-wave character of the resonance but we are almost certain that B-field noise has affected the measurement, preventing us to give a final conclusion.

We have observed a narrow heteronuclear high field Feshbach resonance in the Li$|1\rangle$K$|1\rangle$ spin channel at 2335.2(3) G. To our knowledge, this is the highest field where a Feshbach resonance has been observed so far. Input from theory side would be welcome to assign the resonance which might help to improve the knowledge of the scattering properties of the ^{6}Li-^{40}K mixture.

The author thanks Tobias Tiecke for the fruitful collaboration with our group on the Feshbach spectroscopy paper, which triggered to perform the measurements presented.

Appendix B

p-wave Resonance Splitting

When the ^{6}Li-^{40}K Feshbach resonances had been assigned it was a surprise that the observed p-wave resonances were broader than the s-wave resonances, see chapter 2. This is uncommon but can be understood by the fact, that the difference in the magnetic moment of the unbound atomic state to that of the bound molecular state is small. Thus, the thermally broadened p-wave loss feature is stretched out over a larger magnetic field range. Molecules at p-wave resonances exhibit orbital angular momentum $\ell = 1$ [Tic04]. In order to collide, the atoms have to tunnel through the p-wave barrier. Since the tunneling rate is strongly energy dependent, the shape of the resonance is asymmetric and also depends strongly on the temperature of the atoms.

We consider here only alkali metals in the ground state ($^2S_{1/2}$) where a p-wave molecule can only be created by combining the two spins of the atoms aligned in the same direction. In an external magnetic field the orbital angular momentum is projected onto 3 states, described by the magnetic quantum numbers $m_\ell = 0, \pm 1$. The spin-spin interaction between the two atoms is attractive when the spins are aligned head to tail and it is repulsive when the spins are side by side. In a classical picture, a molecule which rotates in the plane of the magnetic field, figure B.1(a), which corresponds to $m_\ell = 0$, will have the spins some time attracting and the other time repelling each other during the rotation. The net interaction energy will be zero (or close to zero). A molecule rotating in a plane perpendicular to the magnetic field, figure B.2(b), which corresponds to $m_\ell = \pm 1$, will have the spins always interacting repulsively. This leads to an increase of the energy with respect to the case $m_\ell = 0$. The state with $m_\ell = \pm 1$ will create a resonance at a lower field than that with $m_\ell = 0$. We expect the resonance to be split into these two features. Normally, this splitting is small, but for the ^{40}K heteronuclear p-wave resonance around 198.5 G it could be observed and characterized [Tic04]. We became curious about the p-wave resonances in the ^{6}Li-^{40}K-mixture since they are very broad. After we could significantly reduce the temperature of our sample with respect to the first Feshbach scans we wanted to have a closer look on one of them and see if we can resolve the splitting.

Figure B.2 shows the atom loss around the Li$|1\rangle$K$|1\rangle$ p-wave Feshbach resonance at 245 G. The measurement was performed at the three different temperatures indicated. The sample was prepared at around 1180 G where evaporation was done in an optical dipole trap, derived from a 200 W multi-mode 1070 nm single focus beam of 38 μm waist. Li$|1\rangle$ and Li$|2\rangle$ were

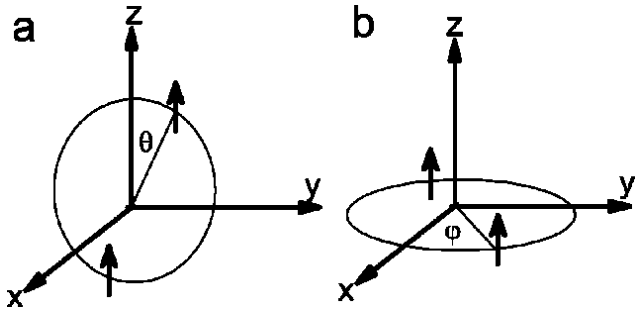

Figure B.1: Classical picture of orbiting spins in different planes relative to the applied B-field (from [Tic04]). (a) If the spins orbit in-plane with the field ($m_\ell = 0$) the spin-spin interaction is repulsive during one half of the orbit and attractive during the other half. The net interaction energy is zero. (b) If the spins orbit in an orthogonal plane to the field ($m_\ell = \pm 1$) the spin-spin interaction is constantly repulsive leading to an increase in energy.

evaporated and K$|1\rangle$ sympathetically cooled. After evaporation, the Li$|2\rangle$ spin state was removed by resonant light to avoid Li_2 molecule formation during the following B-field ramp down to the desired field. The Li$|1\rangle$K$|1\rangle$ sample was hold at the given field for 2 s followed by a field ramp to zero for fluorescence imaging. To get different temperatures, evaporation was stopped at different trap depths. The atom number of ^{6}Li (^{40}K) is around $8{\times}10^5$ ($1.3{\times}10^4$), $5{\times}10^5$ ($8.5{\times}10^3$) and $1{\times}10^5$ ($4{\times}10^3$) for the data at 2.5 μK, 600 nK and 70 nK respectively. The given temperatures correspond to a ratio T/T_F of about 1 (6), 0.5 (3) and 0.2 (1) for ^{6}Li (^{40}K). Note that all numbers here are estimates, since the measurement was done with fluorescence detection and thermometry was performed on another day under slightly different conditions.

We observe a broad splitting into two loss features separated by (4.0 ± 0.1) G. As expected, we see a strong temperature dependence and a strong asymmetry. The high-temperature tail at 2.5 μK (light gray squares) becomes smaller for lower temperature (600 nK, gray triangles), until at 70 nK (black rings) a very narrow feature remains. For a degenerate Fermi gas the Fermi energy defines the width of the loss feature. The lowest temperature of potassium is about T_F, while for lithium it is about $0.2\,T_F$. The low field edge of the loss feature does not change with temperature and can be interpreted as the threshold of the resonance. For the lowest temperature we obtain by Gauss fits the position of the feature which is (241 ± 2) G and (245 ± 2) G for the $m_\ell = \pm 1$ and $m_\ell = 0$ state, respectively. The large error is caused by the uncertainty of the B-field calibration since no radio-frequency determination of the field was made (see appendix D). The $e^{-1/2}$-width of the Gaussian is 0.1 G for both features. Note that the splitting is the relative position of the two features, so it could be determined more precisely.

We tried to obtain the binding energy of the p-wave molecules with the "wiggle spectroscopy" method described in appendix C and as was done for ^{6}Li p-wave molecules in [Fuc08]. But we could not observe any dips corresponding to the molecules. The small difference in the magnetic moment requires to search in a larger field region which makes it more difficult. A technical reason can not be excluded as well, since we encountered later that the used audio amplifier might have switched off during the measurements due to

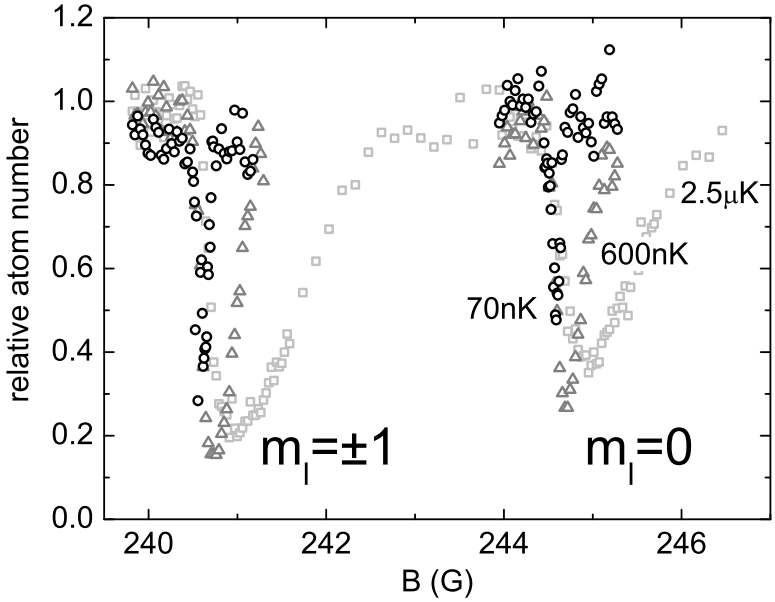

Figure B.2: Potassium atom number after 2 s hold time normalized to the initial atom number. Plotted is the loss for different temperatures: $2.5\,\mu$K$=6\,T_F$ (light gray squares), 600 nK$=3\,T_F$ (gray triangles) and 70 nK$=T_F$ (black rings).

overheating.

In conclusion, we have observed a broad 4 G splitting of a heteronuclear ^{6}Li-^{40}K p-wave resonance. The temperature dependence clearly shows the typical asymmetry. Further experiments have not been carried out on this resonance. It would be easy to get exact positions, lifetimes and loss coefficients. Molecules have been already seen on p-wave resonances [Zha04, Gae07, Mai10]. But they are in general short in lifetime since the least-bound states lie behind the p-wave barrier which can decay via tunneling. On the other hand, the barrier protects the molecules against colliding atoms. Lower lying p-wave molecules would be more stable if the binding energy was below the barrier height. The possibility to specifically select the m_ℓ of the p-wave molecule could be useful.

For the BEC-BCS crossover of pairs with angular momentum a rich phase diagram is expected but p-wave resonances are intrinsically narrow making experiments difficult. Although p-wave resonances have been observed for many years, for example [Reg03c, Sch05], so far Bose condensation and p-wave superfluidity have not been achieved. This would be desirable, especially in the light of high-T_c superconductivity where pairing with angular momentum (namely d-wave) is discussed to play a significant role.

The author is thankful to Devang Naik with whom the presented data was taken and who initiated these measurements on the p-wave resonance.

Appendix C

Wiggle Spectroscopy

After we created our first heteronuclear molecules, section 4.6, we intended to measure the binding energy of them. This would allow to determine the position of the resonance more precisely. Our method was to directly drive a transition between the molecule state and the free atom state by modulating the magnetic field [Tho05b, Pap06, Han07, Fuc08, Web08, Lan09]. This method could be called "magnetic-field modulation spectroscopy", but within our group we name it "wiggle" spectroscopy [Pil09]. It has the advantage in comparison with rf-spectroscopy that the frequencies are lower so that powerful audio amplifiers can be used and the matching of the antenna is not critical. The measurement of the binding energy of the heteronuclear Feshbach molecules of $\mathrm{Li}|1\rangle\mathrm{K}|1\rangle$ states using the wiggle method is presented in this appendix.

Figure C.1 shows one sample spectrum measured at the $\mathrm{Li}|1\rangle\mathrm{K}|1\rangle$ resonance around 168 G. The modulation frequency was 400 kHz and the modulation amplitude was 190 mG (peak-to-peak). Plotted is the remaining atom number of ^{40}K after 200 ms of modulation. Three dips are visible in the atom number. To obtain the position and width of each loss feature we fitted three Gaussians to the data (blue curves). The central dip is on the resonance which we observe even without modulating the field. We loose about 80% of the atoms after 200 ms. The dip at negative detuning from the resonance center is at the field where the binding energy of the molecules coincides with the applied modulation frequency. Note that the amplitude of the modulation is accidentally close to the found ΔB. For a smaller amplitude less atoms are transferred and we observe less pronounced dips in the atom number but the dips are not shifted. The molecular dip in this example is as deep as the loss feature. This is not always the case but it is nearly always narrower than the center feature (a discussion of the width will follow below). We see another dip at positive detuning from the resonance which we interpret by the association of quasi-bound molecules. They can not only decay into lower molecular states but into free atoms as well. This dip is less pronounced and broader than the feature observed for the bound molecules. The broadening could be understood by the reduced lifetime of these molecules.

In figure C.2 we show the result of several spectra where we plotted the position of the dips for different binding energies. We see that the binding energy of the molecules (black squares) has a linear dependency (blue line) on the magnetic field. In the range of the measurement and within the error there is no visible deviation from the linear dependency.

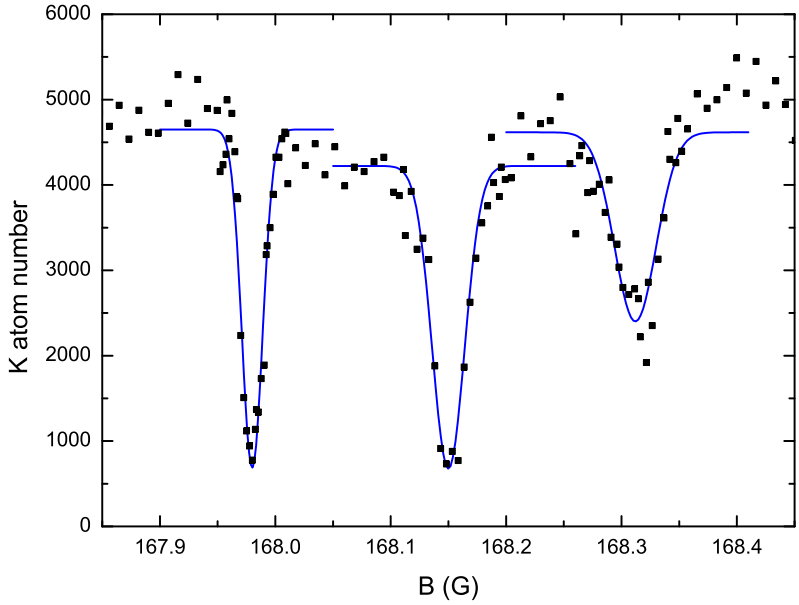

Figure C.1: Remaining K$|1\rangle$ atom number (black squares) after a 200 ms magnetic field modulation with 400 kHz and amplitude of 190 mG (peak-to-peak). Gaussian fits (blue curves) give $\Delta B = (166 \pm 4)$ mG for the position of the molecular two loss features relative to the free atom feature in the center.

The slope $\delta\mu/h = (2.42 \pm 0.01)$ MHz/G corresponds to the difference in the magnetic moment of the free atoms with the magnetic moment of the molecules. This value is close to the 2.5 MHz/G obtained by a coupled channels calculation, see table 5.2. The binding energy becomes zero at $B_c = (168.145 \pm 0.005)$ G. Statistical errors would amount to 1 mG but we assume a 5 mG uncertainty coming from the field determination, see appendix D. The field B_c corresponds to the crossing of the bare molecular state with the free atom state. The actual position of the resonance B_0 is shifted towards higher field by the interaction between the molecule state and the free atom state (i.e. due to the avoided crossing), see [Chi10]. Since the resonance is narrow and closed channel dominated, we assume that $B_0 \approx B_c$ within the uncertainty. The observed loss feature of the free atoms (blue triangles) is only +3 mG towards higher field and confirms our assumption. For the smallest modulation frequency of 100 kHz and 200 kHz the dips in the spectra were already overlapping and 4 or 5 dips were observed. The additional dips are shown as red circles in figure C.2. The field of these dips is exactly at a binding energy which is twice the modulation frequency. Therefore, we interpret these additional dips as a two photon transition which becomes more likely at a high collision rate. It was not possible to modulate at a lower frequency than 100 kHz since no clear dips could be observed even for small modulation amplitude and short waiting time. We assume that the dips are broadened by collisions in the vicinity of the resonance which prevents to have a narrower loss feature.

Figure C.3 shows the width of the observed dips. Symbols and colors are the same as in figure C.2. The error of the width is calculated from the Gaussian fit. For the bound molecules the width seems to be constant around 12 mG while at the position of the reso-

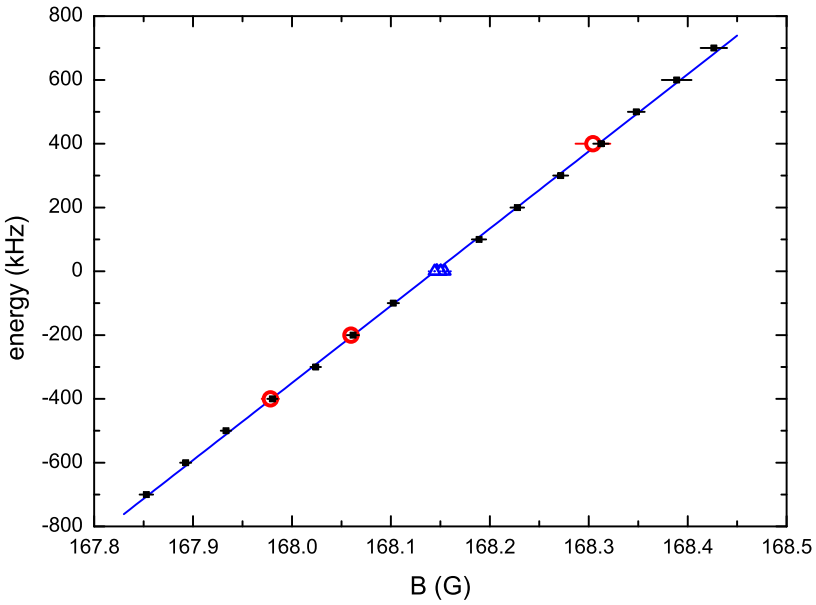

Figure C.2: Molecular binding energy for Li$|1\rangle$K$|1\rangle$ resonance at $B = (168.145 \pm 0.005)$ G. Black squares show the binding energy of the molecules. Blue triangles are the free atoms and red circles show the positions of 2^{nd} molecular dips which were observed for 100 kHz and 200 kHz modulation frequency. Blue line is a fit to all data points and gives a slope of $\delta\mu/h = (2.42 \pm 0.01)$ MHz/G.

nance it shows a sharp increase towards 25 mG for the quasi-bound molecule. This can be interpreted as a reduction in the lifetime of the quasi-bound molecules with respect to the bound molecules. As the binding energy of the quasi-bound molecules is increased the width might decrease again but the noise in the measurement is too large for making conclusions. The increase in width of the free atom loss feature might be related to the increased collision rate on the resonance.

Note that in the figures presented the modulation amplitude was lower for the largest two frequencies of 600 kHz and 700 kHz with 100 mG and 90 mG, respectively. At these frequencies the audio amplifier could not drive anymore the full peak current (of 90 mA) used for all other data points.

For the wiggle spectroscopy we tested several setups with current control. Two were working best: 8 unity-gain buffer OPAmps (BUF634 delivers ±250 mA) in parallel showed very fast rise times which would be advantageous for fast switching of fields. However, they can only be used with maximum ±18 V source voltage which limits the driving capabilities of a coil at high frequencies. Therefore, we switched later to an audio amplifier (LM3886, 68 W, needs good cooling) which can be supplied with ±42 V. All the measurements presented here are done with this amplifier.

In conclusion, we have measured the binding energy of the Li$|1\rangle$K$|1\rangle$ molecules by wiggle spectroscopy. We obtained the position of the resonance and the difference in the magnetic moment of the molecules with respect to the atoms. We could observe loss features associated with quasi-bound molecules. The increased width of these loss features might be understood

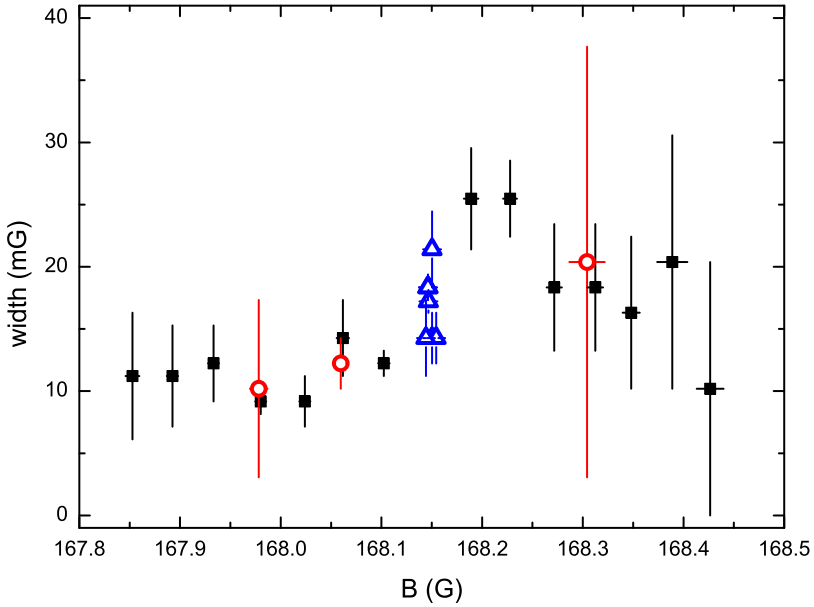

Figure C.3: Width of the loss features. Black squares correspond to molecules, blue triangles to free atoms and red circles are molecules with binding energy of twice the applied modulation frequency. The error of the widths is calculated from the Gaussian fits.

by the reduced lifetime of the quasi-bound molecules but no further analysis was performed.

The author thanks Gerhard Hendl and Florian Schreck for building the amplifiers and Michael Mark for suggesting the method.

Appendix D

Breit-Rabi formula

In the course of our high-precision measurements on the 155-G Feshbach resonance, chapter 5, it was crucial to obtain a good magnetic field stability, see appendix E. Also the magnetic field has to be determined precisely. One of the most reliable ways is to measure the energy difference between two Zeeman states where the magnetic field dependence is well known. For the ground state of Alkali metals the energy difference can be calculated analytically using the Breit-Rabi formula [Bre31]. We investigated the used parameters and corrected a small mistake in our formula. In this section we present the Breit-Rabi formula together with the values of all used input parameters.

Together with our measurements we take always a radio frequency spectrum on either ^{6}Li or ^{40}K at the same current and timing as the measurement. This is done with the other species removed or in an only weakly interacting state in order to be not affected by interaction effects. We obtain the frequency of maximum transfer between two Zeeman states and with the Breit-Rabi formula presented below we calculate from the frequency the magnetic field of the measurement. For this purpose, we use a simple C-program for the calculations. The program uses the Secant method, a variation of Newton's method, to calculate the B-field for a given transition frequency in an iterative way. Note that the experiment is synchronized to line and we compensate line noise as described in appendix E. The radio frequency pulse is Fourier-limited with a width of typically 1 kHz. This gives a frequency resolution of less than 0.5 kHz and results in about 1 mG uncertainty in the determination of the magnetic field.

The Breit-Rabi fomula can be obtained by diagonalizing the Hamiltonian for the hyperfine interaction in an external magnetic field [Geh03a, Tie09a, Ari77, Bre31]:

$$\begin{aligned} H_{int} &= H_{HF} + H_Z \\ &= \frac{A_{HF}}{\hbar^2}\,\mathbf{I}\cdot\mathbf{J} + \frac{B_{HF}}{\hbar^2}\,\frac{6(\mathbf{I}\cdot\mathbf{J})^2 + 3(\mathbf{I}\cdot\mathbf{J}) - 2\mathbf{I}^2\mathbf{J}^2}{2I(2I-1)2J(2J-1)} + (g_J\mathbf{J} + g_I\mathbf{I})\frac{\mu_B}{\hbar}\mathbf{B}\ . \end{aligned} \tag{D.1}$$

Here A_{HF} is the magnetic dipole constant which depends on the states involved and determines the hyperfine splitting at zero magnetic field ΔE_0. For the $^2S_{1/2}$ (ground) state the relation holds:

$$\Delta E_0 = A_{HF}(I + 1/2)\ . \tag{D.2}$$

B_{HF} is the electric quadrupole constant, which is 0 for the $^2S_{1/2}$ and $^2P_{1/2}$ states. For the $^2S_{1/2}$ (ground) state the eigenvalues of the Hamiltonian (D.1) can be calculated analytically, yielding the Breit-Rabi formula for F=I±1/2:

$$E(I,m_F) = -\frac{\Delta E_0}{2(2\,I+1)} + m_F\, g_I\, \mu_B\, B \pm \frac{\Delta E_0}{2}\sqrt{1+\frac{4\,m_F}{2\,I+1}x+x^2} \quad \text{with} \quad x \equiv (g_J - g_I)\,\frac{\mu_B\, B}{\Delta E_0}\ . \tag{D.3}$$

We use the convention that g_I has opposite sign than the magnetic moment, i.e. $\mu = -g_I\mu_B\, B$. The term linear in B above is often neglected since $g_I \ll g_J$. For the precision of our experiment it makes a measurable contribution. For other states numerical solutions can be found. For example, in [Geh03a] the code for the numerical calculation with *Mathematica* is presented.

When one tries to calculate energies with the equation above one needs to be careful which sign to use since not only for the different F-states but also for the stretched states the sign changes. Therefore, we give an explicit form for calculations:

$$\frac{E(I,m_F)}{\Delta E_0} = -\frac{1}{2(2\,I+1)} + \frac{m_F\, x}{g_J/g_I - 1} + (F-I)\begin{cases} 1+\mathrm{sign}(m_F)\,x \\ \sqrt{1+\dfrac{4\,m_F}{2\,I+1}x+x^2} \end{cases}\ . \tag{D.4}$$

The upper case is for stretched states with $\pm m_F = I + 1/2$ and the lower case is for the other states. The prefactor $(F-I)$ can only be $\pm 1/2$ and is used to obtain the correct sign. The used atomic parameters are listed in table D.1 together with the references from where they have been obtained.

Table D.1: Atomic parameter for ^{6}Li and ^{40}K.

symbol	name	^{6}Li	^{40}K	Ref.
I	nuclear spin	1	4	
g_I	nuclear coupling factor	-0.0004476540(3)	0.000176490(34)	[Ari77]
g_J	electron coupling factor $^2S_{1/2}$	2.0023010(7)	2.00229421(24)	[Ari77]
	electron coupling factor $^2P_{1/2}$	0.6668(20)	2/3	[Ari77, Tie09a]
	electron coupling factor $^2P_{3/2}$	1.335(10)	4/3	[Ari77, Tie09a]
A_{HF}	magnet. dipole constant $^2S_{1/2}$	152.1368407(20) MHz	-285.7308(24) MHz	[Ari77]
	magnet. dipole constant $^2P_{1/2}$	17.375(18) MHz	-34.523(25) MHz	[Ari77, Tie09a]
	magnet. dipole constant $^2P_{3/2}$	-1.155(8) MHz	-7.585(10) MHz	[Ari77, Tie09a]
B_{HF}	electr. quadrupole const. $^2P_{3/2}$	-0.10(14) MHz[1]	-3.445(90) MHz	[Ari77, Tie09a]
μ_B	Bohr magneton	1.399624604(35) MHz/G		[Moh08]

[1]The given B_{HF} of ^{6}Li corresponds to the "recommended values" of [Ari77] summarized in their table IX. But in the ^{6}Li section of the same publication they give a 10 times smaller value. The cited reference *Orth et al.* was not obtainable before submission of this thesis, such that it was not possible to check which value is correct. No newer measurement could be found either. For the numerical calculations shown in figure D.1 the value in the table was used, as in [Geh03a]. However, this uncertainty only affects the $2^2P_{3/2}$ state of ^{6}Li and for zero field up to 1 kG the difference in energy is less than 100 kHz.

On pages 104 and 105 the energies of the ground and excited states of ^{6}Li and ^{40}K are shown. For calculating the ground state equation (D.4) was used, while for the excited state the hamiltonian (D.1) was diagonalized numerically using the code by [Geh03a].

The Breit-Rabi formula and the atomic parameters have been evaluated thoroughly by Florian Schreck, Rudi Grimm and the author and consistency between the results obtained by ^{6}Li and ^{40}K has been proved experimentally around the 155-G resonance. Consistency between numerical and analytical results has been checked as well. The formula is very useful to get a precision of 1 mG in the determination of the magnetic field. Nevertheless, the accuracy of the absolute value of the magnetic field determined by the frequency can still suffer from systematics. Therefore, for comparison of different results it might be helpful to compare the frequencies where the field was determined. To make such a comparison easier this appendix was written.

This is a summary of the work of several contributors, cited in the text.

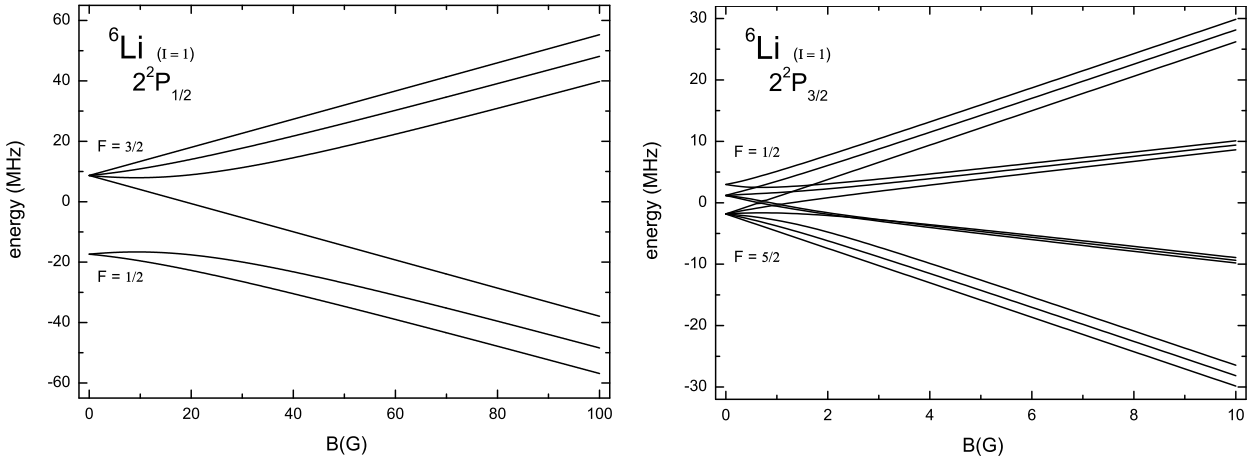

Figure D.1: ^{6}Li first excited state $2^2P_{1/2}$ and second excited state $2^2P_{3/2}$ energies as a function of magnetic field. Numerical results obtained with the code in [Geh03a], using the parameters in table D.1.

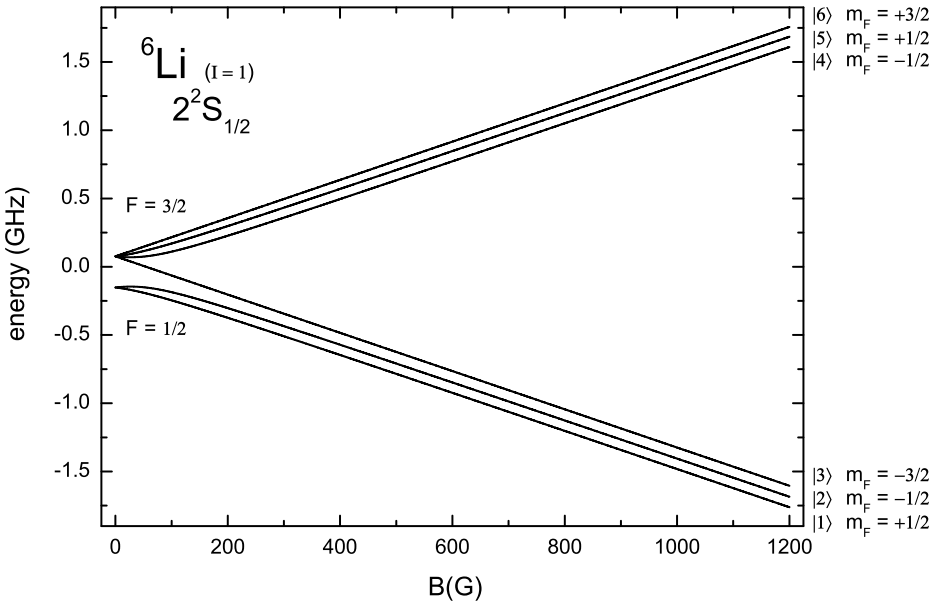

Figure D.2: ^{6}Li ground state $2^2S_{1/2}$ energies as a function of magnetic field obtained from equation (D.4), using the parameters in table D.1.

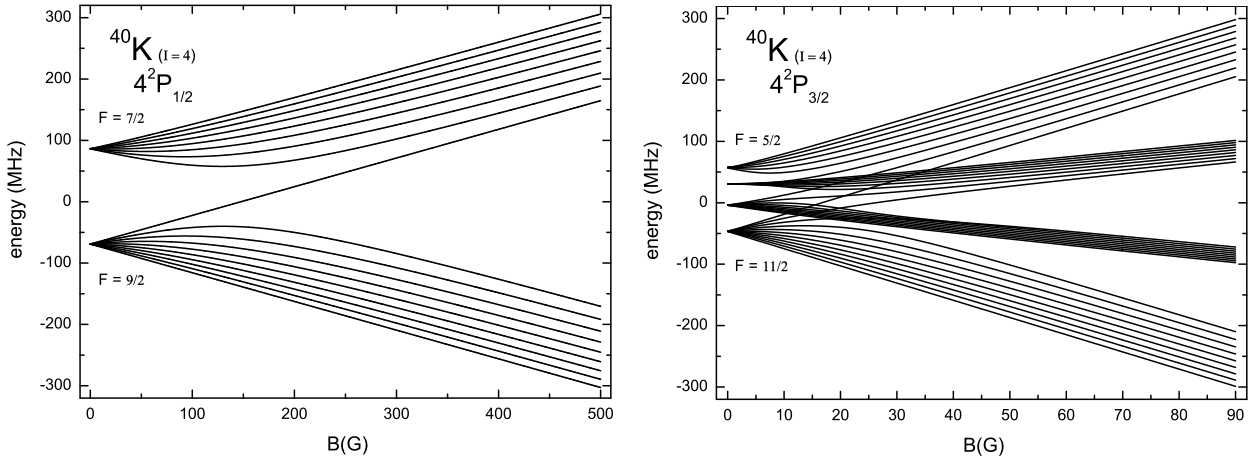

Figure D.3: ^{40}K first excited state $4^2P_{1/2}$ and second excited state $4^2P_{3/2}$ energies as a function of magnetic field. Numerical results obtained with the code in [Geh03a], using the parameters in table D.1.

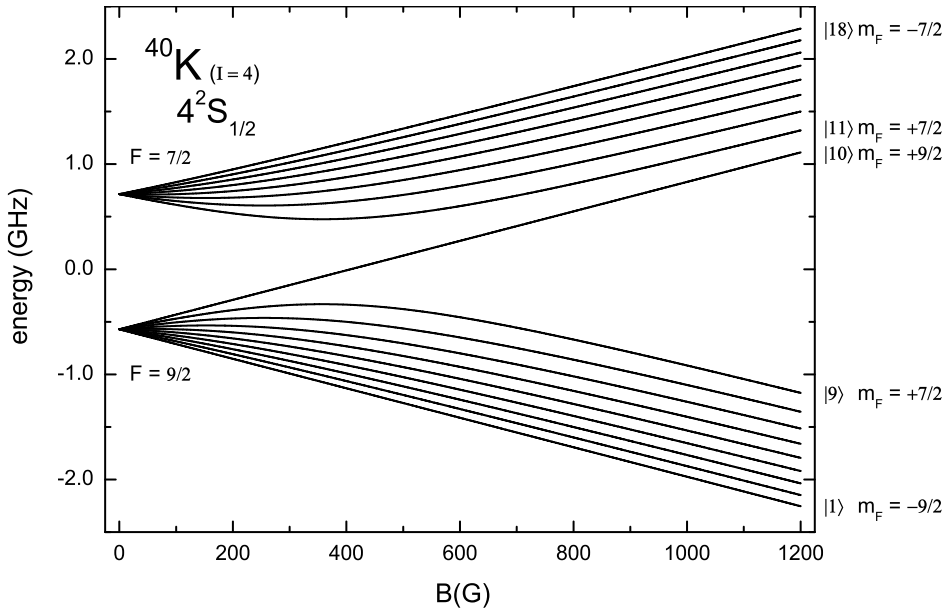

Figure D.4: ^{40}K ground state $4^2S_{1/2}$ energies as a function of magnetic field obtained from equation (D.4), using the parameters in table D.1.

Appendix E

Noise Reduction

We can't solve problems by using the same kind of thinking we used when we created them.

Albert Einstein

Feshbach resonances in the ^{6}Li-^{40}K mixture turned out to be rather narrow, see chapter 2. This makes it a challenge to control the interaction strength precisely in the vicinity of the resonance. One needs a good control over the magnetic field in the mG regime. We have a very stable power supply driven by batteries but additional 50 Hz line noise needs to be compensated. How this is done will be described in this appendix.

The power supply we use for our high-precision measurements is from the company Danfysik (Model 858 with maximum 90/60 A, 5 V output). We upgraded it to get maximum 180 A (by using one winding through the current transducer instead of two or three). It is computer controlled with 18 bit resolution. We can connect it to the Feshbach coils (3.313 G/A) or curvature coils (1.493 G/A) depending on whether we need additional confinement from a magnetic field curvature or not. The current of this power supply is provided by lead acid batteries giving 12 V total (2×EN160-6 and 2×EN100-6 from the company YUASA; each has a capacity of 160 Ah or 100 Ah respectively and gives 6 V nominal voltage; 2×2 in series are connected in parallel). The batteries are charged during MOT loading and evaporation (charging current is limited to 25.5 A at 13.6 V). Afterwards, we ramp linearly the magnetic field from 1180 G to the 155-G Feshbach resonance of Li$|1\rangle$K$|3\rangle$, for example. The power supplies used for evaporation are ramped to zero current while we ramp up the current of the Danfysik power supply. This is possible since the Feshbach or curvature coil can be driven simultaneously by the Danfysik power supply and one of the other power supplies (because they are connected with diodes to the coil). At the field of the resonance all power supplies except the Danfysik power supply are disconnected from the coils with relays. On some power supplies we shorten additionally the output to ensure that no current spike is created when the power supply is reconnected to the coil later.

The Danfysik power supply actively stabilizes the current which is measured with a

sensitive current transducer. The rated stability of the power supply is 3 ppm (parts per million drift within 8 hours) at full current, giving $3\times10^{-6}\times180\,\mathrm{A}=50\,\mathrm{nA}$ which corresponds to a magnetic field stability of $\leq 0.2\,\mathrm{mG}$. This is an impressive number but it turned out that the power supply suffers from several problems: It is very slow and the current has 50 Hz line noise ripples of several 10 mG. It takes typically 2 s to switch on the current from zero to 100 A. This is already much faster than the minimum settle time of 10 s given in the datasheet. This we achieved by the removal of a low-pass filter in the internal control loop. We tried to adjust the PID values but it was difficult because the controller tends to become unstable. Therefore, we left the old values but at currents above 110 A the controller still might start to oscillate. The larger problem are the 50 Hz line ripples. We moved all possible sources of line noise as far away from the atoms as possible but it turned out that the major part of the noise is coming from the Danfysik power supply itself. Although the current for the coils is supplied by batteries, the control electronics is still supplied by line. Moreover, several transformers are inside the housing of the power supply very close to the current transducer. Though the design of the transducer is such that it should be insensitive to external fields, we believe that stray fields can induce the 50 Hz noise into the transducer and control electronics of the supply. Therefore, we unplugged all transformers and feed in the DC voltages needed for the electronics by external power supplies. All fans except one were unplugged. The remaining one was moved outside the housing at the end of a tube through which it blows air into the power supply for cooling. These measures were successful in reducing the 50 Hz line noise but they could not cancel them entirely. It might be that the coils themselves act as an antenna to pick up the line noise. Depending on the current of the Danfysik power supply we measure about 20 to 70 mG (peak-to-peak) noise at 50 to 150 Hz (see below).

An additional ("notch") filter in the control loop could help to damp the induced noise at line frequencies. But this was not tried so far because of the difficulties with the PID. Another solution is to synchronize the experiment with respect to line. Before every experimental run the computer control waits for a line trigger before the experiment is started. This ensures that for each experimental run the line noise, and hence the magnetic field is exactly the same. This method works very well as long as the time spent in the vicinity of the Feshbach resonance is short with respect to 20 ms. But when we were investigating the creation and lifetime of molecules, section 4.6, this approach was not sufficient anymore. One might place one or several sensors close to the atoms to measure the actual field and actively compensate it to a certain value. But this is not very practical since we change the fields frequently. Moreover, it is not easy to find a sensor which does not saturate at the fields we are working and still gives a good sensitivity. Therefore, we decided to measure the noise and compensate it by applying the inverted noise signal with an arbitrary function generator to the atoms.

We drive radio frequency (rf) transitions between Zeeman states of either ^{6}Li or ^{40}K. Here we are not interested in the exact magnitude of the frequency or field (see appendix D) but we vary the delay relative to the line trigger and observe how the frequency of maximum transition varies. From this the magnetic field noise can be calculated easily. In principle the measurement can be done by recording many spectra at different delay times relative to the line trigger. But we can do it faster as will be discussed now.

First we measure a reference spectrum where we vary the frequency at a fixed delay to

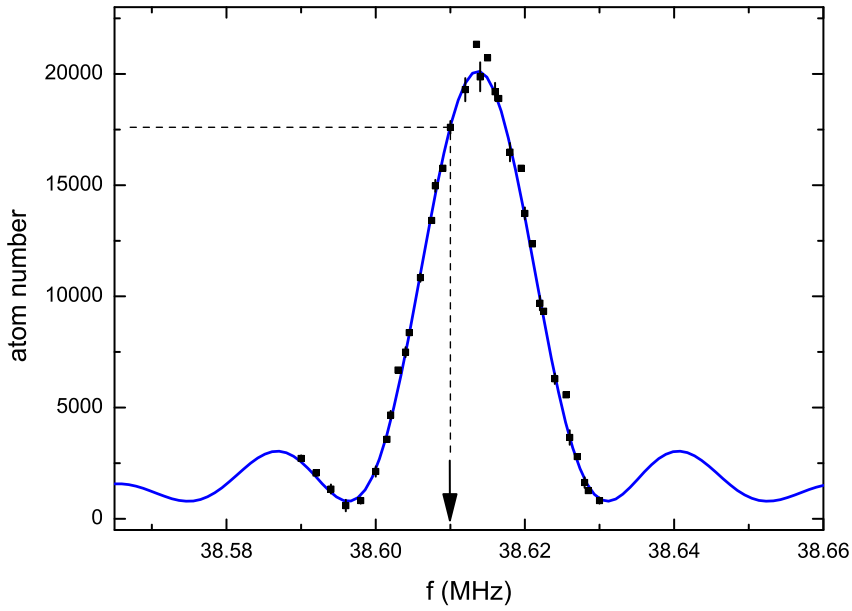

Figure E.1: Reference spectrum (black squares) for an rf pulse on K$|3\rangle \rightarrow |2\rangle$ transition taken without ^{6}Li present. Plotted is the transferred atom number in the K$|2\rangle$ state. The pulse length was t=50 μs. The fit (blue curve) with equation (E.2) gives a center frequency of $f_0 = (38.6138 \pm 0.0001)$ MHz and a Rabi frequency of $\Omega = 2\pi\,(10.1 \pm 0.1) \times 10^3\,\mathrm{s}^{-1}$. The dashed line shows how in figure E.2 the frequency f (arrow) is obtained from the measured atom number. At the field of the maximum transition (154.903±0.001) G the difference in magnetic moment between the K$|2\rangle$ and K$|3\rangle$ states is $\Delta\mu$=195.380 kHz/G. With this the magnetic field noise ΔB in figure E.3 is calculated from the frequency with $\Delta B = (f - f_0)/\Delta\mu$.

the line trigger. A typical spectrum is shown in figure E.1. To understand the spectrum, we consider a two-level system driven with an electrical field at a frequency detuning of $\delta = \omega - \omega_0$ from the atomic transition ω_0. The atom number $N_2(\delta, t)$ of the excited state, which is initially zero, is given by (see for example [Met99]):

$$N_2(\delta, t) \propto \left| -i\frac{\Omega}{\Omega'} \sin\left(\frac{\Omega' t}{2}\right) e^{-i\delta t/2} \right|^2 = \frac{\Omega^2}{\Omega^2 + \delta^2} \sin^2\left(\frac{t}{2}\sqrt{\Omega^2 + \delta^2}\right) . \tag{E.1}$$

The transfered atom number shows Rabi oscillations at a frequency of $\Omega' = \sqrt{\Omega^2 + \delta^2}$ with Ω the Rabi frequency. It depends on the intensity and the wave function overlap of the two states. Experimentally, we adjust the frequency, intensity and pulse length to get maximum transfer. This corresponds to the time $t = \pi/\Omega$ which we insert into equation (E.1) to get the frequency dependency of the Rabi oscillation:

$$N_2(\omega) \propto \frac{\sin^2\left(\frac{\pi}{2}\sqrt{1 + (\frac{\omega - \omega_0}{\Omega})^2}\right)}{1 + (\frac{\omega - \omega_0}{\Omega})^2} . \tag{E.2}$$

In figure E.1 we expect to see such a spectrum which was used in the fit (blue curve) to obtain the frequency of maximum transition and the Rabi frequency. The Rabi frequency should be $\Omega = 2\pi/(2t) = 2\pi \times 10^3\,\mathrm{s}^{-1}$ and matches exactly the result of the fit.

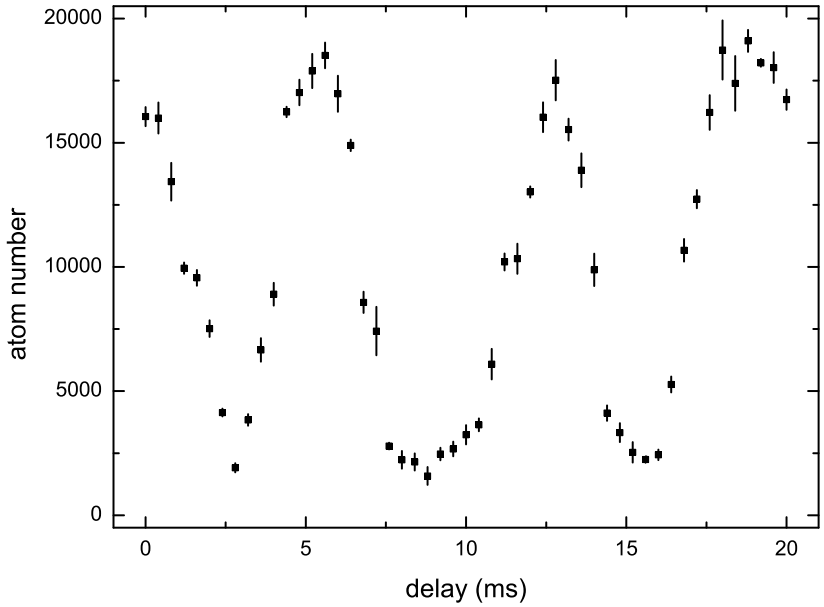

Figure E.2: Measured transferred K$|2\rangle$ atom number for different delay time between line trigger and rf pulse. The pulse frequency is 38.610 MHz (arrow in figure E.1) and the pulse length is 50 μs (as in figure E.1).

For measuring the magnetic field noise we record the transferred atom number for varying delay times relative to the line trigger, see figure E.2. This is done at a fixed radio frequency which we choose typically on one of the slopes of the reference spectrum such that half of the atoms are transferred. But the choice depends on the measured noise and one might need to readjust it. If the field deviation is such that the first zero point or the maximum of the reference spectrum is reached, then the transferred atom number can not be mapped unambiguously to a frequency anymore. These points make a fake signature at the mirror frequency and must be identified. We do this by checking the frequency explicitly at suspicious points or by taking several noise spectra at different pulse frequencies and combine them. To avoid these difficulties one can decrease the pulse length to increase the width of the spectrum. This goes at the expense of reduced resolution but is the simplest method we can recommend. The difference in magnetic moment of ^{6}Li is about half that of ^{40}K at 155 G, so in our experiment we could change to measure the noise with ^{6}Li to increase the span of the observable field noise as well. In the example shown here the frequency of the pulse was chosen to be 38.610 MHz (arrow in figure E.1) where the entire noise spectrum shown in figure E.2 could be recorded at once without any advanced analysis.

From the atom number in the noise spectrum the frequency deviation $\Delta f = f - f_0$ to the pulse frequency f_0 can be calculated easily from the reference spectrum E.1 (dashed lines). This is done numerically with the parameters obtained from the fit with equation (E.2). The difference of the magnetic moment for the K$|2\rangle$ to K$|3\rangle$ state is $\Delta\mu$=195.380 kHz/G which can be calculated from the Breit-Rabi formula discussed in appendix D. With this the magnetic field noise is calculated by $\Delta B = \Delta f/\Delta\mu$ plotted in figure E.3 (black squares).

The result is often noisy such we filtered it by using a fast Fourier transform where we

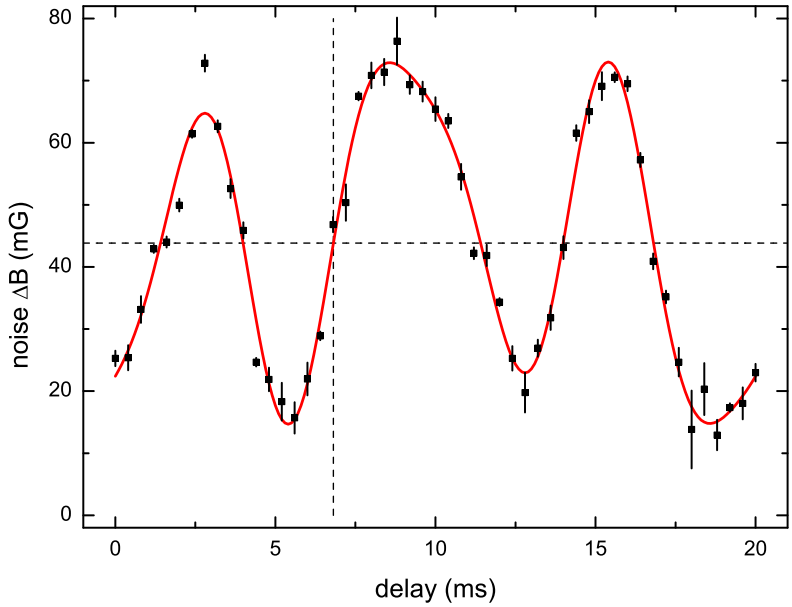

Figure E.3: Magnetic field noise (black squares) calculated from the data in figure E.2 using the reference spectrum in figure E.1. The spectrum is filtered with a fast Fourier transform (red curve) at frequencies of 50 Hz, 100 Hz and 150 Hz. The inverted AC signal is applied to the atoms with an arbitrary function generator to cancel the noise. Dashed lines indicate one zero crossing of the AC signal at 6.811 ms used for adjusting the correct phase as described in the main text.

retain only frequency components of 50 Hz, 100 Hz and 150 Hz (red curve). The noise has 60 mG (peak-to-peak) amplitude with the main frequency component at 150 Hz. Note that the amplitude and frequency depends on the current of the Danfysik power supply. The shown noise is typical for a current of around 104 A needed for the curvature coil to reach the 155-G resonance. If the power supply is connected with the Feshbach coil we need only around 47 G to reach this resonance. At this current the noise is generally smaller (20 mG peak-to-peak) and only 50 Hz noise is present.

We take the measured and filtered noise signal and feed it inverted and without DC offset into an arbitrary function generator connected to an additional coil (anti-curvature coil). This field is permanently switched on and compensates the line noise. The calibration of the coil we have done by using rf transitions again. The function generator is phase locked to line. This is done with a 3 MHz signal, phase locked to the 50 Hz line, which is used as the clock input for a "direct digital synthesizer" (DDS). The DDS generates the 10 MHz needed as the reference signal for the function generator (we are currently building a new phase-locked loop/PLL circuit which gives us the 10 MHz directly without the need of a DDS). We still have to adjust the correct phase for our compensation signal. We trigger an oscilloscope on our rf pulse (detected by a pick up coil) where the delay of the pulse relative to the line trigger is set such that the compensation signal should have a zero crossing at the same time. In figure E.3 a good delay would be at 6.811 ms indicated by the dashed lines. We adjust the phase of the compensation signal such that the zero crossing coincides with the rf

pulse. Since the pulse has a certain length and does not show a perfect square shape in time, we can not perfectly adjust the phase. Because of this reason and due to the noise in the measurements, the compensation can not cancel the noise entirely. Therefore, we measure the residual noise with the compensation switched on, often with a longer pulse to increase the resolution. We check if the compensation works well and usually the entire procedure had to be repeated again with the residual noise added to the initial compensation.

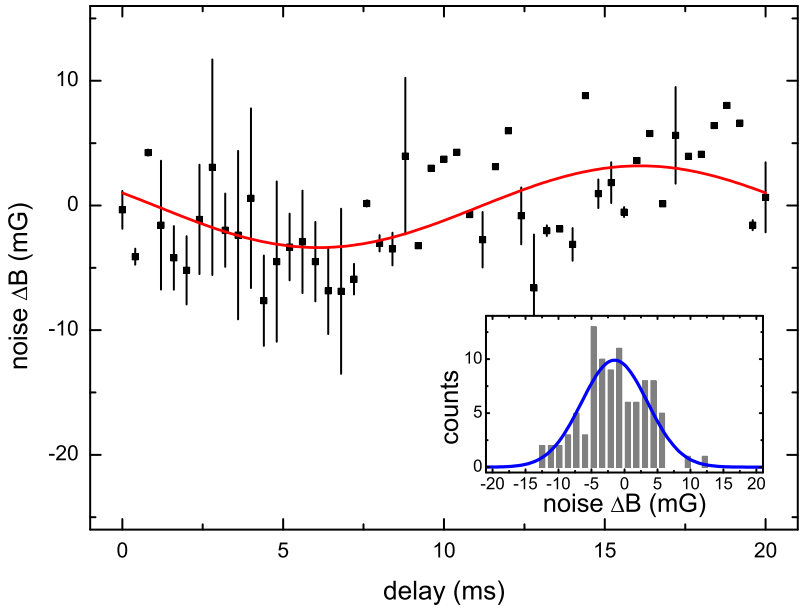

Figure E.4: Residual noise after two iterations of noise corrections. A 50 Hz noise amplitude of about 7 mG (peak-to-peak) is still present. Other noise components are mainly random. Data points without error are measured only once. The inset shows a histogram of the (non-averaged) residual noise. It is fitted with a Gaussian (blue) of a width of 5 mG. The peak-to-peak (95%) noise is 20 mG.

Figure E.4 shows the residual noise (black squares) measured after the 2^{nd} iteration of compensations. A small 7 mG peak-to-peak residual 50 Hz noise component (red curve) is still visible but random fluctuations dominate the spectrum. The histogram of the (non-averaged) residual noise is shown in the inset of the figure. A Gaussian fitted to the histogram (blue curve) gives a peak-to-peak noise of 20 mG ($4\,\sigma \propto 95\%$). This shows the limitations of the used method. Random fluctuations and changes in the amplitude of the noise can not be canceled. When the Danfysik power supply is connected to the Feshbach coil the random fluctuations are smaller in the order of about 10 mG (peak-to-peak).

We showed our method to measure the line noise and how to compensate it. We can reduce the noise amplitude to below 20 mG where we are limited by random fluctuations. Since the main noise component is induced by the Danyfysik power supply we should consider to improve the shielding of this power supply or the current transducer. Improving the PID settings and inserting a 50 Hz line filter in the control loop might reduce the noise significantly. This could help as well to stabilize the control loop which in turn might allow to increase the speed of the power supply.

The upgrade of the Danfysik power supply has been carried out by Devang Naik, Gerhard Hendl and Florian Schreck. The compensation was done by the author.

Bibliography

[All38] J. Allen and A. Misener, *Flow of liquid Helium II*, Nature **141**, 75 (1938).

[Alt07a] A. Altmeyer, S. Riedl, C. Kohstall, M. J. Wright, R. Geursen, M. Bartenstein, C. Chin, J. Hecker Denschlag, and R. Grimm, *Precision Measurements of Collective Oscillations in the BEC-BCS Crossover*, Phys. Rev. Lett. **98**, 040401 (2007).

[Alt07b] A. Altmeyer, S. Riedl, M. J. Wright, C. Kohstall, J. Hecker Denschlag, and R. Grimm, *Dynamics of a strongly interacting Fermi gas: The radial quadrupole mode*, Phys. Rev. A **76**, no. 3, 033610 (2007).

[And95] M. H. Anderson, J. R. Ensher, M. R. Matthews, C. E. Wieman, and E. A. Cornell, *Observation of Bose-Einstein condensation in dilute atomic vapor*, Science **269**, 198 (1995).

[Ari77] E. Arimondo, M. Inguscio, and P. Violino, *Experimental determinations of the hyperfine structure in the alkali atoms*, Rev. Mod. Phys. **49**, 31 (1977).

[AS01] J. R. Abo-Shaeer, C. Raman, J. M. Vogels, and W. Ketterle, *Observation of Vortex Lattices in Bose-Eeinstein Condensates*, Science **292**, 476 (2001).

[Aym05] M. Aymar and O. Dulieu, *Calculation of accurate permanent dipole moments of the lowest $^{1,3}\Sigma^+$ states of heteronuclear alkali dimers using extended basis sets*, J. Chem. Phys. **122**, 204302 (2005).

[Baa10] J. E. Baarsma, K. B. Gubbels, and H. T. C. Stoof, *Population and mass imbalance in atomic Fermi gases*, Phys. Rev. A **82**, 013624 (2010).

[Bar98] R. Barnfield, *An Ode ('As it fell upon a Day') from 'Poems: In divers humors', published with 'The Encomion of Lady Pecunia: or The praise of Money'*, London (1598), see e.g. http://www.archive.org/details/completepoemsofr00barnrich.

[Bar57a] J. Bardeen, L. N. Cooper, and J. R. Schrieffer, *Microscopic Theory of Superconductivity*, Phys. Rev. **106**, 162 (1957).

[Bar57b] J. Bardeen, L. N. Cooper, and J. R. Schrieffer, *Theory of Superconductivity*, Phys. Rev. **108**, 1175 (1957).

[Bar04a] M. Bartenstein, A. Altmeyer, S. Riedl, S. Jochim, C. Chin, J. Hecker Denschlag, and R. Grimm, *Collective Excitations of a Degenerate Gas at the BEC-BCS Crossover*, Phys. Rev. Lett. **92**, 203201 (2004).

[Bar04b] M. Bartenstein, A. Altmeyer, S. Riedl, S. Jochim, C. Chin, J. Hecker Denschlag, and R. Grimm, *Crossover from a Molecular Bose-Einstein Condensate to a Degenerate Fermi Gas*, Phys. Rev. Lett. **92**, 120401 (2004).

[Bar08] M. A. Baranov, C. Lobo, and G. V. Shlyapnikov, *Superfluid pairing between fermions with unequal masses*, Phys. Rev. A **78**, 033620 (2008).

[Bar09] G. Barontini, C. Weber, F. Rabatti, J. Catani, G. Thalhammer, M. Inguscio, and F. Minardi, *Observation of heteronuclear atomic Efimov resonances*, Phys. Rev. Lett. **103**, no. 4, 043201 (2009).

[Bau09] I. Bausmerth, A. Recati, and S. Stringari, *Chandrasekhar-Clogston limit and phase separation in Fermi mixtures at unitarity*, Phys. Rev. A **79**, 043622 (2009).

[Bea97] I. G. Bearden *et al.*, *Collective expansion in high energy heavy ion collisions*, Phys. Rev. Lett. **78**, 2080 (1997).

[Blo08] I. Bloch, J. Dalibard, and W. Zwerger, *Many-body physics with ultracold gases*, Rev. Mod. Phys. **80**, 885 (2008).

[Boh99] J. L. Bohn and P. S. Julienne, *Semianalytic theory of laser-assisted resonant cold collisions*, Phys. Rev. A **60**, 414 (1999).

[Bos24] S. Bose, *Plancks Gesetz und Lichtquantenhypothese*, Z. Phys. **26**, 178 (1924).

[Bou03] T. Bourdel, J. Cubizolles, L. Khaykovich, K. M. F. Magalhães, S. J. J. M. F. Kokkelmans, G. V. Shlyapnikov, and C. Salomon, *Measurement of the Interaction Energy near a Feshbach Resonance in a ^{6}Li Fermi Gas*, Phys. Rev. Lett. **91**, 020402 (2003).

[Bou04] T. Bourdel, L. Khaykovich, J. Cubizolles, J. Zhang, F. Chevy, M. Teichmann, L. Tarruell, S. J. J. M. F. Kokkelmans, and C. Salomon, *Experimental Study of the BEC-BCS Crossover Region in Lithium 6*, Phys. Rev. Lett. **93**, 050401 (2004).

[Bra95] C. C. Bradley, C. A. Sackett, J. J. Tollett, and R. G. Hulet, *Evidence of Bose-Einstein condensation in an atomic gas with attractive interactions*, Phys. Rev. Lett. **75**, 1687 (1995).

[Bra07] P. Braun-Munzinger and J. Stachel, *The quest for the quark-gluon plasma*, Nature **448**, 302 (2007).

[Bre31] G. Breit and I. Rabi, *Measurement of Nuclear Spin*, Phys. Rev. **38**, 2082 (1931).

[Cao11] C. Cao, E. Elliott, J. Joseph, H. Wu, J. Petricka, T. Schäfer, and J. E. Thomas, *Universal Quantum Viscosity in a Unitary Fermi Gas*, Science **331**, 58 (2011).

[Che05a] Q. Chen, J. Stajic, S. Tan, and K. Levin, *BCS-BEC Crossover: From High Temperature Superconductors to Ultracold Superfluids*, Phys. Rep. **412**, 1 (2005).

[Che05b] F. Chevy, E. G. M. van Kempen, T. Bourdel, J. Zhang, L. Khaykovich, M. Teichmann, L. Tarruell, S. J. J. M. F. Kokkelmans, and C. Salomon, *Resonant scattering properties close to a p-wave Feshbach resonance*, Phys. Rev. A **71**, no. 6, 062710 (2005).

[Che09] Q. Chen, Y. He, C.-C. Chien, and K. Levin, *Theory of radio frequency spectroscopy experiments in ultracold Fermi gases and their relation to photoemission in the cuprates*, Rep. Prog. Phys. **72**, 122501 (2009).

[Che10] F. Chevy and C. Mora, *Ultra-cold polarized Fermi gases*, Rep. Prog. Phys. **73**, 112401 (2010).

[Chi04] C. Chin, M. Bartenstein, A. Altmeyer, S. Riedl, S. Jochim, J. Hecker Denschlag, and R. Grimm, *Observation of the Pairing Gap in a Strongly Interacting Fermi Gas*, Science **305**, 1128 (2004).

[Chi10] C. Chin, R. Grimm, P. S. Julienne, and E. Tiesinga, *Feshbach resonances in ultracold gases*, Rev. Mod. Phys. **82**, 1225 (2010).

[Coo56] L. N. Cooper, *Bound Electron Pairs in a Degenerate Fermi Gas*, Phys. Rev. **104**, 1189 (1956).

[Cos10] L. Costa, J. Brachmann, A.-C. Voigt, C. Hahn, M. Taglieber, T. W. Hänsch, and K. Dieckmann, *s-wave interaction in a two-species Fermi-Fermi mixture at a narrow Feshbach resonance*, Phys. Rev. Lett. **105**, 123201 (2010), *ibid.* **105**, 269904(E) (2010).

[Cou98] P. Courteille, R. S. Freeland, D. J. Heinzen, F. A. van Abeelen, and B. J. Verhaar, *Observation of a Feshbach Resonance in Cold Atom Scattering*, Phys. Rev. Lett. **81**, 69 (1998).

[Cra01] S. G. Crane, S. J. Brice, A. Goldschmidt, R. Guckert, A. Hime, J. J. Kitten, D. J. Vieira, and X. Zhao, *Parity Violation Observed in the Beta Decay of Magnetically Trapped ^{82}Rb Atoms*, Phys. Rev. Lett. **86**, 2967 (2001).

[Cub03] J. Cubizolles, T. Bourdel, S. J. J. M. F. Kokkelmans, G. V. Shlyapnikov, and C. Salomon, *Production of Long-Lived Ultracold Li_2 Molecules from a Fermi Gas*, Phys. Rev. Lett. **91**, 240401 (2003).

[Dan10] J. G. Danzl, M. J. Mark, E. Haller, M. Gustavsson, R. Hart, J. Aldegunde, J. M. Hutson, and H.-C. Nägerl, *An ultracold high-density sample of rovibronic ground-state molecules in an optical lattice*, Nature Phys. **6**, 265 (2010).

[Dav95] K. B. Davis, M. O. Mewes, M. R. Andrews, N. J. van Druten, D. S. Durfee, D. M. Kurn, and W. Ketterle, *Bose-Einstein condensation in a gas of sodium atoms*, Phys. Rev. Lett. **75**, 3969 (1995).

[Del10] D. van Delft and P. Kes, *The discovery of Superconductivity*, Phys. Today **63**, no. 9, 38 (2010).

[DeM99] B. DeMarco and D. S. Jin, *Onset of Fermi Degeneracy in a Trapped Atomic Gas*, Science **285**, 1703 (1999).

[Der01] A. Derevianko, J. F. Babb, and A. Dalgarno, *High-precision calculations of van der Waals coefficients for heteronuclear alkali-metal dimers*, Phys. Rev. A **63**, 052704 (2001).

[DeS10] B. J. DeSalvo, M. Yan, P. G. Mickelson, Y. N. Martinez de Escobar, and T. C. Killian, *Degenerate Fermi Gas of* ^{87}Sr, Phys. Rev. Lett. **105**, no. 3, 030402 (2010).

[D'I05] J. P. D'Incao and B. D. Esry, *Scattering length scaling laws for ultracold three-body collisions*, Phys. Rev. Lett. **94**, 213201 (2005).

[D'I08] J. P. D'Incao and B. D. Esry, *Suppression of molecular decay in ultracold gases without Fermi statistics*, Phys. Rev. Lett. **100**, 163201 (2008).

[Die02] K. Dieckmann, C. A. Stan, S. Gupta, Z. Hadzibabic, C. H. Schunck, and W. Ketterle, *Decay of an Ultracold Fermionic Lithium Gas near a Feshbach Resonance*, Phys. Rev. Lett. **89**, 203201 (2002).

[Die10] R. B. Diener and M. Randeria, *BCS-BEC crossover with unequal-mass fermions*, Phys. Rev. A **81**, 033608 (2010).

[Du08] X. Du, L. Luo, B. Clancy, and J. E. Thomas, *Observation of anomalous spin segregation in a trapped Fermi gas*, Phys. Rev. Lett. **101**, 150401 (2008).

[Du09] X. Du, Y. Zhang, and J. E. Thomas, *Inelastic Collisions of a Fermi Gas in the BEC-BCS Crossover*, Phys. Rev. Lett. **102**, no. 25, 250402 (2009).

[Eag69] D. M. Eagles, *Possible pairing without superconductivity at low carrier concentrations in bulk and thin-film superconducting semiconductors*, Phys. Rev. **186**, 456 (1969).

[Efi70] V. Efimov, *Energy levels arising from resonant two-body forces in a three-body system*, Phys. Lett. B **33**, 563 (1970).

[Ein24] A. Einstein, *Quantentheorie des einatomigen idealen Gases*, Sitzungsber. Kgl. Preuss. Akad. Wiss., Phys.-Math. Kl. vom 10. Juli, pp. 261–267 (1924).

[Ein25] A. Einstein, *Quantentheorie des einatomigen idealen Gases. Zweite Abhandlung.*, Sitzungsber. Kgl. Preuss. Akad. Wiss., Phys.-Math. Kl. vom 8. Januar, pp. 3–14 (1925).

[Eng97] J. R. Engelbrecht, M. Randeria, and C. A. R. Sá de Melo, *BCS to Bose Crossover: Broken-Symmetry State*, Phys. Rev. B **55**, 15153 (1997).

[Esr01] B. D. Esry, C. H. Greene, and H. Suno, *Threshold laws for three-body recombination*, Phys. Rev. A **65**, 010705 (2001).

[Fal08] S. Falke, H. Knöckel, J. Friebe, M. Riedmann, E. Tiemann, and C. Lisdat, *Potassium ground-state scattering parameters and Born-Oppenheimer potentials from molecular spectroscopy*, Phys. Rev. A **78**, 012503 (2008).

[Fed96] P. O. Fedichev, Y. Kagan, G. V. Shlyapnikov, and J. T. M. Walraven, *Influence of nearly resonant light on the scattering length in low-temperature atomic gases*, Phys. Rev. Lett. **77**, 2913 (1996).

[Fei09] A. E. Feiguin and M. P. A. Fisher, *Exotic paired states with anisotropic spin-dependent Fermi surfaces*, Phys. Rev. Lett. **103**, 025303 (2009).

[Fer02] G. Ferrari, M. Inguscio, W. Jastrzebski, G. Modugno, G. Roati, and A. Simoni, *Collisional properties of ultracold K-Rb mixtures*, Phys. Rev. Lett. **89**, 053202 (2002).

[Fer03] F. Ferlaino, R. J. Brecha, P. Hannaford, F. Riboli, G. Roati, G. Modugno, and M. Inguscio, *Bipolar oscillations in a quantum degenerate Fermi-Bose atomic mixture*, J. Opt. B: Quantum Semiclass. Opt. **5**, S3 (2003).

[Fer06] F. Ferlaino, C. D'Errico, G. Roati, M. Zaccanti, M. Inguscio, G. Modugno, and A. Simoni, *Feshbach spectroscopy of a K-Rb atomic mixture*, Phys. Rev. A **73**, 040702 (2006).

[Fer09] F. Ferlaino, S. Knoop, and R. Grimm, *Ultracold Feshbach molecules*, in R. V. Krems, B. Friedrich, and W. C. Stwalley (Eds.), *Cold Molecules: Theory, Experiment, Applications*, arXiv:0809.3920 (2009).

[For05] M. M. Forbes, E. Gubankova, W. V. Liu, and F. Wilczek, *Stability criteria for breached-pair superfluidity*, Phys. Rev. Lett. **94**, 017001 (2005).

[Frö11] B. Fröhlich, M. Feld, E. Vogt, M. Koschorreck, W. Zwerger, and M. Köhl, *Radio-Frequency Spectroscopy of a Strongly Interacting Two-Dimensional Fermi Gas*, Phys. Rev. Lett. **106**, 105301 (2011).

[Fuc07] J. Fuchs, G. J. Duffy, G. Veeravalli, P. Dyke, M. Bartenstein, C. J. Vale, P. Hannaford, and W. J. Rowlands, *Molecular BoseEinstein condensation in a versatile low power crossed dipole trap*, J. Phys. B: At. Mol. Opt. Phys. **40**, 4109 (2007).

[Fuc08] J. Fuchs, C. Ticknor, P. Dyke, G. Veeravalli, E. Kuhnle, W. Rowlands, P. Hannaford, and C. J. Vale, *Binding energies of ^{6}Li p-wave Feshbach molecules*, Phys. Rev. A **77**, 053616 (2008).

[Fuk07] T. Fukuhara, Y. Takasu, M. Kumakura, and Y. Takahashi, *Degenerate Fermi gases of ytterbium*, Phys. Rev. Lett. **98**, 030401 (2007).

[Fuk09] T. Fukuhara, S. Sugawa, Y. Takasu, and Y. Takahashi, *All-optical formation of quantum degenerate mixtures*, Phys. Rev. A **79**, 021601(R) (2009).

[Ful64] P. Fulde and R. A. Ferrell, *Superconductivity in a Strong Spin-Exchange Field*, Phys. Rev. **135**, no. 3A, A550 (1964).

[Gae07] J. P. Gaebler, J. T. Stewart, J. L. Bohn, and D. S. Jin, *p-wave Feshbach molecules*, Phys. Rev. Lett. **98**, 200403 (2007).

[Gae10] J. P. Gaebler, J. T. Stewart, T. E. Drake, D. S. Jin, A. Perali, P. Pieri, and G. C. Strinati, *Observation of pseudogap behaviour in a strongly interacting Fermi gas*, Nature Phys. **6**, 569 (2010).

[Geh03a] M. E. Gehm, *Preparation of an Optically-Trapped Degenerate Fermi Gas of ^{6}Li: Finding the Route to Degeneracy*, Ph.D. thesis, Duke University, Durham, North Carolina (2003).

[Geh03b] M. E. Gehm, S. L. Hemmer, S. R. Granade, K. M. O'Hara, and J. E. Thomas, *Mechanical stability of a strongly interacting Fermi gas of atoms*, Phys. Rev. A **68**, 011401 (2003).

[Gel05] B. A. Gelman, E. V. Shuryak, and I. Zahed, *Ultracold strongly coupled gas: A near-ideal liquid*, Phys. Rev. A **72**, 043601 (2005).

[Gen01] S. D. Gensemer and D. S. Jin, *Transition from collisionless to hydrodynamic behavior in an ultracold Fermi gas*, Phys. Rev. Lett. **87**, 173201 (2001).

[Gez08] A. Gezerlis and J. Carlson, *Strongly paired fermions: Cold atoms and neutron matter*, Phys. Rev. C **77**, 032801(R) (2008).

[Gez09] A. Gezerlis, S. Gandolfi, K. E. Schmidt, and J. Carlson, *Heavy-light fermion mixtures at unitarity*, Phys. Rev. Lett. **103**, 060403 (2009).

[Gio08] S. Giorgini, L. P. Pitaevskii, and S. Stringari, *Theory of ultracold atomic Fermi gases*, Rev. Mod. Phys. **80**, 1215 (2008).

[Gra02] S. R. Granade, M. E. Gehm, K. M. O'Hara, and J. E. Thomas, *All-Optical Production of a Degenerate Fermi Gas*, Phys. Rev. Lett. **88**, 120405 (2002).

[Gre03] M. Greiner, C. A. Regal, and D. S. Jin, *Emergence of a Molecular Bose-Einstein Condensate from a Fermi Gas*, Nature **426**, 537 (2003).

[Gri93] G. F. Gribakin and V. V. Flambaum, *Calculation of the scattering length in atomic collisions using the semiclassical approximation*, Phys. Rev. A **48**, 546 (1993).

[Gri00] R. Grimm, M. Weidemüller, and Y. B. Ovchinnikov, *Optical dipole traps for neutral atoms*, Adv. At. Mol. Opt. Phys. **42**, 95 (2000).

[Gri08] R. Grimm, *Ultracold Fermi gases in the BEC-BCS crossover: A review from the Innsbruck perspective*, in Inguscio *et al.* [Ing08], 413–462.

[Gro09] N. Gross, Z. Shotan, S. Kokkelmans, and L. Khaykovich, *Observation of universality in ultracold ^{7}Li three-body recombination*, Phys. Rev. Lett. **103**, 163202 (2009).

[Gro10] N. Gross, Z. Shotan, S. Kokkelmans, and L. Khaykovich, *Nuclear-Spin-Independent Short-Range Three-Body Physics in Ultracold Atoms*, Phys. Rev. Lett. **105**, 103203 (2010).

[Gub03] E. Gubankova, W. V. Liu, and F. Wilczek, *Breached Pairing Superfluidity: Possible Realization in QCD*, Phys. Rev. Lett. **91**, 032001 (2003).

[Gub09] K. B. Gubbels, J. E. Baarsma, and H. T. C. Stoof, *Lifshitz Point in the Phase Diagram of Resonantly Interacting 6Li-40K Mixtures*, Phys. Rev. Lett. **103**, 195301 (2009).

[Gün05] K. Günter, T. Stöferle, H. Moritz, M. Köhl, and T. Esslinger, *p-Wave Interactions in Low-Dimensional Fermionic Gases*, Phys. Rev. Lett. **95**, 230401 (2005).

[Gup03] S. Gupta, Z. Hadzibabic, M. W. Zwierlein, C. A. Stan, K. Dieckmann, C. H. Schunck, E. G. M. van Kempen, B. J. Verhaar, and W. Ketterle, *Radio-Frequency Spectroscopy of Ultracold Fermions*, Science **300**, 1723 (2003).

[Had02] Z. Hadzibabic, C. A. Stan, K. Dieckmann, S. Gupta, M. W. Zwierlein, A. Görlitz, and W. Ketterle, *Two-Species Mixture of Quantum Degenerate Bose and Fermi Gases*, Phys. Rev. Lett. **88**, 160401 (2002).

[Han07] T. M. Hanna, T. Köhler, and K. Burnett, *Association of molecules using a resonantly modulated magnetic field*, Phys. Rev. A **75**, no. 1, 013606 (2007).

[Han09] T. M. Hanna, E. Tiesinga, and P. S. Julienne, *Prediction of Feshbach resonances from three input parameters*, Phys. Rev. A **79**, 040701 (2009).

[Hei01] H. Heiselberg, *Fermi systems with long scattering lengths*, Phys. Rev. A **63**, 043606 (2001).

[HM10] F. Heidrich-Meisner, A. E. Feiguin, U. Schollwöck, and W. Zwerger, *BCS-BEC crossover and the disappearance of Fulde-Ferrell-Larkin-Ovchinnikov correlations in a spin-imbalanced one-dimensional Fermi gas*, Phys. Rev. A **81**, 023629 (2010).

[Ho04] T.-L. Ho, *Universal Thermodynamics of Degenerate Quantum Gases in the Unitarity Limit*, Phys. Rev. Lett. **92**, 090402 (2004).

[Hod05] E. Hodby, S. T. Thompson, C. A. Regal, M. Greiner, A. C. Wilson, D. S. Jin, E. A. Cornell, and C. E. Wieman, *Production efficiency of ultracold Feshbach molecules in bosonic and fermionic systems*, Phys. Rev. Lett. **94**, 120402 (2005).

[Hu07] H. Hu, P. D. Drummond, and X.-J. Liu, *Universal thermodynamics of strongly interacting Fermi gases*, Nature Phys. **3**, 469 (2007).

[Huc09] J. H. Huckans, J. R. Williams, E. L. Hazlett, R. W. Stites, and K. M. O'Hara, *Three-body recombination in a three-state Fermi gas with widely tunable interactions*, Phys. Rev. Lett. **102**, no. 16, 165302 (2009).

[Hut07] J. M. Hutson, *Feshbach resonances in the presence of inelastic scattering: threshold behavior and suppression of poles in scattering lengths*, New J. Phys. **9**, 152 (2007).

[Ina08] Y. Inada, M. Horikoshi, S. Nakajima, M. Kuwata-Gonokami, M. Ueda, and T. Mukaiyama, *Critical Temperature and Condensate Fraction of a Fermion Pair Condensate*, Phys. Rev. Lett. **101**, 180406 (2008).

[Ing08] M. Inguscio, W. Ketterle, and C. Salomon (Eds.), *Ultracold Fermi gases, Proceedings of the international school of physics "Enrico Fermi", Course CLXIV, Varenna, June 2006*, IOS Press, Amsterdam (2008).

[Ino98] S. Inouye, M. R. Andrews, J. Stenger, H.-J. Miesner, D. M. Stamper-Kurn, and W. Ketterle, *Observation of Feshbach resonances in a Bose-Einstein condensate*, Nature **392**, 151 (1998).

[Ino04] S. Inouye, J. Goldwin, M. L. Olsen, C. Ticknor, J. L. Bohn, and D. S. Jin, *Observation of Heteronuclear Feshbach Resonances in a Mixture of Bosons and Fermions*, Phys. Rev. Lett. **93**, 183201 (2004).

[Isk06] M. Iskin and C. A. R. Sá de Melo, *Two-Species Fermion Mixtures with Population Imbalance*, Phys. Rev. Lett. **97**, 100404 (2006).

[Isk07] M. Iskin and C. A. R. Sá de Melo, *Superfluid and Insulating Phases of Fermion Mixtures in Optical Lattices*, Phys. Rev. Lett. **99**, 080403 (2007).

[Isk08] M. Iskin and C. J. Williams, *Trap-imbalanced fermion mixtures*, Phys. Rev. A **77**, 013605 (2008).

[Jac10] B. Jacak and P. Steinberg, *Creating the perfect liquid in heavy-ion collisions*, Phys. Today **63**, no. 5, 39 (2010).

[Jo09] G.-B. Jo, Y.-R. Lee, J.-H. Choi, C. A. Christensen, T. H. Kim, J. H. Thywissen, D. E. Pritchard, and W. Ketterle, *Itinerant Ferromagnetism in a Fermi Gas of Ultracold Atoms*, Science **325**, 1521 (2009).

[Joc03a] S. Jochim, M. Bartenstein, A. Altmeyer, G. Hendl, C. Chin, J. Hecker Denschlag, and R. Grimm, *Pure Gas of Optically Trapped Molecules Created from Fermionic Atoms*, Phys. Rev. Lett **91**, 240402 (2003).

[Joc03b] S. Jochim, M. Bartenstein, A. Altmeyer, G. Hendl, S. Riedl, C. Chin, J. Hecker Denschlag, and R. Grimm, *Bose-Einstein Condensation of Molecules*, Science **302**, 2101 (2003).

[Joc04] S. Jochim, *Bose-Einstein Condensation of Molecules*, Ph.D. thesis, Innsbruck University (2004).

[Joh10] C. V. Johnson and P. Steinberg, *What black holes teach about strongly coupled particles*, Phys. Today **63**, no. 5, 29 (2010).

[Jos07] J. Joseph, B. Clancy, L. Luo, J. Kinast, A. Turlapov, and J. E. Thomas, *Measurement of Sound Velocity in a Fermi Gas near a Feshbach Resonance*, Phys. Rev. Lett. **98**, 170401 (2007).

[Kap38] P. Kapitza, *Viscosity of liquid Helium below the λ-point*, Nature **141**, 74 (1938).

[Ket08] W. Ketterle and M. W. Zwierlein, *Making, probing and understanding ultracold Fermi gases*, in Inguscio *et al.* [Ing08], 95–287, see also arXiv:0801.2500v1.

[Kin04a] J. Kinast, S. L. Hemmer, M. E. Gehm, A. Turlapov, and J. E. Thomas, *Evidence for Superfluidity in a Resonantly Interacting Fermi Gas*, Phys. Rev. Lett. **92**, 150402 (2004).

[Kin04b] J. Kinast, A. Turlapov, and J. E. Thomas, *Breakdown of Hydrodynamics in the Radial Breathing Mode of a Strongly Interacting Fermi Gas*, Phys. Rev. A **70**, 051401(R) (2004).

[Kin05a] J. Kinast, A. Turlapov, and J. E. Thomas, *Damping of a Unitary Fermi Gas*, Phys. Rev. Lett. **94**, 170404 (2005).

[Kin05b] J. Kinast, A. Turlapov, J. E. Thomas, Q. Chen, J. Stajic, and K. Levin, *Heat Capacity of a Strongly Interacting Fermi Gas*, Science **307**, 1296 (2005).

[Kno09] S. Knoop, F. Ferlaino, M. Mark, M. Berninger, H. Schöbel, H.-C. Nägerl, and R. Grimm, *Observation of an Efimov-like trimer resonance in ultracold atom-dimer scattering*, Nature Phys. **5**, 227 (2009).

[Kno11] S. Knoop, T. Schuster, R. Scelle, A. Trautmann, J. Appmeier, M. K. Oberthaler, E. Tiesinga, and E. Tiemann, *Feshbach spectroscopy and analysis of the interaction potentials of ultracold sodium*, Phys. Rev. A **83**, 042704 (2011).

[Köh05] T. Köhler, E. Tiesinga, and P. S. Julienne, *Spontaneous Dissociation of Long-Range Feshbach Molecules*, Phys. Rev. Lett. **94**, no. 2, 020402 (2005).

[Köh06] T. Köhler, K. Góral, and P. S. Julienne, *Production of cold molecules via magnetically tunable Feshbach resonances*, Rev. Mod. Phys. **78**, 1311 (2006).

[Kra06] T. Kraemer, M. Mark, P. Waldburger, J. G. Danzl, C. Chin, B. Engeser, A. D. Lange, K. Pilch, A. Jaakkola, H.-C. Nägerl, and R. Grimm, *Evidence for Efimov quantum states in an ultracold gas of caesium atoms*, Nature **440**, 315 (2006).

[Kuh10] E. D. Kuhnle, H. Hu, X.-J. Liu, P. Dyke, M. Mark, P. D. Drummond, P. Hannaford, and C. J. Vale, *Universal Behavior of Pair Correlations in a Strongly Interacting Fermi Gas*, Phys. Rev. Lett. **105**, 070402 (2010).

[Kuh11] E. D. Kuhnle, S. Hoinka, P. Dyke, H. Hu, P. Hannaford, and C. J. Vale, *Temperature Dependence of the Universal Contact Parameter in a Unitary Fermi Gas*, Phys. Rev. Lett. **106**, 170402 (2011).

[Lan08] F. Lang, K. Winkler, C. Strauss, R. Grimm, and J. Hecker Denschlag, *Ultracold Triplet Molecules in the Rovibrational Ground State*, Phys. Rev. Lett. **101**, 133005 (2008).

[Lan09] A. D. Lange, K. Pilch, A. Prantner, F. Ferlaino, B. Engeser, H.-C. Nägerl, R. Grimm, and C. Chin, *Determination of atomic scattering lengths from measurements of molecular binding energies near Feshbach resonances*, Phys. Rev. A **79**, 013622 (2009).

[Lar65] A. I. Larkin and Y. N. Ovchinnikov, *Inhomogeneous state of superconductors*, Sov. Phys. JETP **20**, 762 (1965).

[Leg80] A. J. Leggett, in A. Pekalski and R. Przystawa (Eds.), *Modern Trends in the Theory of Condensed Matter*, volume 115 of *Lecture Notes in Physics*, 13, Springer Verlag, Berlin (1980).

[Leg01] A. J. Leggett, *Bose-Einstein condensation in the alkali gases: Some fundamental concepts*, Rev. Mod. Phys. **73**, 307 (2001).

[Leg06] A. J. Leggett, *Quantum Liquids: Bose Condensation and Cooper Pairing in Condensed-matter Systems*, Oxford University Press, Oxford (2006).

[Lev09] J. Levinsen, T. G. Tiecke, J. T. M. Walraven, and D. S. Petrov, *Atom-dimer scattering and long-lived trimers in fermionic mixtures*, Phys. Rev. Lett. **103**, 153202 (2009).

[Lif80] E. M. Lifshitz and L. P. Pitaevskii, *Statistical Physics Part 2, vol. 9 (Course of theoretical physics)*, Butterworth-Heinemann, Oxford (1980).

[Liu03] W. V. Liu and F. Wilczek, *Interior Gap Superfluidity*, Phys. Rev. Lett. **90**, 047002 (2003).

[Liu04] W. V. Liu, F. Wilczek, and P. Zoller, *Spin-dependent Hubbard model and a quantum phase transition in cold atoms*, Phys. Rev. A **70**, 033603 (2004).

[Luo07] L. Luo, B. Clancy, J. Joseph, J. Kinast, and J. E. Thomas, *Measurement of the Entropy and Critical Temperature of a Strongly Interacting Fermi Gas*, Phys. Rev. Lett. **98**, 080402 (2007).

[Luo09] L. Luo and J. E. Thomas, *Thermodynamic Measurements in a Strongly Interacting Fermi Gas*, J. Low Temp. Phys. **154**, 1 (2009).

[Mad00a] P. Maddaloni, M. Modugno, C. Fort, F. Minardi, and M. Inguscio, *Collective oscillations of two colliding Bose-Einstein condensates*, Phys. Rev. Lett. **85**, 2413 (2000).

[Mad00b] K. W. Madison, F. Chevy, W. Wohlleben, and J. Dalibard, *Vortex Formation in a Stirred Bose-Einstein Condensate*, Phys. Rev. Lett. **84**, 806 (2000).

[Mai10] R. A. W. Maier, C. Marzok, C. Zimmermann, and P. W. Courteille, *Radio-frequency spectroscopy of ^{6}Li p-wave molecules: Towards photoemission spectroscopy of a p-wave superfluid*, Phys. Rev. A **81**, 064701 (2010).

[Mas11] P. Massignan and G. M. Bruun, *Repulsive polarons and itinerant ferromagnetism in strongly polarized Fermi gases* (2011), arXiv:1102.0121v2 [cond-mat.quant-gas].

[Mat99] M. R. Matthews, B. P. Anderson, P. C. Haljan, D. S. Hall, C. E. Wieman, and E. A. Cornell, *Vortices in a Bose-Einstein Condensate*, Phys. Rev. Lett. **83**, 2498 (1999).

[McN06] J. M. McNamara, T. Jeltes, A. S. Tychkov, W. Hogervorst, and W. Vassen, *Degenerate Bose-Fermi Mixture of Metastable Atoms*, Phys. Rev. Lett. **97**, 080404 (2006).

[Met99] H. J. Metcalf and P. van der Straten, *Laser Cooling and Trapping*, Springer, New York (1999).

[Mie96] F. H. Mies, C. J. Williams, P. S. Julienne, and M. Krauss, *Estimating bounds on collisional relaxation rates of spin-polarized Rb-87 atoms at ultracold temperatures*, J. Res. Natl. Inst. Stand. Technol. **101**, 521 (1996).

[Moe95] A. J. Moerdijk, B. J. Verhaar, and A. Axelsson, *Resonances in ultracold collisions of ^{6}Li, ^{7}Li, and ^{23}Na*, Phys. Rev. A **51**, 4852 (1995).

[Moh08] P. J. Mohr, B. N. Taylor, and D. B. Newell, *CODATA recommended values of the fundamental physical constants: 2006*, Rev. Mod. Phys. **80**, 633 (2008), see also http://physics.nist.gov/constants.

[Mor09] C. Mora and F. Chevy, *Ground state of a tightly bound composite dimer immersed in a Fermi sea*, Phys. Rev. A **80**, 033607 (2009).

[Mot65] N. F. Mott and H. Massey, *The Theory of Atomic Collisions*, Oxford (1965).

[Mud02] M. Mudrich, S. Kraft, K. Singer, R. Grimm, A. Mosk, and M. Weidemüller, *Sympathetic Cooling with Two Atomic Species in an Optical Trap*, Phys. Rev. Lett. **88**, no. 25, 253001 (2002).

[Nai11] D. Naik, A. Trenkwalder, C. Kohstall, F. M. Spiegelhalder, M. Zaccanti, G. Hendl, F. Schreck, R. Grimm, T. M. Hanna, and P. S. Julienne, *Feshbach resonances in the ^{6}Li-^{40}K Fermi-Fermi mixture: Elastic versus inelastic interactions*, Eur. Phys. J. D (2011), published online, doi:10.1140/epjd/e2010-10591-2.

[Nak10] S. Nakajima, M. Horikoshi, T. Mukaiyama, P. Naidon, and M. Ueda, *Nonuniversal Efimov Atom-Dimer Resonances in a Three-Component Mixture of ^{6}Li*, Phys. Rev. Lett. **105**, 023201 (2010).

[Nas10] S. Nascimbène, N. Navon, K. J. Jiang, F. Chevy, and C. Salomon, *Exploring the thermodynamics of a universal Fermi gas*, Nature **463**, 1057 (2010).

[Nav10] N. Navon, S. Nascimbène, F. Chevy, and C. Salomon, *The Equation of State of a Low-Temperature Fermi Gas with Tunable Interactions*, Science **328**, 729 (2010).

[Ni08] K.-K. Ni, S. Ospelkaus, M. H. G. de Miranda, A. Pe'er, B. Neyenhuis, J. J. Zirbel, S. Kotochigova, P. S. Julienne, D. S. Jin, and J. Ye, *A High Phase-Space-Density Gas of Polar Molecules*, Science **322**, 231 (2008).

[Nis08] Y. Nishida and S. Tan, *Universal Fermi gases in mixed dimensions*, Phys. Rev. Lett. **101**, 170401 (2008).

[Nis09a] Y. Nishida, *Induced p-wave superfluidity in two dimensions: Brane world in cold atoms and nonrelativistic defect CFTs*, Ann. Phys. **324**, 897 (2009).

[Nis09b] Y. Nishida and S. Tan, *Confinement-induced Efimov resonances in Fermi-Fermi mixtures*, Phys. Rev. A **79**, 060701(R) (2009).

[Nis10] Y. Nishida, *Phases of a bilayer Fermi gas*, Phys. Rev. A **82**, 011605 (2010).

[Noz85] P. Nozières and S. Schmitt-Rink, *Bose condensation in an attractive fermion gas: From weak to strong coupling superconductivity*, J. Low Temp. Phys. **59**, 195 (1985).

[O'H02] K. M. O'Hara, S. L. Hemmer, M. E. Gehm, S. R. Granade, and J. E. Thomas, *Observation of a Strongly Interacting Degenerate Fermi Gas*, Science **298**, 2179 (2002).

[Ore00] J. Orenstein and A. J. Millis, *Advances in the Physics of High-Temperature Superconductivity*, Science **288**, 468 (2000).

[Ors07] G. Orso, *Attractive Fermi Gases with Unequal Spin Populations in Highly Elongated Traps*, Phys. Rev. Lett. **98**, 070402 (2007).

[Ors08] G. Orso, L. P. Pitaevskii, and S. Stringari, *Equilibrium and dynamics of a trapped superfluid Fermi gas with unequal masses*, Phys. Rev. A **77**, 033611 (2008).

[Osh72] Q. D. Osheroff, R. C. Richardson, and D. M. Lee, *Evidence for a New Phase of Solid He^3*, Phys. Rev. Lett. **28**, 885 (1972).

[Ott08] T. B. Ottenstein, T. Lompe, M. Kohnen, A. N. Wenz, and S. Jochim, *Collisional stability of a three-component degenerate Fermi gas*, Phys. Rev. Lett. **101**, no. 20, 203202 (2008).

[Paa06] T. Paananen, J.-P. Martikainen, and P. Törmä, *Pairing in a three-component Fermi gas*, Phys. Rev. A **73**, 053606 (2006).

[Pap06] S. B. Papp and C. E. Wieman, *Observation of heteronuclear Feshbach molecules from a ^{85}Rb-^{87}Rb gas*, Phys. Rev. Lett. **97**, 180404 (2006).

[Par06a] G. B. Partridge, W. Li, R. I. Kamar, Y. Liao, and R. G. Hulet, *Pairing and Phase Separation in a Polarized Fermi Gas*, Science **311**, 503 (2006).

[Par06b] G. B. Partridge, W. Li, Y. A. Liao, R. G. Hulet, M. Haque, and H. T. C. Stoof, *Deformation of a Trapped Fermi Gas with Unequal Spin Populations*, Phys. Rev. Lett. **97**, 190407 (2006).

[Par07] M. M. Parish, F. M. Marchetti, A. Lamacraft, and B. D. Simons, *Polarized Fermi Condensates with Unequal Masses: Tuning the Tricritical Point*, Phys. Rev. Lett. **98**, 160402 (2007).

[Pek11] D. Pekker, M. Babadi, R. Sensarma, N. Zinner, L. Pollet, M. W. Zwierlein, and E. Demler, *Competition between Pairing and Ferromagnetic Instabilities in Ultracold Fermi Gases near Feshbach Resonances*, Phys. Rev. Lett. **106**, 050402 (2011).

[Per04] A. Perali, P. Pieri, and G. C. Strinati, *Quantitative Comparison between Theoretical Predictions and Experimental Results for the BCS-BEC Crossover*, Phys. Rev. Lett. **93**, 100404 (2004).

[Per11] A. Perali, F. Palestini, P. Pieri, G. C. Strinati, J. T. Stewart, J. P. G. T. E. Drake, and D. S. Jin, *Evolution of the Normal State of a Strongly Interacting Fermi Gas from a Pseudogap Phase to a Molecular Bose Gas*, Phys. Rev. Lett. **106**, 060402 (2011).

[Pet04a] D. S. Petrov, *Three-boson problem near a narrow Feshbach resonance*, Phys. Rev. Lett. **93**, 143201 (2004).

[Pet04b] D. S. Petrov, C. Salomon, and G. V. Shlyapnikov, *Weakly Bound Dimers of Fermionic Atoms*, Phys. Rev. Lett. **93**, 090404 (2004).

[Pet05] D. S. Petrov, C. Salomon, and G. V. Shlyapnikov, *Diatomic molecules in ultracold Fermi gases-novel composite bosons*, J. Phys. B: At. Mol. Opt. Phys. **38**, S645 (2005).

[Pet07] D. S. Petrov, G. E. Astrakharchik, D. J. Papoular, C. Salomon, and G. V. Shlyapnikov, *Crystalline Phase of Strongly Interacting Fermi Mixtures*, Phys. Rev. Lett. **99**, 130407 (2007).

[Pil09] K. Pilch, *Optical trapping and Feshbach spectroscopy of an ultracold Rb-Cs mixture*, Ph.D. thesis, Innsbruck University (2009).

[Pol09] S. E. Pollack, D. Dries, and R. G. Hulet, *Universality in three- and four-body bound states of ultracold atoms*, Science **326**, 1683 (2009).

[Rad10] L. Radzihovsky and D. E. Sheehy, *Imbalanced Feshbach-resonant Fermi gases*, Rep. Prog. Phys. **73**, 076501 (2010).

[Reg03a] C. A. Regal and D. S. Jin, *Measurement of Positive and Negative Scattering Lengths in a Fermi Gas of Atoms*, Phys. Rev. Lett. **90**, 230404 (2003).

[Reg03b] C. A. Regal, C. Ticknor, J. L. Bohn, and D. S. Jin, *Creation of Ultracold Molecules from a Fermi Gas of Atoms*, Nature **424**, 47 (2003).

[Reg03c] C. A. Regal, C. Ticknor, J. L. Bohn, and D. S. Jin, *Tuning p-wave Interactions in an Ultracold Fermi Gas of Atoms*, Phys. Rev. Lett. **90**, 053201 (2003).

[Reg04a] C. A. Regal, M. Greiner, and D. S. Jin, *Lifetime of Molecule-Atom Mixtures near a Feshbach Resonance in* ^{40}K, Phys. Rev. Lett. **92**, 083201 (2004).

[Reg04b] C. A. Regal, M. Greiner, and D. S. Jin, *Observation of Resonance Condensation of Fermionic Atom Pairs*, Phys. Rev. Lett. **92**, 040403 (2004).

[Reg05] C. Regal, *Experimental realization of BCS-BEC crossover physics with a Fermi gas of atoms*, Ph.D. thesis, University of Colorado, Boulder (2005).

[Rid11] A. Ridinger, S. Chaudhuri, T. Salez, U. Eismann, D. R. Fernandes, K. Magalhães, D. Wilkowski, C. Salomon, and F. Chevy, *Large atom number dual-species magneto-optical trap for fermionic* ^{6}Li *and* ^{40}K *atoms*, Eur. Phys. J. D (2011).

[Rie11] S. Riedl, E. R. S. Guajardo, C. Kohstall, J. Hecker Denschlag, and R. Grimm, *Superfluid quenching of the moment of inertia in a strongly interacting Fermi gas*, New J. Phys. **13**, 035003 (2011).

[Rob98] J. L. Roberts, N. R. Claussen, J. J. P. Burke, C. H. Greene, E. A. Cornell, and C. E. Wieman, *Resonant magnetic field control of elastic scattering in cold* ^{85}Rb, Phys. Rev. Lett. **81**, 5109 (1998).

[Sa 93] C. A. R. Sa de Melo, M. Randeria, and J. R. Engelbrecht, *Crossover from BCS to Bose Superconductivity: Transition Temperature and Time-Dependent Ginzburg-Landau Theory*, Phys. Rev. Lett. **71**, 3202 (1993).

[Sak94] J. J. Sakurai, *Modern Quantum Mechanics*, Addison-Wesley, Reading, MA, revised edition (1994).

[Sal07] H. Salami, A. J. Ross, P. Crozet, W. Jastrzebski, P. Kowalczyk, and R. J. L. Roy, *A full analytic potential energy curve for the* $a^3\Sigma^+$ *state of KLi from a limited vibrational data set*, J. Chem. Phys. **126**, 194313 (2007).

[Sar63] G. Sarma, *On the influence of a uniform exchange field acting on the spins of the conduction electrons in a superconductor*, J. Phys. Chem. Solids **24**, no. 8, 1029 (1963).

[Sch93] A. Schilling, M. Cantoni, J. D. Guo, and H. R. Ott, *Superconductivity above 130 K in Hg-Ba-Ca-Cu-O system*, Nature **363**, 56 (1993).

[Sch01] F. Schreck, L. Khaykovich, K. L. Corwin, G. Ferrari, T. Bourdel, J. Cubizolles, and C. Salomon, *Quasipure Bose-Einstein Condensate Immersed in a Fermi Sea*, Phys. Rev. Lett. **87**, 080403 (2001).

[Sch05] C. H. Schunck, M. W. Zwierlein, C. A. Stan, S. M. F. Raupach, W. Ketterle, A. Simoni, E. Tiesinga, C. J. Williams, and P. S. Julienne, *Feshbach Resonances in Fermionic ^6Li*, Phys. Rev. A **71**, 045601 (2005).

[Sch09a] T. Schäfer and D. Teaney, *Nearly perfect fluidity: from cold atomic gases to hot quark gluon plasmas*, Rep. Prog. Phys. **72**, 126001 (2009).

[Sch09b] A. Schirotzek, C.-H. Wu, A. Sommer, and M. W. Zwierlein, *Observation of Fermi polarons in a tunable Fermi liquid of ultracold atoms*, Phys. Rev. Lett. **102**, 230402 (2009).

[Shi06] Y. Shin, M. W. Zwierlein, C. H. Schunck, A. Schirotzek, and W. Ketterle, *Observation of Phase Separation in a Strongly Interacting Imbalanced Fermi Gas*, Phys. Rev. Lett. **97**, 030401 (2006).

[Shi07] Y. Shin, C. H. Schunck, A. Schirotzek, and W. Ketterle, *Tomographic rf Spectroscopy of a Trapped Fermi Gas at Unitarity*, Phys. Rev. Lett. **99**, 090403 (2007).

[Shi08a] Y. Shin, *Determination of the equation of state of a polarized Fermi gas at unitarity*, Phys. Rev. A **77**, 041603 (2008).

[Shi08b] Y. Shin, C. H. Schunck, A. Schirotzek, and W. Ketterle, *Phase diagram of a two-component Fermi gas with resonant interactions*, Nature **451**, 689 (2008).

[Sil05] C. Silber, S. Gunther, C. Marzok, B. Deh, P. W. Courteille, and C. Zimmermann, *Quantum-Degenerate Mixture of Fermionic Lithium and Bosonic Rubidium Gases*, Phys. Rev. Lett. **95**, 170408 (2005).

[Sim96] J. E. Simsarian, A. Ghosh, G. Gwinner, L. A. Orozco, G. D. Sprouse, and P. A. Voytas, *Magneto-Optic Trapping of ^{210}Fr*, Phys. Rev. Lett. **76**, 3522 (1996).

[Sim03] A. Simoni, F. Ferlaino, G. Roati, G. Modugno, and M. Inguscio, *Magnetic Control of the Interaction in Ultracold K-Rb Mixtures*, Phys. Rev. Lett. **90**, no. 16, 163202 (2003).

[Spi09] F. M. Spiegelhalder, A. Trenkwalder, D. Naik, G. Hendl, F. Schreck, and R. Grimm, *Collisional stability of ^{40}K immersed in a strongly interacting Fermi Gas of ^6Li*, Phys. Rev. Lett. **103**, 223203 (2009).

[Spi10] F. M. Spiegelhalder, A. Trenkwalder, D. Naik, G. Kerner, E. Wille, G. Hendl, F. Schreck, and R. Grimm, *All-optical production of a degenerate mixture of ^6Li and ^{40}K and creation of heteronuclear molecules*, Phys. Rev. A **81**, 043637 (2010), because of a calibration error the magnetic field values in the vicinity of the 168 G resonance in the *aa* channel need to be corrected by −47 mG.

[Sta04] C. A. Stan, M. W. Zwierlein, C. H. Schunck, S. M. F. Raupach, and W. Ketterle, *Observation of Feshbach Resonances between Two Different Atomic Species*, Phys. Rev. Lett. **93**, 143001 (2004).

[Ste06] J. T. Stewart, J. P. Gaebler, C. A. Regal, and D. S. Jin, *Potential Energy of a ^{40}K Fermi Gas in the BCS-BEC Crossover*, Phys. Rev. Lett. **97**, 220406 (2006).

[Ste09] S. Stellmer, M. K. Tey, B. Huang, R. Grimm, and F. Schreck, *Bose-Einstein condensation of strontium*, Phys. Rev. Lett. **103**, 200401 (2009).

[Ste10a] S. Stellmer, M. K. Tey, R. Grimm, and F. Schreck, *Bose-Einstein condensation of ^{86}Sr*, Phys. Rev. A **82**, no. 4, 041602 (2010).

[Ste10b] J. T. Stewart, J. P. Gaebler, T. E. Drake, and D. S. Jin, *Verification of Universal Relations in a Strongly Interacting Fermi Gas*, Phys. Rev. Lett. **104**, 235301 (2010).

[Sto88] H. T. C. Stoof, J. M. V. A. Koelman, and B. J. Verhaar, *Spin-exchange and dipole relaxation rates in atomic hydrogen: rigorous and simplified calculations*, Phys. Rev. B **38**, 4688 (1988).

[Str03] K. E. Strecker, G. B. Partridge, and R. G. Hulet, *Conversion of an Atomic Fermi Gas to a Long-Lived Molecular Bose Gas*, Phys. Rev. Lett. **91**, no. 8, 080406 (2003).

[Tag06] M. Taglieber, A.-C. Voigt, F. Henkel, S. Fray, T. W. Hänsch, and K. Dieckmann, *Simultaneous magneto-optical trapping of three atomic species*, Phys. Rev. A **73**, 011402(R) (2006).

[Tag08] M. Taglieber, A.-C. Voigt, T. Aoki, T. W. Hänsch, and K. Dieckmann, *Quantum Degenerate Two-Species Fermi-Fermi Mixture Coexisting with a Bose-Einstein Condensate*, Phys. Rev. Lett. **100**, 010401 (2008).

[Tan08a] S. Tan, *Energetics of a strongly correlated Fermi gas*, Ann. Phys. **323**, 2952 (2008).

[Tan08b] S. Tan, *Generalized virial theorem and pressure relation for a strongly correlated Fermi gas*, Ann. Phys. **323**, 2987 (2008).

[Tan08c] S. Tan, *Large momentum part of a strongly correlated Fermi gas*, Ann. Phys. **323**, 2971 (2008).

[Tey10] M. K. Tey, S. Stellmer, R. Grimm, and F. Schreck, *Double-degenerate Bose-Fermi mixture of strontium*, Phys. Rev. A **82**, no. 1, 011608 (2010).

[Tho05a] S. T. Thompson, E. Hodby, and C. E. Wieman, *Spontaneous dissociation of ^{85}Rb Feshbach molecules*, Phys. Rev. Lett. **94**, 020401 (2005).

[Tho05b] S. T. Thompson, E. Hodby, and C. E. Wieman, *Ultracold molecule production via a resonant oscillating magnetic field*, Physical Review Letters **95**, no. 19, 190404 (2005).

[Tho10] J. E. Thomas, *The nearly perfect Fermi gas*, Phys. Today **63**, no. 5, 34 (2010).

[Tic04] C. Ticknor, C. A. Regal, D. S. Jin, and J. L. Bohn, *Multiplet structure of Feshbach resonances in nonzero partial waves*, Phys. Rev. A **69**, 042712 (2004).

[Tie09a] T. G. Tiecke, *Feshbach resonances in ultracold mixtures of the fermionic quantum gases ^6Li and ^{40}K*, Ph.D. thesis, University of Amsterdam (2009).

[Tie09b] T. G. Tiecke, S. D. Gensemer, A. Ludewig, and J. T. M. Walraven, *High-flux two-dimensional magneto-optical-trap source for cold lithium atoms*, Phys. Rev. A **80**, 013409 (2009).

[Tie09c] E. Tiemann, H. Knöckel, P. Kowalczyk, W. Jastrzebski, A. Pashov, H. Salami, and A. J. Ross, *Coupled system $a\Sigma 3+$ and $X\Sigma 1+$ of KLi: Feshbach resonances and corrections to the Born-Oppenheimer approximation*, Phys. Rev. A **79**, 042716 (2009).

[Tie10a] T. G. Tiecke, M. R. Goosen, A. Ludewig, S. D. Gensemer, S. Kraft, S. J. J. M. F. Kokkelmans, and J. T. M. Walraven, *Broad Feshbach resonance in the ^6Li-^{40}K mixture*, Phys. Rev. Lett. **104**, 053202 (2010).

[Tie10b] T. G. Tiecke, M. R. Goosen, J. T. M. Walraven, and S. J. J. M. F. Kokkelmans, *Asymptotic-bound-state model for Feshbach resonances*, Phys. Rev. A **82**, 042712 (2010).

[Tre11] A. Trenkwalder, C. Kohstall, M. Zaccanti, D. Naik, A. I. Sidorov, F. Schreck, and R. Grimm, *Hydrodynamic Expansion of a Strongly Interacting Fermi-Fermi Mixture*, Phys. Rev. Lett. **106**, 115304 (2011).

[Tru01] A. G. Truscott, K. E. Strecker, W. I. McAlexander, G. B. Partridge, and R. G. Hulet, *Observation of Fermi Pressure in a Gas of Trapped Atoms*, Science **291**, 2570 (2001).

[Voi09] A.-C. Voigt, M. Taglieber, L. Costa, T. Aoki, W. Wieser, T. W. Hänsch, and K. Dieckmann, *Ultracold heteronuclear Fermi-Fermi molecules*, Phys. Rev. Lett. **102**, 020405 (2009), *ibid.* **105**, 269904(E) (2010).

[Wan09] B. Wang, H.-D. Chen, and S. Das Sarma, *Quantum phase diagram of fermionic mixtures with population imbalance in one-dimensional optical lattices*, Phys. Rev. A **79**, 051604(R) (2009).

[Web08] C. Weber, G. Barontini, J. Catani, G. Thalhammer, M. Inguscio, and F. Minardi, *Association of ultracold double-species bosonic molecules*, Phys. Rev. A **78**, 061601(R) (2008).

[Wen09] A. N. Wenz, T. Lompe, T. B. Ottenstein, F. Serwane, G. Zürn, and S. Jochim, *Universal trimer in a three-component Fermi gas*, Phys. Rev. A **80**, 040702(R) (2009).

[Wie10] A. W. Wiederkehr, S. D. Hogan, B. Lambillotte, M. Andrist, H. Schmutz, J. Agner, Y. Salathe, and F. Merkt, *Trapping deuterium atoms*, Phys. Rev. A **81**, 021402(R) (2010).

[Wil08] E. Wille, F. M. Spiegelhalder, G. Kerner, D. Naik, A. Trenkwalder, G. Hendl, F. Schreck, R. Grimm, T. G. Tiecke, J. T. M. Walraven, S. J. J. M. F. Kokkelmans, E. Tiesinga, and P. S. Julienne, *Exploring an ultracold Fermi-Fermi mixture: Interspecies Feshbach resonances and scattering properties of ^6Li and ^{40}K*, Phys. Rev. Lett. **100**, no. 5, 053201 (2008).

[Wil09a] E. Wille, *Preparation of an Optically Trapped Fermi-Fermi Mixture of ^6Li and ^{40}K Atoms and Characterization of the Interspecies Interactions by Feshbach Spectroscopy*, Ph.D. thesis, Innsbruck University (2009).

[Wil09b] J. R. Williams, E. L. Hazlett, J. H. Huckans, R. W. Stites, Y. Zhang, and K. M. O'Hara, *Evidence for an excited-state Efimov trimer in a three-component Fermi gas*, Phys. Rev. Lett. **103**, 130404 (2009).

[Wri07] M. J. Wright, S. Riedl, A. Altmeyer, C. Kohstall, E. R. Sánchez Guajardo, J. Hecker Denschlag, and R. Grimm, *Finite-temperature collective dynamics of a Fermi gas in the BEC-BCS crossover*, Phys. Rev. Lett. **99**, 150403 (2007).

[Wu11] C.-H. Wu, I. Santiago, J. W. Park, P. Ahmadi, and M. W. Zwierlein, *Strongly Interacting Isotopic Bose-Fermi Mixture Immersed in a Fermi Sea*, arXiv:1103.4630v1 [cond-mat.quant-gas] (2011).

[Yag05] K. Yagi, T. Hatsuda, and Y. Miake, *Quark-Gluon Plasma: From Big Bang to Little Bang*, Cambridge University Press (2005).

[Zac09] M. Zaccanti, B. Deissler, C. D'Errico, M. Fattori, M. Jona-Lasinio, S. Müller, G. Roati, M. Inguscio, and G. Modugno, *Observation of an Efimov spectrum in an atomic system*, Nature Phys. **5**, 586 (2009).

[Zha04] J. Zhang, E. G. M. van Kempen, T. Bourdel, L. Khaykovich, J. Cubizolles, F. Chevy, M. Teichmann, L. Tarruell, S. J. J. M. F. Kokkelmans, and C. Salomon, *P-wave Feshbach Resonances of ultracold ^6Li*, Phys. Rev. A **70**, 030702(R) (2004).

[Zwe09] W. Zwerger, *Itinerant Ferromagnetism with Ultracold Atoms*, Science **325**, 1507 (2009).

[Zwi03] M. W. Zwierlein, C. A. Stan, C. H. Schunck, S. M. F. Raupach, S. Gupta, Z. Hadzibabic, and W. Ketterle, *Observation of Bose-Einstein Condensation of Molecules*, Phys. Rev. Lett. **91**, 250401 (2003).

[Zwi04] M. W. Zwierlein, C. A. Stan, C. H. Schunck, S. M. F. Raupach, A. J. Kerman, and W. Ketterle, *Condensation of Pairs of Fermionic Atoms near a Feshbach Resonance*, Phys. Rev. Lett. **92**, 120403 (2004).

[Zwi05] M. W. Zwierlein, J. R. Abo-Shaeer, A. Schirotzek, C. H. Schunck, and W. Ketterle, *Vortices and Superfluidity in a Strongly Interacting Fermi Gas*, Nature **435**, 1047 (2005).

[Zwi06a] M. W. Zwierlein, A. Schirotzek, C. H. Schunck, and W. Ketterle, *Direct observation of the superfluid phase transition in ultracold Fermi gases*, Nature **442**, 54 (2006).

[Zwi06b] M. W. Zwierlein, A. Schirotzek, C. H. Schunck, and W. Ketterle, *Fermionic Superfluidity with Imbalanced Spin Populations*, Science **311**, 492 (2006).